

Cellular balancing under dynamic conditions

A systems biology-based discovery using experimental and modelling approaches

Verhagen, K.J.A.

DOI

[10.4233/uuid:d43f7180-be04-4e5b-a090-993f52433513](https://doi.org/10.4233/uuid:d43f7180-be04-4e5b-a090-993f52433513)

Publication date

2023

Document Version

Final published version

Citation (APA)

Verhagen, K. J. A. (2023). *Cellular balancing under dynamic conditions: A systems biology-based discovery using experimental and modelling approaches*. [Dissertation (TU Delft), Delft University of Technology]. <https://doi.org/10.4233/uuid:d43f7180-be04-4e5b-a090-993f52433513>

Important note

To cite this publication, please use the final published version (if applicable). Please check the document version above.

Copyright

Other than for strictly personal use, it is not permitted to download, forward or distribute the text or part of it, without the consent of the author(s) and/or copyright holder(s), unless the work is under an open content license such as Creative Commons.

Takedown policy

Please contact us and provide details if you believe this document breaches copyrights. We will remove access to the work immediately and investigate your claim.

Cellular balancing under dynamic conditions

A systems biology-based discovery using experimental and modelling approaches

Dissertation

for the purpose of obtaining the degree of doctor

at the Delft University of Technology

by the authority of the Rector Magnificus Prof.dr.ir. T.H.J.J. van der Hagen,

chair of the Board for Doctorates

to be defended publicly on

Thursday 6 April 2023 at 12:30 o'clock

by

Koen Johannes Anthonius VERHAGEN

Master of Science in Life Science and Technology, Delft University of Technology, the Netherlands

born in Delft, the Netherlands

This dissertation has been approved by the promotor.

Composition of the doctoral committee:

Rector Magnificus	chairperson
Prof.dr. P.A.S. Daran-Lapujade	Delft University of Technology, promotor
Prof.dr. S.A. Wahl	Friedrich-Alexander-Universität Erlangen-Nürnberg, Germany, promotor

Independent members:

Prof.dr. P. Branduardi	University of Milano-Bicocca, Italy
Prof.dr. F.J. Bruggeman	Vrije Universiteit Amsterdam
Prof.dr. A. Grünberger	Karlsruhe Institute of Technology, Germany
Prof.dr.ir. H.J. Noorman	Delft University of Technology / DSM
Dr. K Nöh	Forschungszentrum Jülich, Germany
Prof.dr. F. Hollmann	Delft University of Technology, reserve member

The research presented in this thesis was performed at the Cell Systems Engineering and Industrial Microbiology groups, Department of Biotechnology, Faculty of Applied Sciences, Delft University of Technology, the Netherlands and was funded by a grant from the Building Blocks of Life research program of the Netherlands Organization for Scientific Research (NWO, project number 737.016.001) and by Koninklijke DSM N.V..

© 2023, Koen Verhagen

All rights reserved

Printed by Ipskamp Printing

Table of contents

Summary		1
Samenvatting		5
Chapter 1	General Introduction	9
Chapter 2	Using kinetic modelling to infer adaptations in <i>Saccharomyces cerevisiae</i> carbohydrate storage metabolism to feast/famine regimes	27
Chapter 3	Predicting metabolic adaptation under dynamic substrate conditions using a resource dependent kinetic model: A case study using <i>Saccharomyces cerevisiae</i>	63
Chapter 4	A dive into yeast's sugar diet – Comparing the metabolic response of glucose, fructose, sucrose & maltose under dynamic feast/famine conditions	95
Chapter 5	Outlook	125
Acknowledgements		133
About the Author		137

Summary

Saccharomyces cerevisiae, also known as baker's yeast, is a robust microorganism frequently used in industrial biotechnology. The scale of its applications ranges from several millilitres for research and process development in the lab to hundreds of cubic meters for cultivation in industrial production processes. In large-scale reactors mixing limitations inherently lead to physiochemical gradients in substrate and oxygen concentrations, pH or temperature. Such inhomogeneous environment in production processes can cause a reduced yield or titer compared to the small-scale development processes. Such scale performance differences can lead to significant worse process economics and increase costs and development time.

The scope of this thesis is to study and understand the regulation of *Saccharomyces cerevisiae* metabolism under dynamic substrate conditions, using both experimental and modelling approaches.

Chapter 1 provides a general introduction to *S. cerevisiae* central carbon metabolism, especially focused on dynamic conditions. Here, earlier experimental studies monitoring the metabolic response to various dynamic substrate conditions in *S. cerevisiae* are summarized and discussed, together with an overview of the currently published kinetic models of *S. cerevisiae* metabolism. Furthermore, the current challenges and remaining knowledge gaps are described.

In **Chapter 2**, a large, comprehensive dynamic model of yeast carbon metabolism was used to identify relevant mechanisms regulating the metabolic response to prolonged repetitive dynamic "feast/famine" conditions. This study is based on multi-omics data, containing quantitative metabolomics and fluxomics, as well as ¹³C labelling data. A novel parameter estimation pipeline using combinatorial enzyme selection was applied to identify the minimal enzyme and parameter adjustments to reproduce the adaptation in metabolic response from chemostat to feast/famine conditions. Especially, proteomic changes in glucose transport and phosphorylation reactions were identified as most relevant for reproducing the adapted dynamic metabolic response. These predictions were confirmed through comparison with experimental proteome data.

Chapter 3 describes the development of a proteome-dependent kinetic model of yeast central carbon metabolism. In contrast to earlier resource allocation approaches, able to predict optimal proteomes under (quasi) steady-state conditions, this model can be applied to dynamic cultivation conditions as well. The model was constructed by combining published kinetic models and calibrating its parameters to published fluxomics and proteomics datasets. The calibrated model was able to predict proteomes for different steady-state chemostat dilution rates. The predictions suggested that the onset of aerobic fermentation, also known as the Crabtree effect, is not the result of space limitations in the total proteome, but rather an effect of mitochondrial constraints. Predictions of proteome allocation under dynamic feast/famine conditions showed that, compared to steady-state conditions, less proteome space was available for non-metabolic proteins. This suggests that the experimentally measured 'overcapacity' in proteomes at steady-state might ensure robustness of cells to dynamic conditions. Comparison of predicted proteomes under dynamic conditions with experimental proteome measurements confirmed the ability of this model to accurately predict proteome adaptation trends.

Chapter 4 provides a comprehensive experimental comparison of four different sugar substrates, namely glucose, fructose, sucrose and maltose, under dynamic substrate conditions in *S. cerevisiae*. While these substrates are chemically very similar to each other, the transport of these sugars into the cell differs significantly, with glucose and fructose being transported passively, while maltose is transported actively into the cell. Sucrose on the other hand is hydrolysed extracellularly, followed by passive transport of the resulting mono-saccharides into the cell. These differences in transport were expected to modulate the metabolic response under dynamic substrate conditions. To unravel the impact of these different carbon sources under dynamic substrate gradients, both steady-state and

dynamic feast/famine conditions were compared with respect to physiology, intracellular metabolome and proteome. Dynamic gradients of maltose lead to a significant decrease in biomass yield, which was not observed for the other sugar gradients.

While the averaged physiology was very comparable for glucose, fructose and sucrose, the intracellular metabolic response was very different, with reduced glycolytic responses for fructose and sucrose compared to glucose. Additionally, the concentration of enzymes of the upper glycolysis were found to be decreased for glucose, while increased for fructose and sucrose conditions upon exposure to dynamic substrate conditions. Nonetheless, a stable energy charge between 0.78 and 0.89 was observed for all dynamic sugar conditions, contrary to observations from single-pulse experiments.

Chapter 5 summarizes the main findings of this work and the remaining open questions, challenges and opportunities for future research are discussed. Future experimental and modelling challenges include 1) the accounting for differences in enzyme kinetics due to intracellular pH changes, isoenzyme expression and post-translational modifications, 2) quantification of intracellular transport and compartmentation, and 3) population dynamics.

Samenvatting

Saccharomyces cerevisiae, ook wel bekend als bakkergist, is een robuust micro-organisme dat veel wordt gebruikt in de industriële biotechnologie. De schaal van zijn verschillende toepassingen varieert van enkele milliliters bij onderzoek en procesontwikkeling in het lab tot honderden kubiek meters bij cultivatie in industriële productieprocessen. Op grote schaal zullen beperkingen in het mengen van de reactor van nature leiden tot fysiochemische gradiënten in de substraat en zuurstof concentraties, pH en temperatuur. Zo'n inhomogeen milieu kan in productieprocessen leiden tot een verminderde productopbrengst in vergelijking met kleine schaal processen voor procesontwikkeling. Dit soort verschillen in opbrengst kunnen leiden tot significant slechtere winstmarges en tot verhoogde kosten en een langere ontwikkelingstijd.

Het doel van dit proefschrift is het bestuderen en begrijpen van de regulatie van het metabolisme van *Saccharomyces cerevisiae* bij blootstelling aan substraatgradiënten, door gebruik te maken van zowel experimentele als modelmatige methoden.

Hoofdstuk 1 geeft een algemene introductie tot het centrale koolstofmetabolisme van *S. cerevisiae*, met een specifieke focus op dynamische omstandigheden. Voorgaande experimentele onderzoeken van de metabole respons van *S. cerevisiae* op verscheidene dynamische substraatomstandigheden zijn samengevat en worden hier besproken, samen met de tot op heden gepubliceerde kinetische modellen van het metabolisme van *S. cerevisiae*. Hiernaast worden ook de huidige uitdagingen en kennislacunes beschreven.

In **Hoofdstuk 2** is een groot, uitgebreid dynamisch model van het koolstofmetabolisme van gist gebruikt om de belangrijke mechanismen, verantwoordelijk voor het reguleren van de metabole respons op langdurige herhaaldelijke dynamische "feast/famine" omstandigheden, te identificeren. Deze studie is gebaseerd op multi-omics data, bestaande uit zowel kwantitatieve metabolomics en fluxomics data, als ¹³C labelling data. Om kinetische parameters te schatten is een nieuwe pijplijn, gebruikmakend van combinatorische enzymselectie, toegepast om de aanpassing van de metabole respons van chemostaat naar feast/famine omstandigheden te reproduceren. Hierbij werden proteoomveranderingen in glucose transport en fosforyleringsreacties geïdentificeerd als het belangrijkste voor het reproduceren van de aangepaste metabole respons. Deze voorspellingen werden bevestigd door vergelijking met experimentele proteoom data.

Hoofdstuk 3 beschrijft de ontwikkeling van een proteoom-afhankelijk kinetisch model van het centrale koolstofmetabolisme van gist. In tegenstelling tot eerdere resource allocation modellen, die in staat waren om de optimale proteoomsamenstelling onder (quasi) steady-state omstandigheden te voorspellen, kan dit model ook gebruikt worden met dynamische cultivatie omstandigheden. Het model is opgebouwd door gepubliceerde kinetische modellen met elkaar te combineren en de parameters ervan te kalibreren op gepubliceerde fluxomics en proteomics datasets. De voorspellingen suggereerden dat het begin van aerobe fermentatie, ook wel bekend als het Crabtree-effect, niet het resultaat is van ruimtebeperkingen in het totale proteoom, maar eerder een effect is van mitochondriale beperkingen. Voorspellingen van proteoomverdeling onder dynamische feast/famine omstandigheden toonden aan dat, in vergelijking met steady-state omstandigheden, er minder proteoomruimte beschikbaar was voor niet-metabole eiwitten. Dit suggereert dat de experimenteel gemeten 'overcapaciteit' in proteomen bij steady-state de robuustheid van cellen voor dynamische omstandigheden zou kunnen garanderen. Vergelijking van voorspelde proteomen onder dynamische omstandigheden met experimentele proteoommetingen bevestigden het vermogen van dit model om proteoomaanpassingstrends accuraat te kunnen voorspellen.

Hoofdstuk 4 biedt een uitgebreide experimentele vergelijking van vier verschillende suikersubstraten, namelijk glucose, fructose, sucrose en maltose, onder dynamische substraatomstandigheden in *S. cerevisiae*. Hoewel deze substraten chemisch gezien erg op elkaar lijken, verschilt het transport van deze suiker naar de cel aanzienlijk, waarbij glucose en fructose passief worden getransporteerd, terwijl maltose actief de cel in wordt getransporteerd. Sucrose daarentegen wordt extracellulair gehydrolyseerd, gevolgd door passief transport naar de cel van de resulterende monosacchariden. Verwacht werd dat deze verschillen in transport de metabole respons onder dynamische substraatomstandigheden zouden moduleren. Om de impact van deze verschillende koolstofbronnen onder dynamische substraatgradiënten te ontrafelen, werden zowel steady-state als feast/famine omstandigheden vergeleken met betrekking tot fysiologie, intracellulair metabooloom en proteoom. Dynamische gradiënten van maltose leidden tot een significante daling in de biomassaopbrengst, hetgeen niet werd waargenomen bij de andere suikergradiënten.

Hoewel de gemiddelde fysiologie zeer vergelijkbaar was voor glucose, fructose en sucrose, was de intracellulaire metabole respons heel anders, met verminderde glycolytische responsen voor fructose en sucrose in vergelijking met glucose. Bovendien bleek de concentratie van enzymen van de hogere glycolyse verlaagd te zijn voor glucose, terwijl deze juist verhoogd was voor fructose- en sucroseomstandigheden bij blootstelling aan dynamische substraatomstandigheden. Desalniettemin werd er een stabiele energielading tussen 0.78 en 0.89 waargenomen voor alle dynamische suikercondities, in tegenstelling tot waarnemingen van experimenten met één enkele substraatpuls.

Hoofdstuk 5 vat de belangrijkste bevindingen van dit werk samen en hiernaast worden de resterende open vragen, uitdagingen en kansen voor toekomstig onderzoek besproken. Toekomstige experimentele en modelleringsuitdagingen omvatten 1) het rekening houden met de verschillen in enzymkinetiek als gevolg van intracellulaire pH veranderingen, isoenzymexpressie en post-translationele modificaties, 2) kwantificering van intracellulair transport en compartimentering, en 3) dynamiek in populaties.

1

General Introduction

Background

Saccharomyces cerevisiae, also commonly known as baker's yeast, is one of the most used microorganisms in biotechnology. It has been used by mankind for thousands of years, having engrained itself in our society as a successful domestication project. *S. cerevisiae* is a prominent cell factory involved in the food, beverages, and biofuels industries [1–5]. On top of its tractability and robustness, genetic engineering has allowed for the introduction of novel pathways, mechanisms of protein secretion, as well as improvement of a plethora of cellular mechanisms, such as those involved in protein secretion, stress tolerance and substrate requirements, generating new strains that have widened its range of applications [6,7]. Nonetheless, scaling up from laboratory to commercial production is a challenging stage in which developed strains may emerge as inefficient [8]. When scaling up a reactor, all dimensions are enlarged, however, relevant parameters, such as power input per volume are far more difficult to scale. As such, both shear stress and mixing times are increased, presenting a major problem, as these parameters heavily affect metabolic performance of the cells including *S. cerevisiae*. This is because long circulation times and nonideal mixing results in significant gradients in substrate, oxygen, pH and temperature in the large-scale reactor [9–12]. As yeast cells experience these gradients, extracellular fluxes into the cell are constantly changing, which is something to which these cells need to continuously adapt their metabolism, often deteriorating process yields [13]. Understanding the regulatory mechanisms behind this behaviour is essential to improve the development of large-scale bioprocesses.

However, cell factories are apart from the product pathway, not designed, but rather evolved in natural environments. Our understanding of the multifaceted regulation of metabolism and adaptation to different environments is still limited. A cell contains many different molecules, together forming a biological system regulating the metabolic behaviour of the cell. Following the central dogma of biology [14], the genome, in the form of DNA, acts as the blueprint of the cell, from which mRNA molecules are transcribed. These mRNA molecules are subsequently translated into proteins. Proteins in turn catalyse the reactions converting substrates into energy, biomass and various metabolites and products. Together, these levels of metabolism, genome, transcriptome, proteome and metabolome, shape the metabolic behaviour of the cell. Systems biology is the field of study which aims to identify how these different levels interact with each other to produce the metabolic behaviour of the cell. It does this by combining mechanistic or heuristic modelling based on extensive datasets describing these biological levels, in the form of fluxomics, genomics, metabolomics, proteomics and transcriptomics [15].

In this thesis, several of these -omics technologies have been used in synergy with metabolic modelling to describe and understand the metabolic behaviour of *S. cerevisiae* under different, dynamic cultivation conditions.

S. cerevisiae metabolism under dynamic conditions

Glycolysis can be found at the core of the metabolic network of *S. cerevisiae*. This pathway converts intracellular hexose into pyruvate and produces energy in the form of ATP and glycolytic intermediates that support anabolic reactions [16]. How glycolysis contributes to the metabolic processes inside the cell depends on multiple factors. The presence or absence of oxygen determines if pyruvate is fully oxidized to CO₂ or fermented to ethanol [17,18]. Still, this conspicuously simple explanation is challenged at high-substrate concentrations or higher growth rates, where the maximum respiratory capacity is reached and fermentation takes place even if oxygen is present [19,20], in what is known as 'overflow metabolism' or Crabtree effect [21]. While these phenomena can be explained by different optimality criteria, it is not clear how such behaviours are regulated on a metabolic level.

By nature, glycolysis (see Figure 1.1) is thermodynamically set up in a so-called 'turbo design', with ATP produced from glucose being reinvested to consume even more substrate, producing a further surplus of ATP, optimizing flux through glycolysis [22]. However, when substrate-limited cells are suddenly exposed to an excess of substrate, this 'turbo design' of glycolysis has been observed to cause a phenomenon called substrate accelerated death. In wild-type yeast cells, this phenomenon has been observed specifically for maltose, but not for glucose, which indicated the presence of specific regulatory systems to prevent this from occurring. The response of glycolysis to fluctuations in glucose concentration in the extracellular space is controlled by different regulatory layers. The first, fast mechanism is metabolic, i.e. the diversion of flux to storage, glycogen and trehalose when glucose uptake exceeds the glycolytic processing capacity [23]. Furthermore, allosteric and post-translation regulation take place [24]: Hexokinase (HXK) is allosterically inhibited by trehalose-6-phosphate (T6P), pyruvate kinase (PYK) is activated by fructose-1,6-bis-phosphate (FBP) and multiple metabolites act on phosphofructokinase (PFK) [25,26]. Simultaneously, the cAMP-protein kinase A (PKA) pathway is activated upon glucose perturbation and starts a regulation cascade in central carbon metabolism (CCM) [27] and possible targets for Post-Translational Modifications (PTMs) have been found in multiple enzymes along the CCM [28]. Finally, to adapt to different growth conditions, yeast cells use different enzyme isoforms. For instance, expression of hexokinases and glucokinases is balanced to adapt to different glucose concentrations [29], with hexokinases specifically playing a significant role in glucose repression [30] and the regulation of intracellular pH is compartment-specific, carried out by different ATPases [31].

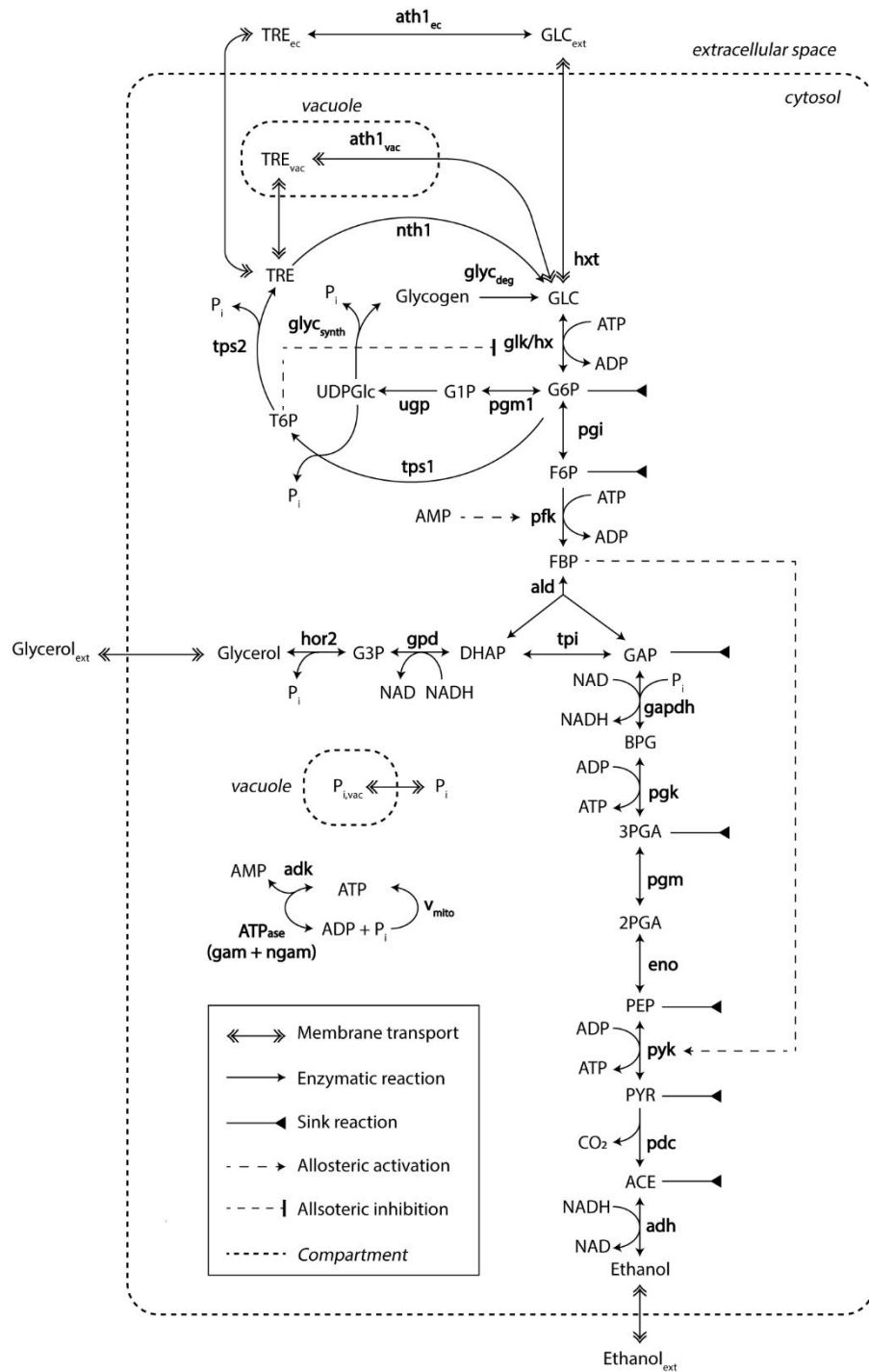


Figure 1.1. Schematic overview of the central carbon metabolism of yeast, with in the centre glycolysis, with associated pathways for the trehalose cycle, glycerol pathway, TCA cycle, PPP and ethanol fermentation.

Developments in monitoring the dynamic metabolic response in *S. cerevisiae*

Scale-down approaches have been developed to understand long-standing performance problems in industrial bioreactors. Although this has granted valuable knowledge, essential intracellular properties such as *in vivo* fluxes and kinetics have been captured with only limited resolution, constraining model development. In fact, this has become one of the main challenges in the development of high quality predictive kinetic models, since often multiple variables from the transcriptome, metabolome and fluxome, interact to result in the final response [32].

Early models on *in vitro* and *in vivo* metabolic responses to periodic glucose fluctuations only used small datasets, reducing their range of implementation. On most occasions only extracellular data such as growth and nutrient exchange rates was available [33] or a few metabolites at most [34], until *in vivo* quantification of metabolite concentrations and fluxes became a common practice, where most cofactors, glycolytic intermediates and rates were simultaneously observable [35]. A major challenge in this type of experiments is the accurate monitoring of the actual metabolic state at the time of sampling, followed by the accurate measurement of intracellular metabolites, which are all present in very low concentration. For rapid sampling of cultures, many different setups have been developed [36–40]. However, accurate measurement of metabolite concentrations is also dependent on quenching and processing of the samples, where one has to take metabolite leakage and extracellular metabolites into account [41–44]. To account for degradation of metabolites during processing steps, an internal (^{13}C) standard can be added prior to processing [45].

Later, a commonly used dynamic glucose perturbation experimental setup with yeast strains from the CEN.PK lineage [46] was adopted (see Table 1). This consisted of glucose-limited chemostat cultures at dilution rate of 0.1 h^{-1} (about 25% of the maximum growth rate of this yeast), followed by an external glucose perturbation in the form of a single pulse, where extracellular concentration increased to 1 g L^{-1} . These stimulus response experiments were used to infer more physiological patterns [36] and the use of Nuclear Magnetic Resonance (NMR) and Mass Spectroscopy (MS) techniques made a wide range of intracellular metabolites measurable. From only a few glycolytic concentrations, datasets gradually grew to include most metabolites in glycolysis, the trehalose cycle, the tricarboxylic acid (TCA) cycle, and the pentose phosphate pathway (PPP). These studies focused on a single substrate pulse, which is a good tool to study the metabolic makeup of cells grown under limiting conditions (i.e. the previous chemostat).

To study cells in their industrial setting, other setups that mimic the large-scale conditions are required, so called scale-down experiments. One such setup is the feast/famine cycle regime [47] which uses repetitive cycles of short glucose pulses (Figure 1.2). Extensive datasets are now available for *S. cerevisiae*, however they have not yet been used for the purpose of model development [48,49]. Suarez-Mendez et al. [49] used a feast/famine cycle setup to monitor *in vivo* metabolic activity during cycles of 400 s. These feast/famine cycles were characterized by a 20 s feed ('feast'), followed by 380 s of no feed ('famine') (Figure 1.2). These feast/famine cycles were maintained for 50 hours.

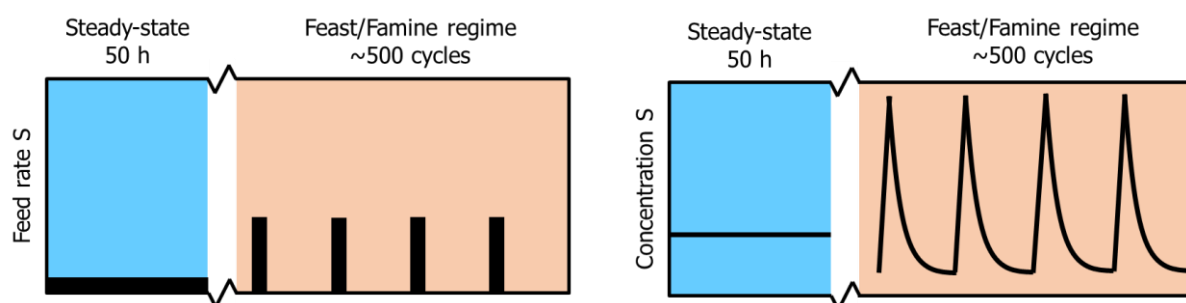


Figure 1.2. Profile of the experimental feeding and resulting substrate concentration conditions. After a glucose-limited chemostat phase (reference steady-state) of 50 h, a block-wise feed is applied in a 400 s cycle at the same average substrate supply and dilution rate for another 50 h (adapted from [49]).

It was observed that under these feast/famine conditions, *S. cerevisiae* cultures show a different metabolic response to a substrate perturbation compared to steady-state cultures [49]. For instance, the ethanol production typically observed upon single glucose pulse to a glucose-limited yeast culture, is not observed after pulsing glucose in feast/famine conditions. Interestingly, an increase rather than a decrease in ATP is observed. Additionally, a quick and maintained accumulation of glycolytic metabolites is observed upon a single glucose pulse to a chemostat culture, which is not observed for

feast/famine cultures. These differences in metabolic response suggest metabolic adaptation to long-term exposure to the feast/famine regime [50–52], although the exact mechanism behind this adaptation is not well understood.

In general, three levels of metabolic regulation can be distinguished [53]: 1) Allosteric regulation, which is the regulation of enzyme activity through non-covalent binding with metabolites. The response time of this form of regulation is almost instantaneous, providing important feedback loops within metabolic pathways [54]. 2) Post-translational modifications (PTMs), in which the enzyme activity is regulated through covalent binding of specific molecular attachments, such as phosphate groups. This form of regulation acts on the timescale of seconds to minutes, and is utilized as part of short-term responses to stress situations, such as sudden changes in the extracellular environment [55,56]. Finally, 3) translational regulation, which directly affects the composition of the proteome, accounting for longer-term adaptations [57]. Together, these mechanisms regulate the adjustment of the metabolic response. Next to aforementioned metabolomics, the quantification of mRNA transcripts and proteins, respectively known as transcriptomics and proteomics, provides a useful tool to further understand the role of these three levels of regulation in the observed metabolic adaptation to long-term exposure to repetitive substrate fluctuations.

Table 1.1. Overview of experiments with glucose concentration perturbation to substrate-limited cultures of *S. cerevisiae*. Only studies with intracellular metabolome quantification are shown. The only exception is the study by Walther et al. [58] in which growth limitation is reached by trehalose feeding in batch (shake-flask) culture. Metabolite pools: glycolysis (GLYCO), tricarboxylic acid cycle (TCA), pentose phosphate pathway (PPP), trehalose cycle (TRE), nucleotides (NUC), Amino acids (AAs).

	Rizzi et al. [59]	Theobald et al. [36]	Vaseghi et al. [60]	Visser et al. [25]
Glucose input regime	Glucose-limited to glucose pulse (0.25 g L ⁻¹)	Glucose-limited to glucose pulse (1 g L ⁻¹)	Glucose-limited to glucose pulse (1 g L ⁻¹)	Glucose-limited to glucose pulse (1 g L ⁻¹)
Experimental setup	30 °C, pH5, aerobic, D = 0.1 h ⁻¹ , direct sampling	30 °C, pH5, aerobic, D = 0.1 h ⁻¹ , direct sampling	30 °C, pH5, aerobic, D = 0.1 h ⁻¹ , direct sampling	30 °C, pH5, aerobic, D = 0.05 h ⁻¹ , BioScope sampling
Duration	500 s	180 s	180 s	80 s
Strain	CBS 7336 (ATCC 32167)	CBS 7336 (ATCC 32167)	CBS 7336 (ATCC 32167)	CEN.PK113-7D
Measurement technique	Enzymatic assay	Enzymatic assay: metabolites, NAD(H) HPLC: adenine nucleotides	Enzymatic assay: metabolites, NAD(H)	Enzymatic assay: ATP, NADX and G6P MS: glycolytic intermediates
Intracellular variables measured	GLYCO: G6P.	GLYCO: G6P, F6P, FBP, GAP, 3PG, PEP, PYR. NUC: NAD(H), AXP (whole cell and cytoplasmic). Pi.	GLYCO: G6P, F6P. PPP: 6PG. NUC: NADP(H).	GLYCO: G6P, F6P, G1P, FBP, 2GP+3PG, PEP, PYR. NUC: ATP, NADX.
	Mashego et al. [37]	Kresnowati et al. [61]	Wu et al. [62]	Walther et al. [58]
Glucose input regime	Glucose-limited to glucose pulse (1 g L ⁻¹)	Glucose-limited to glucose pulse (1 g L ⁻¹)	Glucose-limited to glucose pulse (1 g L ⁻¹)	Trehalose-limited to glucose pulse (20 g L ⁻¹)

Experimental setup	30 °C, pH5, aerobic, D = 0.05 h ⁻¹ , BioScope sampling	30 °C, pH5, aerobic, D = 0.05 h ⁻¹ , BioScope sampling	30 °C, pH5, aerobic, D = 0.05 h ⁻¹ , direct sampling	30 °C, pH4.8, aerobic, direct sampling.
Duration	180 s	180 s	300 s	30 min
Strain	CEN.PK113-7D	CEN.PK113-7D	CEN.PK113-7D	BY4741
Measurement technique	MS	Enzymatic analysis: NAD(H) MS	MS	MS
Intracellular variables measured	GLYCO: G6P, F6P, FBP, 2/3PG, PEP, PYR. TCA: ISOCIT, FUM, MAL, AKG, SUC. PPP: 6PG. TRE: G1P, T6P, TRE. NUC: AXP, NADH:NAD ratio.	GLYCO: G6P, F6P, F1,6P2, F2,6P2, 2/3PG, PEP. TCA: ISOCIT, AKG, SUC, FUM, MAL. PPP: 6PG. TRE: G1P, T6P. NUC: AXP, NADH:NAD ratio.	GLYCO: G6P, F6P, F1,6P2, F2,6P2, 2/3PG, PEP. TCA: ISOCIT, AKG, SUC, FUM, MAL. PPP: 6PG. TRE: G1P, T6P. NUC: AXP, NADH:NAD ratio. AAs.	GLYCO: G6P, F6P, FBP, G3P, 2/3PG, PEP. TCA: AKG, MAL. PPP: 6PG, R5P, R1P. TRE: T6P, G1P. NUC: ATP, ADP, AMP, IMP, INO, HYP, GTP, GDP, GMP.
	Van Heerden et al. [63]	Suarez-Mendez et al. [49], Suarez-Mendez et al. [64]		
Glucose input regime	Glucose-limited to glucose pulse (20 g L ⁻¹)	Glucose-limited to feast–famine cycles (0.08 g L ⁻¹ max.)		
Experimental setup	30 °C, pH5, aerobic, D = 0.1 h ⁻¹ , BioScope sampling	30 °C, pH5, aerobic, D = 0.1 h ⁻¹ , direct sampling		
Duration	340 s	400 s		
Strain	CEN.PK113-7D	CEN.PK113-7D		
Measurement technique	MS; Reaction rates calculated by piecewise affine approximation (13C data)	MS; Reaction rates calculated by piecewise affine approximation (13C data)		
Intracellular variables measured	GLYCO: G6P, F6P, FBP. TRE: G1P, UDPG, T6P, TRE. PPP: 6PG. NUC: AXP, cAMP, UXP, GXP. Fluxes within glycolysis and trehalose cycle.	GLYCO: G6P, F6P, FBP, G3P, GLYC, DHAP, GAP, 2PG, 3PG, PEP, PYR. TCA: CIT, FUM, ISOCIT, MAL, AKG, SUC. PPP: 6PG, E4P, R5P, RBUP5, S7P, X5P. TRE: G1P, UDPG, T6P, TRE. NUC: AXP. Fluxes within glycolysis and trehalose cycle.		

As described in Table 1.1, previous research on understanding the metabolic effect of substrate concentration perturbations has mostly focused on glucose. However, industrially used substrates often contain different sugars besides glucose, such as sucrose, a glucose-fructose dimer, from sugarcane [10]. As these sugars have different affinities [65], or even different transport mechanisms [66], respective metabolic responses are also different [67]. The presence, concentration and nature of sugars is sensed by yeast and transduced via complex signalling pathways. Different substrates therefore triggers different signals and thereby different responses. TOR kinase and protein kinase A (PKA) are two of the main signalling cascades for sugar sensing in yeast, and regulating cell growth in response to sugar nature and abundance [68]. The G-protein-coupled receptor system (Gpr1-Gpa2) upstream of PKA pathway has very different affinities for different substrates. Its higher affinity for sucrose, but a lower affinity for fructose compared to glucose [69], results in sugar-dependent metabolic responses. Further research, especially into the effect of repetitive perturbations of different sugars, is required to evaluate both the effect of different sugar feedstock for industrial processes, as well as the effect of different sugar transport mechanisms on the metabolic regulation under dynamic substrate conditions. This will be explored in Chapter 4 of this thesis.

Identification and understanding of Key Glycolytic Properties through the Development of Metabolic Models

Many applications of metabolic modeling are based on stoichiometric genome scale models, which allow for extensive structural analysis of metabolic networks, playing an important role in model-driven metabolic engineering approaches. Nonetheless, stoichiometry alone does not describe the kinetics of metabolism and the response to glucose perturbations is a dynamic process where stoichiometry cannot explain mechanisms that act at different time scales or the appearance of metabolic bistability, among others [32,70]. As a result, kinetic models, which integrate the kinetic parameters of enzymes upon the stoichiometric network, enable to gain a deeper understanding of glycolytic properties. Thanks to the abundant data available for *S. cerevisiae*, models of the glycolytic networks have reached a high level of maturity for this organism.

The first kinetic models developed focused on understanding the metabolic response to glucose fluctuations in non-growing yeast cultures [33,34,71–77]. Most enzymatic reactions were lumped (except [71,76]) but they acknowledged the important role of the allosterically-regulated phosphofructokinase (PFK), and showed its kinetic sensitivity to different glucose, oxygen, and acetaldehyde concentrations.

Later studies focused on understanding control properties and glycolytic responses upon a single glucose perturbation experiment, based on the experimental data described in the previous section, [22,78–81]. Thanks to a progressive increase in experimental data available, more detailed models were developed [63,82–84]. Much of the focus was on understanding how mutant strains lacking a functional trehalose cycle would undergo growth arrest upon the glucose perturbation [23,26]. This was found to be due to a metabolic imbalance between upper and lower glycolysis, as ATP has to be invested first, before it can be produced downstream in the pathway [22]. Later, van Heerden et al. [63] more precisely identified the role played by the trehalose cycle in the glycolytic response and highlighted how the intracellular concentrations of metabolites at a given time point modulate metabolic responses.

In this process, glycolytic models have become more interconnected with other pathways, allowing for a more complete understanding of the metabolic responses. Teusink et al. [84] introduced glycolytic byproduct branch reactions to trehalose, glycogen, glycerol and succinate that were necessary to reproduce the experimentally observed metabolic steady state. Other works modeled pathways that are directly linked to yeast glycolysis. For instance, detailed descriptions of glycerol synthesis, the

trehalose cycle and the pentose phosphate pathway (PPP) were developed in [60,85,86], respectively. Later, a PPP model was connected to glycolysis in [87], and another model of glycolysis together with the tricarboxylic acid cycle (TCA) was developed in [35]. These networks were used to understand the control properties of glycolysis, pointing to glucose transport (GLT) and PFK for being the steps with the highest flux controlling coefficients [79,80,88–90]. For a complete overview of metabolic models developed to understand dynamic perturbations, see Table 2.

Furthermore, the regulation exerted by cofactors has gradually become more evident, resulting in a more comprehensive understanding of glycolysis. The depletion of inorganic phosphate concentration that was shown to be crucial in [63] had been overlooked in previous works where it was assumed to be constant over time. Furthermore, adenosine nucleotides were mostly assumed to be a conserved moiety [82]; but, under some experimental conditions this is not the case [58,91], which can be relevant considering that controlling enzyme PFK is allosterically regulated by ATP and AMP.

Table 1.2. Properties of *S. cerevisiae* models developed to understand dynamic glucose perturbation response: glycolysis (GLYCO), tricarboxylic acid cycle (TCA), pentose phosphate pathway (PPP), trehalose cycle (TRE). Number of ‘+’ sign according to how advantageous the property is. Cofactor conservation moieties are sumAXP and sumNADX. N/A when reactions were not modeled, or data was not shown in article. Van Eunen et al. and Kesten et al. [35,83] fitted different parameter sets to multiple data sets. Other models used a unique parameter set.

	Rizzi et al. [78]	Teusink et al. [22]	Teusink et al. [84]	van Eunen et al. [83]
Contribution to glycolytic understanding	Dynamic models can accurately describe glucose perturbation.	ATP surplus can cause the observed overactivation of initial glycolytic steps in DTps1 mutant strains.	<i>In vivo</i> behavior cannot be predicted <i>with in vitro</i> kinetics.	Implementation of allosteric regulation and <i>in vivo</i> measured parameter values is necessary to reproduce GP data.
GLYCO	Individual + branch reactions (++)	Lumped reactions (+)	Individual + branch reactions (++)	Individual + branch reactions (++)
TRE	N/A	N/A	N/A	T6P regulation (+)
TCA	Individual reactions (++)	N/A	N/A	N/A
PPP	N/A	N/A	N/A	N/A
Cofactors	Conservation moiety (+)	Conservation moiety (+)	Conservation moiety (+)	Conservation moiety (+)
Parameters	Computational, <i>in vivo</i> (++)	Computational, toy model (+)	Computational, <i>in vivo</i> (++)	Experimental and computational, <i>in vivo</i> (++)
Data	Single GP experiment (++)	Single GP, toy data (+)	SS data point (+)	Single GP experiment and multiple SS (+++)
	Smallbone et al. [82]	Van Heerden et al. [63]	Messiha et al. [87]	Kesten et al. [35]
Contribution to glycolytic understanding	Broad quantification of enzymatic kinetic constants in <i>in</i>	Glycolytic dynamics combined with cell heterogeneity	Feasibility of constructing larger network models by	Cooperativity PYK-PYR and ADH-PDH bypass play a major role in the

	<i>vivo</i> -like conditions.	determine cell fate.	merging smaller pathway models.	onset of the Crabtree effect.
GLYCO	Individual + branch reactions + isozymes (+++)	Individual + branch reactions (++)	Individual + branch reactions (++)	Individual + branch reactions (++)
TRE	N/A	T6P regulation (+)	N/A	N/A
TCA	N/A	N/A	N/A	Individual reactions (++)
PPP	N/A	N/A	Individual reactions (++)	N/A
Cofactors	Conservation moiety (+)	Conservation moiety + dynamic Pi (++)	Conservation moiety (+)	Conservation moiety (+)
Parameters	Experimental, <i>in vivo</i> (++)	Experimental, <i>in vivo</i> (++)	Experimental, <i>in vivo</i> (++)	Computational, <i>in vivo</i> (++)
Data	N/A	Single GP experiment (++)	Single GP experiment (++)	Single GP experiment (++)

From Glycolysis to Central Carbon Metabolism: Understanding Response to Glucose Perturbations Is Limited by Model Complexity

The development of kinetic models of metabolism has often been constrained to a subset of the whole network. In *S. cerevisiae* models, each next step forward in the understanding of glycolysis encountered a new limitation due to the inherent complexity of the pathway.

Models studying glycolytic oscillations or single glucose pulse experiments led to an in-depth understanding of glycolytic dynamics, but to understand central carbon metabolism performance, more pathways than only glycolysis must be considered. For the synthesis of biomass, a significant fraction of glucose-derived carbon is taken up at different points in glycolysis [92]. To account for this, a relatively simple option is to implement branches or sink reactions (developed for *Escherichia coli* in [93]). This led *S. cerevisiae* models to reproduce glycolytic steady state where imbalance had been mistakenly predicted [84]. Still, dynamic regulation of storage metabolism is more complex than a sink reaction [63,64] and later models gradually added complexity to the trehalose cycle kinetics to avoid the imbalance from happening upon dynamic perturbation [63,83]. A similar situation could happen for other closely linked pathways such as the TCA or PPP, which have mostly been lumped into a single reaction, even though a few exceptions exist [35,60,78,87].

Factors such as growth rate, compartmentation, or transport of metabolites other than glucose, regulate glycolytic responses but have barely been considered to date. First, the growth rate determines how sink reactions behave [92], but most models focus only on a unique growth rate of 0.1 h^{-1} . Since the effect of this variable has not been explicitly considered, models simulating different growth rates had no other alternative than to fit a different parameter set each time [83]. Second, compartmentation and transport reactions have barely been considered. This is for instance relevant in trehalose regulation since trehalose is known to accumulate in compartments other than the cytosol [47,94]. Third, transport of metabolites such as gases oxygen (O_2) and carbon dioxide (CO_2) could allow models to explain differences between respiratory and fermentative behavior [21,25,95] but neither of these has been implemented.

Finally, a key challenge is the representation of metabolites that are not part of the carbon flux, such as cofactors. In most models these are assumed constant or expressed with moiety conservation cycles [96], such as the sum of intracellular adenine nucleotides ($[\text{ATP}] + [\text{ADP}] + [\text{AMP}] = [\text{AXP}]$) or inorganic phosphate [83]. Nonetheless, under intense glucose perturbations, both variables behave in a dynamic

manner [36,58,78,97] and alter glycolytic responses. A well described example of this is the ATP paradox, which occurs when ATP and the sum of adenine nucleotides transiently decay [98]. Furthermore it was shown that adenine nucleotides exert allosteric regulation on the important controlling enzyme PFK [99]. Next to AxP, understanding cytosolic Pi as a dynamic variable and implementation of import from the vacuole turned out to be central in understanding the glycolytic imbalance, with the availability of Pi being essential for lower glycolysis progression via GAPDH [63].

Scope of thesis

The aim of this thesis is to deliver a validated, widely applicable model for the prediction and design of new *S. cerevisiae* processes that can reduce the bioprocess development time significantly. In the extensive literature review, following knowledge gaps were identified:

- 1) Metabolic models that cover different cultivation conditions, e.g., steady-state chemostat, single substrate pulse & repetitive substrate perturbation conditions.
- 2) Integration of kinetics with theory of resource allocation by including proteome capacity in the kinetic modelling.
- 3) Extension of the range of studied substrates for dynamic conditions beyond glucose, including other sugar substrates with different transport mechanisms.

Combining experimental and computational approaches, these are addressed in the different chapters of the thesis.

In **Chapter 2**, available metabolomics and fluxomics data from literature were combined with a large and comprehensive dynamic kinetic model of yeast central carbon metabolism, to identify and predict the minimum enzyme and parameter adjustments from steady-state to feast/famine. These predictions were subsequently compared against experimental proteome measurements to identify the difference in metabolic adaptation between steady-state and feast/famine conditions.

To gain a better understanding of the mechanisms underlying proteome allocation, in **Chapter 3**, a proteome-dependent kinetic model of central carbon metabolism was constructed and exposed to different dynamic conditions. Current proteome allocation models are able to explain (pseudo) steady-state metabolic phenotypes, but lack kinetics to explain short-term dynamics. We therefore developed a proteome-dependent kinetic model to evaluate and understand the impact of the allocation of proteins in the cellular proteome on the metabolic fitness of a yeast cell under short-term extracellular substrate dynamics. Predicted proteome allocations for feast/famine conditions were also evaluated against experimental proteome allocation data to validate the model.

The metabolic response to dynamic substrate conditions has been extensively studied for glucose, however, other sugar substrates, some of which utilize different transport mechanisms, have not been extensively studied under dynamic conditions. In **Chapter 4**, fructose, sucrose and maltose perturbations were used as carbon source in feast/famine regime in *S. cerevisiae* cultures, studying how the metabolic response upon dynamic repetitive substrate perturbations changes with different sugars and thereby transport mechanisms.

Finally, in **Chapter 5**, the main findings of this work are summarised and remaining open questions and opportunities for future research are discussed.

References

1. Rao Z, Ma Z, Shen W, Fang H, Zhuge J, Wang X: **Engineered *Saccharomyces cerevisiae* that produces 1,3-propanediol from d-glucose.** *J Appl Microbiol* 2008, **105**:1768–1776.
2. Hong K-K, Nielsen J: **Metabolic engineering of *Saccharomyces cerevisiae*: a key cell factory platform for future biorefineries.** *Cell Mol Life Sci CMLS* 2012, **69**:2671–2690.
3. Parapouli M, Vasileiadis A, Afendra A-S, Hatziloukas E: ***Saccharomyces cerevisiae* and its industrial applications.** *AIMS Microbiol* 2020, **6**:1–31.
4. Tippmann S, Scalcinati G, Siewers V, Nielsen J: **Production of farnesene and santalene by *Saccharomyces cerevisiae* using fed-batch cultivations with RQ -controlled feed: Production of Farnesene and Santalene.** *Biotechnol Bioeng* 2016, **113**:72–81.
5. Steen EJ, Chan R, Prasad N, Myers S, Petzold CJ, Redding A, Ouellet M, Keasling JD: **Metabolic engineering of *Saccharomyces cerevisiae* for the production of n-butanol.** *Microb Cell Factories* 2008, **7**:36.
6. Nielsen J, Larsson C, van Maris A, Pronk J: **Metabolic engineering of yeast for production of fuels and chemicals.** *Curr Opin Biotechnol* 2013, **24**:398–404.
7. Steensels J, Snoek T, Meersman E, Picca Nicolino M, Voordeckers K, Verstrepen KJ: **Improving industrial yeast strains: exploiting natural and artificial diversity.** *FEMS Microbiol Rev* 2014, **38**:947–995.
8. Crater JS, Lievens JC: **Scale-up of industrial microbial processes.** *FEMS Microbiol Lett* 2018, **365**:fny138.
9. Haringa C, Tang W, Deshmukh AT, Xia J, Reuss M, Heijnen JJ, Mudde RF, Noorman HJ: **Euler-Lagrange computational fluid dynamics for (bio)reactor scale down: An analysis of organism lifelines.** *Eng Life Sci* 2016, **16**:652–663.
10. Oosterhuis NMG, Kossen NWF: **Dissolved oxygen concentration profiles in a production-scale bioreactor.** *Biotechnol Bioeng* 1984, **26**:546–550.
11. Haringa C, Deshmukh AT, Mudde RF, Noorman HJ: **Euler-Lagrange analysis towards representative down-scaling of a 22 m 3 aerobic *S. cerevisiae* fermentation.** *Chem Eng Sci* 2017, **170**:653–669.
12. Enfors S-O, Jahic M, Rozkov A, Xu B, Hecker M, Jürgen B, Krüger E, Schweder T, Hamer G, O’Beirne D, et al.: **Physiological responses to mixing in large scale bioreactors.** *J Biotechnol* 2001, **85**:175–185.
13. Attfield PV: **Stress tolerance: the key to effective strains of industrial baker’s yeast.** *Nat Biotechnol* 1997, **15**:1351–1357.
14. Crick FH: **On protein synthesis.** *Symp Soc Exp Biol* 1958, **12**:138–163.
15. Kerkhoven EJ, Lahtvee P-J, Nielsen J: **Applications of computational modeling in metabolic engineering of yeast.** *FEMS Yeast Res* 2014, doi:10.1111/1567-1364.12199.
16. Lunt SY, Vander Heiden MG: **Aerobic glycolysis: meeting the metabolic requirements of cell proliferation.** *Annu Rev Cell Dev Biol* 2011, **27**:441–464.

17. Ishtar Snoek IS, Yde Steensma H: **Factors involved in anaerobic growth of *Saccharomyces cerevisiae***. *Yeast Chichester Engl* 2007, **24**:1–10.
18. Wiebe MG, Rintala E, Tamminen A, Simolin H, Salusjärvi L, Toivari M, Kokkonen JT, Kiuru J, Ketola RA, Jouhten P, et al.: **Central carbon metabolism of *Saccharomyces cerevisiae* in anaerobic, oxygen-limited and fully aerobic steady-state conditions and following a shift to anaerobic conditions**. *FEMS Yeast Res* 2008, **8**:140–154.
19. Vemuri GN, Eiteman MA, McEwen JE, Olsson L, Nielsen J: **Increasing NADH oxidation reduces overflow metabolism in *Saccharomyces cerevisiae***. *Proc Natl Acad Sci* 2007, **104**:2402–2407.
20. Nilsson A, Nielsen J: **Metabolic Trade-offs in Yeast are Caused by F1F0-ATP synthase**. *Sci Rep* 2016, **6**:22264.
21. Otterstedt K, Larsson C, Bill RM, Ståhlberg A, Boles E, Hohmann S, Gustafsson L: **Switching the mode of metabolism in the yeast *Saccharomyces cerevisiae***. *EMBO Rep* 2004, **5**:532–537.
22. Teusink B, Walsh MC, van Dam K, Westerhoff HV: **The danger of metabolic pathways with turbo design**. *Trends Biochem Sci* 1998, **23**:162–169.
23. François J, Parrou JL: **Reserve carbohydrates metabolism in the yeast *Saccharomyces cerevisiae***. *FEMS Microbiol Rev* 2001, **25**:125–145.
24. Kochanowski K, Sauer U, Noor E: **Posttranslational regulation of microbial metabolism**. *Curr Opin Microbiol* 2015, **27**:10–17.
25. Visser D, van Zuylen GA, van Dam JC, Eman MR, Proll A: **Analysis of *in vivo* kinetics of glycolysis in aerobic *Saccharomyces cerevisiae* by application of glucose and ethanol pulses**. *Biotechnol Bioeng* 2004, **88**:12.
26. Blázquez MA, Lagunas R, Gancedo C, Gancedo JM: **Trehalose-6-phosphate, a new regulator of yeast glycolysis that inhibits hexokinases**. *FEBS Lett* 1993, **329**:51–54.
27. Thevelein JM, de Winde JH: **Novel sensing mechanisms and targets for the cAMP-protein kinase A pathway in the yeast *Saccharomyces cerevisiae***. *Mol Microbiol* 1999, **33**:904–918.
28. Tripodi F, Nicastro R, Reghellin V, Coccetti P: **Post-translational modifications on yeast carbon metabolism: Regulatory mechanisms beyond transcriptional control**. *Biochim Biophys Acta BBA - Gen Subj* 2015, **1850**:620–627.
29. Muratsubaki H, Katsume T: **Distribution of hexokinase isoenzymes depending on a carbon source in *Saccharomyces cerevisiae***. *Biochem Biophys Res Commun* 1979, **86**:1030–1036.
30. Rose M, Albig W, Entian K-D: **Glucose repression in *Saccharomyces cerevisiae* is directly associated with hexose phosphorylation by hexokinases PI and PII**. *Eur J Biochem* 1991, **199**:511–518.
31. Orij R, Brul S, Smits GJ: **Intracellular pH is a tightly controlled signal in yeast**. *Biochim Biophys Acta BBA - Gen Subj* 2011, **1810**:933–944.
32. Almquist J, Cvijovic M, Hatzimanikatis V, Nielsen J, Jirstrand M: **Kinetic models in industrial biotechnology – Improving cell factory performance**. *Metab Eng* 2014, **24**:38–60.

33. Grosz R, Stephanopoulos G: **Physiological, biochemical, and mathematical studies of micro-aerobic continuous ethanol fermentation by *Saccharomyces cerevisiae*. I: Hysteresis, oscillations, and maximum specific ethanol productivities in chemostat culture.** *Biotechnol Bioeng* 1990, **36**:1006–1019.
34. Boiteux A, Busse H-G: **Circuit analysis of the oscillatory state in glycolysis.** *Biosystems* 1989, **22**:231–240.
35. Kesten D, Kummer U, Sahle S, Hübner K: **A new model for the aerobic metabolism of yeast allows the detailed analysis of the metabolic regulation during glucose pulse.** *Biophys Chem* 2015, **206**:40–57.
36. Theobald U, Mailinger W, Baltus M, Rizzi M, Reuss M: ***In vivo* analysis of metabolic dynamics in *Saccharomyces cerevisiae* : I. Experimental observations.** *Biotechnol Bioeng* 1997, **55**:305–316.
37. Mashego MR, van Gulik WM, Vinke JL, Visser D, Heijnen JJ: ***In vivo* kinetics with rapid perturbation experiments in *Saccharomyces cerevisiae* using a second-generation BioScope.** *Metab Eng* 2006, **8**:370–383.
38. Lange HC, Eman M, van Zuijlen G, Visser D, van Dam JC, Frank J, de Mattos MJT, Heijnen JJ: **Improved rapid sampling for *in vivo* kinetics of intracellular metabolites in *Saccharomyces cerevisiae*.** *Biotechnol Bioeng* 2001, **75**:406–415.
39. Buziol S, Bashir I, Baumeister A, Claaßen W, Noisommit-Rizzi N, Mailinger W, Reuss M: **New bioreactor-coupled rapid stopped-flow sampling technique for measurements of metabolite dynamics on a subsecond time scale: Bioreactor-Coupled Rapid Stopped-Flow Sampling Technique.** *Biotechnol Bioeng* 2002, **80**:632–636.
40. Schaefer U, Boos W, Takors R, Weuster-Botz D: **Automated Sampling Device for Monitoring Intracellular Metabolite Dynamics.** *Anal Biochem* 1999, **270**:88–96.
41. Canelas AB, Ras C, ten Pierick A, van Dam JC, Heijnen JJ, van Gulik WM: **Leakage-free rapid quenching technique for yeast metabolomics.** *Metabolomics* 2008, **4**:226–239.
42. Canelas AB, ten Pierick A, Ras C, Seifar RM, van Dam JC, van Gulik WM, Heijnen JJ: **Quantitative Evaluation of Intracellular Metabolite Extraction Techniques for Yeast Metabolomics.** *Anal Chem* 2009, **81**:7379–7389.
43. Douma RD, de Jonge LP, Jonker CTH, Seifar RM, Heijnen JJ, van Gulik WM: **Intracellular metabolite determination in the presence of extracellular abundance: Application to the penicillin biosynthesis pathway in *Penicillium chrysogenum*.** *Biotechnol Bioeng* 2010, **107**:105–115.
44. Tillack J, Paczia N, Nöh K, Wiechert W, Noack S: **Error Propagation Analysis for Quantitative Intracellular Metabolomics.** *Metabolites* 2012, **2**:1012–1030.
45. Mashego MR, Wu L, Van Dam JC, Ras C, Vinke JL, Van Winden WA, Van Gulik WM, Heijnen JJ: **MIRACLE: mass isotopomer ratio analysis of U-13C-labeled extracts. A new method for accurate quantification of changes in concentrations of intracellular metabolites.** *Biotechnol Bioeng* 2004, **85**:620–628.
46. Entian K-D, Kötter P: **25 Yeast Genetic Strain and Plasmid Collections.** In *Methods in Microbiology*. Elsevier; 2007:629–666.

47. Suarez-Mendez CA, Hanemaaijer M, ten Pierick A, Wolters JC, Heijnen JJ, Wahl SA: **Interaction of storage carbohydrates and other cyclic fluxes with central metabolism: A quantitative approach by non-stationary ^{13}C metabolic flux analysis.** *Metab Eng Commun* 2016, **3**:52–63.
48. Kumar K, Venkatraman V, Bruheim P: **Adaptation of central metabolite pools to variations in growth rate and cultivation conditions in *Saccharomyces cerevisiae*.** *Microb Cell Factories* 2021, **20**:64.
49. Suarez-Mendez C, Sousa A, Heijnen J, Wahl A: **Fast “Feast/Famine” Cycles for Studying Microbial Physiology Under Dynamic Conditions: A Case Study with *Saccharomyces cerevisiae*.** *Metabolites* 2014, **4**:347–372.
50. Jöers A, Tenson T: **Growth resumption from stationary phase reveals memory in *Escherichia coli* cultures.** *Sci Rep* 2016, **6**:24055.
51. Brejning J, Jespersen L: **Protein expression during lag phase and growth initiation in *Saccharomyces cerevisiae*.** *Int J Food Microbiol* 2002, **75**:27–38.
52. Abulesz E-M, Lyberatos G: **Periodic operation of a continuous culture of Baker’s yeast.** *Biotechnol Bioeng* 1989, **34**:741–749.
53. Wegner A, Meiser J, Weindl D, Hiller K: **How metabolites modulate metabolic flux.** *Curr Opin Biotechnol* 2015, **34**:16–22.
54. Pincus D, Resnekov O, Reynolds KA: **An evolution-based strategy for engineering allosteric regulation.** *Phys Biol* 2017, **14**:025002.
55. Karim MdR, Kawanago H, Kadowaki M: **A quick signal of starvation induced autophagy: Transcription versus post-translational modification of LC3.** *Anal Biochem* 2014, **465**:28–34.
56. Oliveira AP, Sauer U: **The importance of post-translational modifications in regulating *Saccharomyces cerevisiae* metabolism.** *FEMS Yeast Res* 2012, **12**:104–117.
57. Cohen AA, Geva-Zatorsky N, Eden E, Frenkel-Morgenstern M, Issaeva I, Sigal A, Milo R, Cohen-Saidon C, Liron Y, Kam Z, et al.: **Dynamic Proteomics of Individual Cancer Cells in Response to a Drug.** *Science* 2008, **322**:1511–1516.
58. Walther T, Novo M, Rössger K, Létisse F, Loret M-O, Portais J-C, François J-M: **Control of ATP homeostasis during the respiro-fermentative transition in yeast.** *Mol Syst Biol* 2010, **6**.
59. Rizzi M, Theobald U, Querfurth E, Rohrhirsch T, Baltés M, Reuss M: **In vivo investigations of glucose transport in *Saccharomyces cerevisiae*.** *Biotechnol Bioeng* 2000, **49**:316–327.
60. Vaseghi S, Baumeister A, Rizzi M, Reuss M: **In Vivo Dynamics of the Pentose Phosphate Pathway in *Saccharomyces cerevisiae*.** *Metab Eng* 1999, **1**:128–140.
61. Kresnowati MTAP, van Winden WA, Almering MJH, ten Pierick A, Ras C, Knijnenburg TA, Daran-Lapujade P, Pronk JT, Heijnen JJ, Daran JM: **When transcriptome meets metabolome: fast cellular responses of yeast to sudden relief of glucose limitation.** *Mol Syst Biol* 2006, **2**:49.
62. Wu L, van Dam J, Schipper D, Kresnowati MTAP, Proell AM, Ras C, van Winden WA, van Gulik WM, Heijnen JJ: **Short-Term Metabolome Dynamics and Carbon, Electron, and ATP Balances**

- in Chemostat-Grown *Saccharomyces cerevisiae* CEN.PK 113-7D following a Glucose Pulse. *Appl Environ Microbiol* 2006, **72**:3566–3577.
63. van Heerden JH, Wortel MT, Bruggeman FJ, Heijnen JJ, Bollen YJM, Planque R, Hulshof J, O'Toole TG, Wahl SA, Teusink B: **Lost in Transition: Start-Up of Glycolysis Yields Subpopulations of Nongrowing Cells.** *Science* 2014, **343**:1245114–1245114.
 64. Suarez-Mendez CA, Ras C, Wahl SA: **Metabolic adjustment upon repetitive substrate perturbations using dynamic ¹³C-tracing in yeast.** *Microb Cell Factories* 2017, **16**.
 65. Bisson LF, Fraenkel DG: **Involvement of kinases in glucose and fructose uptake by *Saccharomyces cerevisiae*.** *Proc Natl Acad Sci* 1983, **80**:1730–1734.
 66. Stambuk BU, Batista AS, De Araujo PS: **Kinetics of active sucrose transport in *Saccharomyces cerevisiae*.** *J Biosci Bioeng* 2000, **89**:212–214.
 67. Postma E, Verduyn C, Kuiper A, Scheffers WA, Van Dijken JP: **Substrate-accelerated death of *Saccharomyces cerevisiae* CBS 8066 under maltose stress.** *Yeast* 1990, **6**:149–158.
 68. Powers T, Dilova I, Chen C-Y, Wedaman K: **Yeast TOR Signaling: A Mechanism for Metabolic Regulation.** In *TOR*. Edited by Thomas G, Sabatini DM, Hall MN. Springer Berlin Heidelberg; 2004:39–51.
 69. Lemaire K, Van de Velde S, Van Dijck P, Thevelein JM: **Glucose and Sucrose Act as Agonist and Mannose as Antagonist Ligands of the G Protein-Coupled Receptor Gpr1 in the Yeast *Saccharomyces cerevisiae*.** *Mol Cell* 2004, **16**:293–299.
 70. Payne JL, Wagner A: **Function does not follow form in gene regulatory circuits.** *Sci Rep* 2015, **5**:13015.
 71. Hynne F, Danø S, Sørensen PG: **Full-scale model of glycolysis in *Saccharomyces cerevisiae*.** *Biophys Chem* 2001, **94**:121–163.
 72. Hess B, Boiteux A: **Mechanism of Glycolytic Oscillation in Yeast, I. Aerobic and anaerobic growth conditions for obtaining glycolytic oscillation.** *Hoppe-Seyler's Z Für Physiol Chem* 1968, **349**:1567–1574.
 73. Richter O, Betz A, Giersch C: **The response of oscillating glycolysis to perturbations in the NADH/NAD system: A comparison between experiments and a computer model.** *Biosystems* 1975, **7**:137–146.
 74. Sel'Kov EE: **Stabilization of Energy Charge, Generation of Oscillations and Multiple Steady States in Energy Metabolism as a Result of Purely Stoichiometric Regulation.** *Eur J Biochem* 1975, **59**:151–157.
 75. Richter PH, Ross J: **Oscillations and efficiency in glycolysis.** *Biophys Chem* 1980, **12**:285–297.
 76. du Preez FB, van Niekerk DD, Kooi B, Rohwer JM, Snoep JL: **From steady-state to synchronized yeast glycolytic oscillations I: model construction: Constructing a model for yeast glycolytic oscillations.** *FEBS J* 2012, **279**:2810–2822.

77. Boiteux A, Goldbeter A, Hess B: **Control of oscillating glycolysis of yeast by stochastic, periodic, and steady source of substrate: a model and experimental study.** *Proc Natl Acad Sci* 1975, **72**:3829–3833.
78. Rizzi M, Baltés M, Theobald U, Reuss M: **In vivo analysis of metabolic dynamics in *Saccharomyces cerevisiae*: II. Mathematical model.** *Biotechnol Bioeng* 1997, **55**:592–608.
79. Galazzo JL, Bailey JE: **Fermentation pathway kinetics and metabolic flux control in suspended and immobilized *Saccharomyces cerevisiae*.** *Enzyme Microb Technol* 1990, **12**:162–172.
80. Delgado J, Meruane J, Liao JC: **Experimental determination of flux control distribution in biochemical systems: In vitro model to analyze transient metabolite concentrations: FLUX CONTROL IN VITRO.** *Biotechnol Bioeng* 1993, **41**:1121–1128.
81. Rizzi M, Baltés M, Mailinger W, Theobald U, Reuss M: **Modelling of Short Term Crabtree-Effect in Baker's Yeast.** *IFAC Proc Vol* 1995, **28**:124–129.
82. Smallbone K, Messiha HL, Carroll KM, Winder CL, Malys N, Dunn WB, Murabito E, Swainston N, Dada JO, Khan F, et al.: **A model of yeast glycolysis based on a consistent kinetic characterisation of all its enzymes.** *FEBS Lett* 2013, **587**:2832–2841.
83. van Eunen K, Kiewiet JAL, Westerhoff HV, Bakker BM: **Testing Biochemistry Revisited: How In Vivo Metabolism Can Be Understood from In Vitro Enzyme Kinetics.** *PLoS Comput Biol* 2012, **8**:e1002483.
84. Teusink B, Passarge J, Reijenga CA, Esgalhado E, van der Weijden CC, Schepper M, Walsh MC, Bakker BM, van Dam K, Westerhoff HV, et al.: **Can yeast glycolysis be understood in terms of in vitro kinetics of the constituent enzymes? Testing biochemistry: Do we understand yeast glycolysis?** *Eur J Biochem* 2000, **267**:5313–5329.
85. Voit EO: **Biochemical and genomic regulation of the trehalose cycle in yeast: review of observations and canonical model analysis.** *J Theor Biol* 2003, **223**:55–78.
86. Cronwright GR, Rohwer JM, Prior BA: **Metabolic Control Analysis of Glycerol Synthesis in *Saccharomyces cerevisiae*.** *Appl Environ Microbiol* 2002, **68**:4448–4456.
87. Messiha HL, Kent E, Malys N, Carroll KM, Swainston N, Mendes P, Smallbone K: **Enzyme characterisation and kinetic modelling of the pentose phosphate pathway in yeast.** *PeerJ Prepr* 2014, doi:10.7287/peerj.preprints.146v4.
88. Liao JC, Lightfoot EN, Jolly SO, Jacobson GK: **Application of characteristic reaction paths: Rate-limiting capability of phosphofructokinase in yeast fermentation.** *Biotechnol Bioeng* 1988, **31**:855–868.
89. Cortassa S, Aon MA: **Metabolic control analysis of glycolysis and branching to ethanol production in chemostat cultures of *Saccharomyces cerevisiae* under carbon, nitrogen, or phosphate limitations.** *Enzyme Microb Technol* 1994, **16**:761–770.
90. Pritchard L, Kell DB: **Schemes of flux control in a model of *Saccharomyces cerevisiae* glycolysis: Flux control in yeast glycolysis.** *Eur J Biochem* 2002, **269**:3894–3904.

91. Bakker BM, van Eunen K, Jeneson JAL, van Riel NAW, Bruggeman FJ, Teusink B: **Systems biology from micro-organisms to human metabolic diseases: the role of detailed kinetic models.** *Biochem Soc Trans* 2010, **38**:1294–1301.
92. Canelas AB, Ras C, ten Pierick A, van Gulik WM, Heijnen JJ: **An *in vivo* data-driven framework for classification and quantification of enzyme kinetics and determination of apparent thermodynamic data.** *Metab Eng* 2011, **13**:294–306.
93. Chassagnole C, Noisommit-Rizzi N, Schmid JW, Mauch K, Reuss M: **Dynamic modeling of the central carbon metabolism of *Escherichia coli*.** *Biotechnol Bioeng* 2002, **79**:53–73.
94. Jules M, Guillou V, François J, Parrou J-L: **Two Distinct Pathways for Trehalose Assimilation in the Yeast *Saccharomyces cerevisiae*.** *Appl Environ Microbiol* 2004, **70**:2771–2778.
95. Mashego MR, Van Gulik WM, Heijnen JJ: **Metabolome dynamic responses of *Saccharomyces cerevisiae* to simultaneous rapid perturbations in external electron acceptor and electron donor: Metabolome dynamic responses of *Saccharomyces cerevisiae*.** *FEMS Yeast Res* 2007, **7**:48–66.
96. Hofmeyr J-HS, Kacser H, Merwe KJ: **Metabolic control analysis of moiety-conserved cycles.** *Eur J Biochem* 1986, **155**:631–640.
97. Aledo JC, Jiménez-Rivárez S, Cuesta-Munoz A, Romero JM: **The role of metabolic memory in the ATP paradox and energy homeostasis: Metabolic memory and the ATP paradox.** *FEBS J* 2008, **275**:5332–5342.
98. Somsen OJG, Hoeben MA, Esgalhado E, Snoep JL, Visser D, Heijden RTJM, Heijnen JJ, Westerhoff HV: **Glucose and the ATP paradox in yeast.** *Biochem J* 2000, **352**:593–599.
99. Mensonides FIC, Bakker BM, Cremazy F, Messiha HL, Mendes P, Boogerd FC, Westerhoff HV: **A new regulatory principle for *in vivo* biochemistry: Pleiotropic low affinity regulation by the adenine nucleotides - Illustrated for the glycolytic enzymes of *Saccharomyces cerevisiae*.** *FEBS Lett* 2013, **587**:2860–2867.

2

Using kinetic modelling to infer adaptations in *Saccharomyces cerevisiae* carbohydrate storage metabolism to feast/famine regimes

D. Lao-Martil, K. J. A. Verhagen, A.H. Valdeira Caetano, I.H. Pardijs,
N.A.W. van Riel and S. A. Wahl

Published in *Metabolites* (2023)

DOI: [10.3390/metabo13010088](https://doi.org/10.3390/metabo13010088)

Abstract

Microbial metabolism is strongly dependent on the environmental conditions. While these can be well controlled under laboratory conditions, large-scale bioreactors are characterized by inhomogeneities and consequently dynamic conditions for the organisms. How *Saccharomyces cerevisiae* responds to frequent perturbations in industrial bioreactors is still not understood mechanistically. To study the adjustments to prolonged dynamic conditions, experiments under a feast/famine regime were performed and analysed using modelling approaches. Multiple types of data were integrated; including quantitative metabolomics, ^{13}C incorporation and flux quantification. Kinetic metabolic modelling was applied to unravel the relevant intracellular metabolic response mechanisms. An existing model of yeast central carbon metabolism was extended, and different subsets of enzymatic kinetic constants were estimated. A novel parameter estimation pipeline based on combinatorial enzyme selection, supplemented by regularization, was developed to identify and predict the minimum enzyme and parameter adjustments from steady-state to feast famine conditions. This approach predicted proteomic changes in hexose transport and phosphorylation reactions, which was additionally confirmed by proteome measurements. Nevertheless, the modelling also hints to a yet unknown kinetic or regulation phenomenon. Some intracellular fluxes could not be reproduced by mechanistic rate laws, including hexose transport and intracellular trehalase activity during feast famine cycles.

Introduction

Saccharomyces cerevisiae, also commonly known as baker's yeast, has been used by mankind for thousands of years for the production of relevant beverages, foods and chemicals. However, despite its extensive usage in industry [1–3], scaling especially new *S. cerevisiae* production processes to industrial scale poses several interesting and fundamental challenges. Source of most challenges are spatial inhomogeneities due to mixing limitations in large-scale bioreactors leading to gradients throughout the reactor. A cell dispersed in the reactor is therefore exposed to rapid changes in its extracellular environment, which in turn will impact intracellular metabolic regulation [4,5]. Similarly, the natural habitat will commonly have oscillations resp. perturbations of environmental conditions like temperature, pH and substrate availabilities.

Although dynamic conditions are encountered for industrial applications as well as environmental habitats, many physiological studies on yeast are performed under (pseudo-) steady-state conditions. Clearly, with the vast available reference data, reliable measurements, and reproducibility, steady-state (SS) experiments are very useful in the quantification of intracellular fluxes. However, for the identification of *in vivo* kinetic parameters, dynamic metabolic experiments are required [6]. To bridge this gap, dynamic perturbation experiments can be performed, and many studies have focused on elucidating the metabolic response from single pulse (SP) experiments [6–12].

While this SP approach is very useful for the identification of kinetic parameters of networks adapted to the pre-perturbation limited steady-state, it cannot describe adaptations that may occur upon the subsequent perturbations observed under industrial conditions [5]. To emulate such an environment, a system of periodic perturbations, known as a feast/famine (FF) regime, was developed. The FF regime produces repetitive substrate concentration gradients in time, which allow for accurate and reproducible sampling of the intracellular metabolism (Figure 2.1) [13,14]. Suarez-Mendez et al. [13] used this FF setup to monitor the *in vivo* metabolic activity during FF cycles of 400 s. At this timescale it is assumed that the metabolic response within one cycle is mainly governed by metabolic interactions, as enzyme concentrations will remain basically constant during these 400 s [15]. In a FF cycle, feed was provided block-wise i.e. 20 s feeding, followed by 380 s of no feed (Figure 2.1).

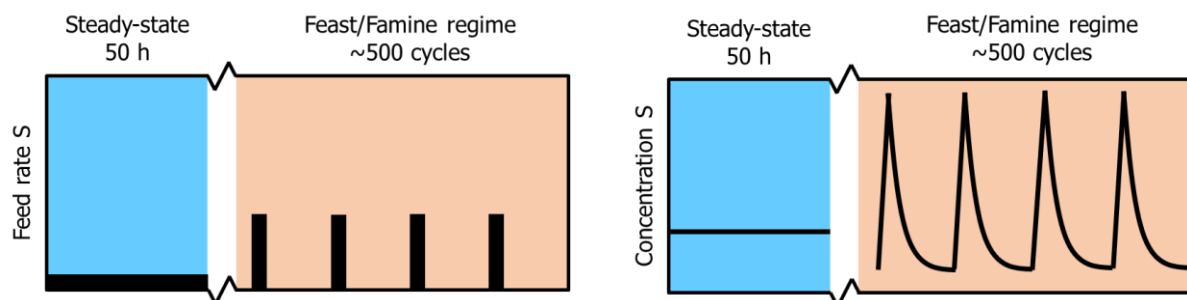


Figure 2.1. Left, the profile of the experimental feeding regime. After a chemostat phase (reference steady-state) of 50 h, a block-wise feed is applied in a 400 s cycle at the same average substrate supply and dilution rate for another 50 h (adapted from [13]). On the right, the resulting extracellular substrate concentration profile in the fermentation broth is shown.

Under such FF conditions, *S. cerevisiae* cultures show different metabolic phenotypes compared to SP or SS cultures [13]. After a pulse in FF, an increase rather than a decrease in ATP, no ethanol production, and no accumulation of glycolytic metabolites was observed. These differences in metabolic response suggest a proteomic adaptation, induced by the prior dynamic growth conditions [16–18]. Especially, translational regulation can lead to condition specific proteome compositions [19]. In fact, distinct proteome compositions have been observed under changing glucose availability conditions [20], both for sugar transporters and intracellular enzymes [21,22], and distinct isoenzymes

have different kinetic properties that can include glucose sensitivity as well [23]. However, the mechanisms behind this adaptation are not well understood.

For the identification of kinetic parameters and putative regulation mechanisms, quantitative data from different omics approaches will be required. Especially, to generate comprehensive models, in addition to intracellular concentrations, carbon tracing is required to identify bidirectional, cyclic or parallel reactions [24,25]. Work with ^{13}C -labelling indicated that storage metabolism is a major metabolic sink upon changes in the glycolytic flux, with in average 15% of the carbon flux being diverted through the glycogen and trehalose cycles [26]. This diversion of flux is in accordance with earlier studies into the importance of the trehalose cycle under SP conditions [9].

Understanding metabolism, especially under dynamic conditions requires integration of stoichiometry and enzyme kinetics. Such kinetic metabolic models have been developed for *S. cerevisiae* using either *in vitro* and *in vivo* parameters [22,27], additional allosteric regulation [28] or subpopulation dynamics [9]. Nonetheless, the conditioning of the cells was mostly at steady-state [29], leading to putative mismatches when applied to large-scale, dynamic cultivation conditions.

Under dynamic conditions, further pathways have been described to play a regulatory role – glycogen and trehalose metabolism. For both, the reaction stoichiometry is known, and *in vitro* parameters have been broadly studied [30–33], but no *in vivo* based parameter values have been derived.

Especially for cyclic pathways like the trehalose cycle, quantifying *in vivo* parameters can be challenging as both in- and outfluxes influence the concentration change and no in- or outflux is directly observable. This correlation, plus the fact that the networks are getting larger, leads to a danger posed by local minima and ill-conditioning, and “sloppy parameter” estimates [34]. To overcome this challenge and identify a minimal set of necessary changes in kinetic constants, the divide and conquer approach has been developed. Here, a decomposition of the global estimation problem into independent subproblems [35] is used. Furthermore, to consider the already known parameter values for the enzymes under study [22,29], L1 or Tikhonov regularization can favour a given parameter set, as long as experimental data is properly reproduced [36–38].

Here, we specifically studied the impact of proteome adaptation to substrate perturbations on the changed metabolic response. To this end, we have expanded upon existing state-of-the-art kinetic models, integrating both metabolomics and fluxomics as well as ^{13}C enrichment data, to evaluate which proteome changes are most relevant to explain the experimentally observed change in metabolic response.

Results and discussion

Continuous and feast famine grown cells demonstrate different enzymatic levels and metabolic responses – experimental observations

As mentioned before, cells exposed to a block-wise feeding (feast/famine conditions), showed a remarkable different response compared to glucose-limited cells from chemostat conditions. The proteome during both conditions was measured and subsequently analysed on their composition [39]. Major changes were observed within the glycolytic and transporter enzymes, specifically in the expression levels of hexose transporters (Hxt), hexokinase (Hxk) and glyceraldehyde dehydrogenase (Tdh) (Figure 2.2). The expression of hexose transporters, especially Hxt7p, has been shown to correlate with the (maximal) substrate uptake rate [40]. The observed decrease in protein concentration can be interpreted as an adaptation to limit rapid influx of glucose upon glucose pulse. In contrast, glucokinase (Glk) is slightly upregulated. Hxk is highly regulated through inhibition by T6P, however, GLK is not inhibited by trehalose-6-P (T6P) up to a level of 5 mM [41]. As such the lower concentration of Hxk in combination with the upregulation of GLK will likely result in an adaptation in the regulation of the glycolytic flux. The downregulation of upper glycolysis (Hxk), in combination with the upregulation of lower glycolysis (Tdh) may additionally allow for improvement of flux capacity through glycolysis upon glucose influx [9].

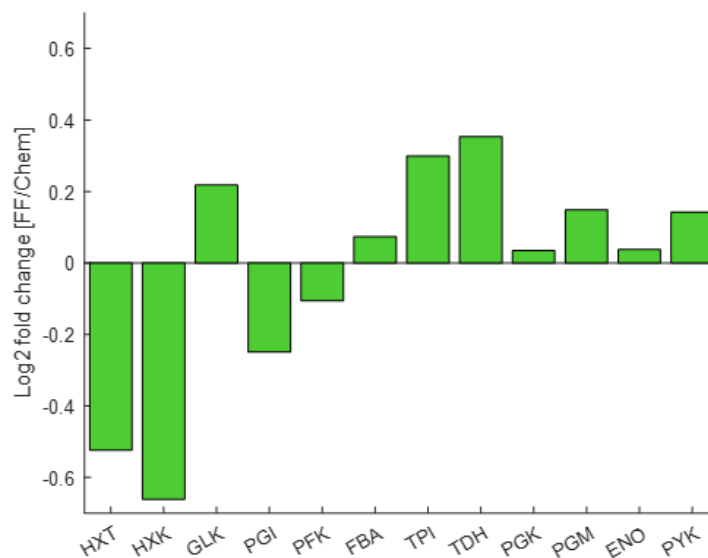


Figure 2.2. The protein concentration log₂ fold change from chemostat to feast/famine conditions of selected glycolytic and transporter proteins. Feast/famine proteome samples were taken at the end of the cycle.

Liebermeister et al. [42] observed that long-term adaptation of the proteome composition had a major influence on the adjustment of the metabolic response of the cell. In our work, to assess whether the observed metabolic response in feast/famine conditions can indeed be explained by the measured proteome changes, combinatorial enzyme selection and regularization was used to identify key parameter adaptations. Next to this, the effect of individual iso-enzymes was considered and evaluated as a factor influencing the observed metabolic response. Furthermore, the kinetics and implementation of the storage metabolism were evaluated.

Carbon storage physiology differs between continuous and feast famine limitation

A kinetic model of yeast glycolysis was previously developed to fit various SS and SP data sets [29]. For the FF conditions, the model was extended with regard to trehalose metabolism in different compartments and glycogen synthesis and degradation (Figure 2.3).

The model simulations could reproduce most of the experimental data properly, after several kinetic constants of Hxt and Hxk were estimated (this is explained in detail in the next section), but with a few exceptions (Figure 2.4A). For instance, glucose 6-phosphate (G6P) and fructose 6-phosphate (F6P) simulated concentrations were smaller, which was already documented in the original model and attributed to underdetermined phosphofructokinase (Pfk) reaction kinetics [29]. Other metabolites also deviated, such as fructose bis-phosphate (FBP), glucose 1-phosphate (G1P) or trehalose 6-phosphate (T6P). This could be explained by affinity constants undergoing changes during FF cycles, here unaccounted for. Furthermore, reaction rates, estimated from ^{13}C enrichment data, were in close agreement (Figure 2.4B), except for the maximum simulated rate for Hxt with a simulated maximum lower than observed experimentally.

In the FF simulations, the increase in residual glucose during feeding resulted in transient changes in glycolytic metabolites, which returned to the initial value by the end of the cycle (Figure 2.4C). Upper glycolysis metabolites reached their maximum concentration within 50 seconds, except glucose, due to recirculation via storage metabolism. Glycerol branch and storage kinetics followed a similar response, but with delay. Due to the slower reaction rate for enzyme GAPDH [43], the entry in lower glycolysis was delayed and BPG reaches its maximum at about 130 seconds. Nonetheless, the increase in FBP activated pyruvate kinase (Pyk), reducing concentrations of 3-phosphoglycerate (3PG), 2-phosphoglycerate (2PG) and phosphoenolpyruvate (PEP). As FBP decreased, its activation dissipated, and these lower glycolysis metabolites reached maximum concentrations in about 230 to 250 seconds of cycle. This trend is in agreement with the known allosteric regulation of FBP on Pyk [12].

Trehalose metabolic dynamics were different in FF and SP conditions. During FF, the maximum flux towards production of trehalose was less than 10% of the Hxk reaction rate, in comparison to the 30% observed in SP [9], and a part was secreted to the extracellular space, what is commonly regarded as stress protection [44,45]. Nonetheless, glycogen took up a greater portion during the feast famine regime, implying that carbon storage is predominant over the stress response by the trehalose cycle and suggesting that the cell is indeed adapted to the FF setup.

Small changes in protein expression occur between cells in a population. One way to examine the possible resulting phenotypes of the network upon perturbation is by means of ensemble modelling [46,47]. To test the robustness of the model, 10000 simulations were performed with random parameter values deviating within a range of $\pm 10\%$ from the model parameter set obtained for the best fit. The concentration and reaction rate profiles were very consistent (see appendix Concentration and reaction rate model fit), especially for reaction rates, where the relative deviation between fluxes was very small. This suggested that the model dynamics are consistent within the parameter range tested.

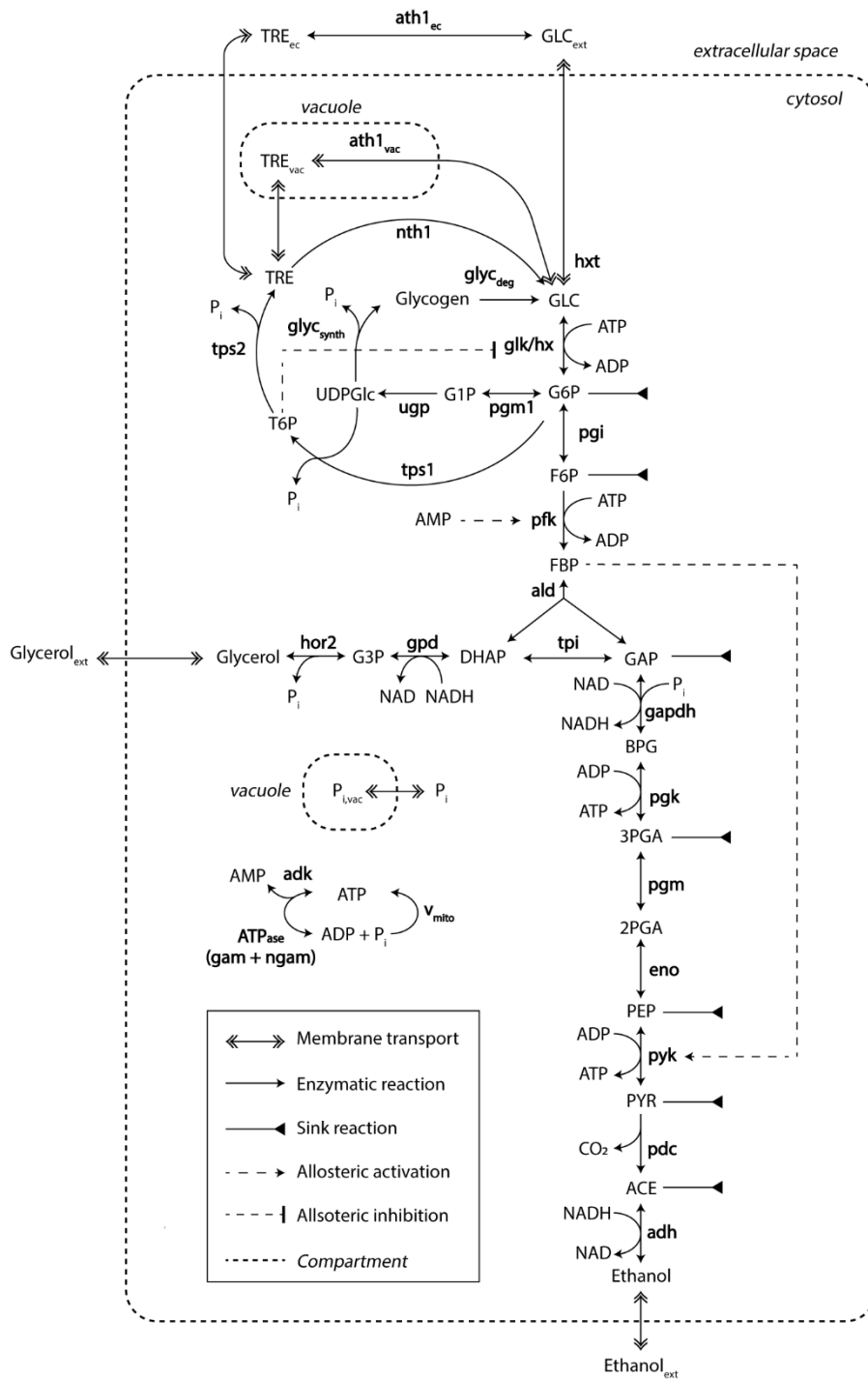


Figure 2.3. Kinetic metabolic model with a detailed description of trehalose and glycogen metabolism. Sink reactions account for fluxes towards the TCA, PPP and biomass synthesis. This model was adapted from [29]. The diagram style was adapted from van Heerden et al.[9].

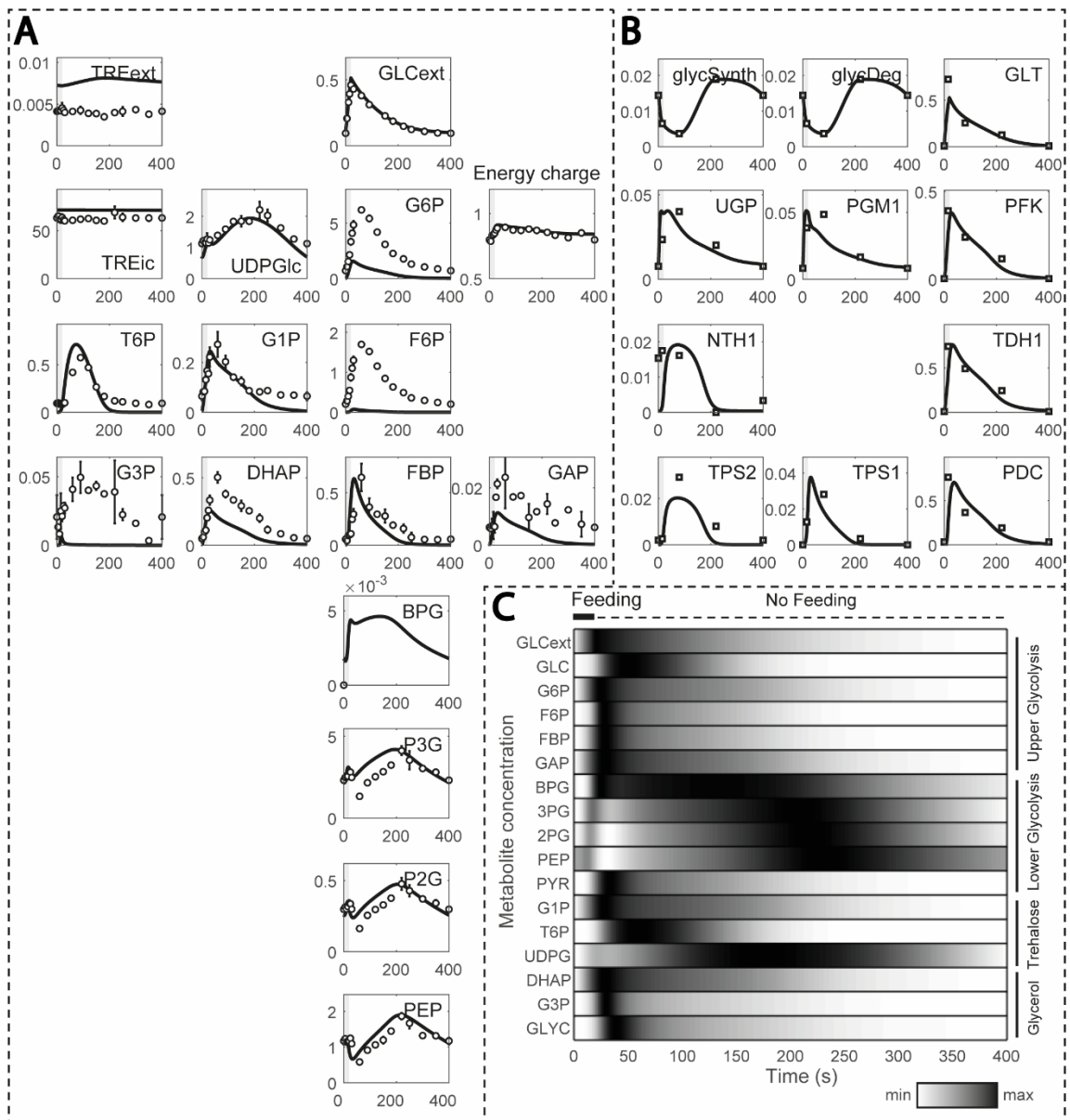


Figure 2.4. Model simulations in comparison to experimental observations. (A) Metabolite concentrations with standard deviation (average metabolite relative error of 5.5 %) and (B) reaction rates estimated from 13C enrichment data over one cycle (400 s). Metabolite concentrations and reaction rates are displayed in the y-axis (in mM and mM s⁻¹, respectively) and time in the x-axis. (C) Normalized metabolite concentrations during one feeding cycle. Darker colours indicate values closer to the maximum, while brighter ones to the minimum.

Glucose transport and phosphorylation identified as key adaptations from combinatorial parameter estimation

Glycolytic enzymes expression changed from chemostat to feast/famine conditions, most notably for Hxt and Hxk (Figure 2.2). As each iso-enzyme has specific kinetic properties, the catalytic (k_{cat}) and Michaelis-Menten (K_M) constants also differ [22]. To identify changes in kinetic parameters, parameter estimation based on the FF datasets was performed and interpreted in light of the measured proteome changes. However, estimating all kinetic parameters simultaneously can lead to multiple local minima and ill-conditioning [34]. To bypass this problem and identify which are the key parameters that change between the cells adapted to continuous and feast famine conditions respectively, we adapted the scale and setup of the parameter estimation problem. Two stages were applied (Figure 2.5): (1) Parameters were estimated for multiple combination of enzymes in parallel assays, to isolate which enzymes were key to reproduce the data properly, and (2) Regularization was implemented, i.e., parameters were re-estimated for the best selection of enzymes found and with a penalty for deviation from the reference parameter set.

In step 1 (Figure 2.5A), good fits were achieved when Hxt, Hxk/Glk and the trehalose cycle were included in the parameter estimation, suggesting that these are the relevant enzymes undergoing changes. Note that for some optimizations, the addition of an extra enzyme parameter set to the optimization resulted in a slightly higher model error. While counter-intuitive, this is likely a result of the solver using different timesteps, hitting the solver tolerance at a slightly different local minimum. In step 2, regularization was used to decide on the trade-off between model error (the normalized deviation between model prediction and data) and parameter deviation from the reference parameter set, shown in Figure 2.5B for Glk kinetics. This overcame dependencies between kinetic constants of the reaction and pointed to $K_{m,\text{GLC}}$, $K_{i,\text{T6P}}$ and V_{max} being the key parameter alterations with respect to the reference parameter set from Lao-Martil et al. [29] (Figure 2.5C). Compared with other toolboxes available to perform parameter estimation in complex kinetic metabolic models [22,34,36,48,49], this pipeline incorporates regularization for known *in vitro* parameter values into a combinatorial enzyme selection approach, with the added value that intracellular flux data is used. Flux data has been available only for a decade and few works have used it for yeast kinetic model development and validation [9,29].

As a result of this pipeline, some kinetic constant changes were suggested for the glucose transport and phosphorylation reactions (Table 2.1). For Hxt, the maximal reaction rate (V_{max}) decreased from 8.13 to 1.7 mM s^{-1} , which is actually close to the value in other published models [27,28] and consistent with the experimental Hxt concentration decrease (Figure 2.2). Changes in Hxt isoenzymes proportions could also lead to changes in affinity; *In vitro* K_M measurements have shown a high variability for the Hxt1-7p subunits [21,50]. Nevertheless, the shift in isoenzymes here did not lead to drastic changes in affinity, the K_M did only change from 1.01 to 0.90 mM.

For the hexose phosphorylation reaction, several kinetic constants changed. $K_{m,\text{glucose}}$ decreased from 0.35 to 0.11 mM, in line with the experimental increase in Glk/Hxk ratio (Figure 2.2), given that the affinity constant for glucose was found lower in Glk than Hxk both *in vitro* and *in vivo*-like conditions [22,51]. Furthermore, the T6P inhibition constant ($K_{i,\text{T6P}}$) increased from 0.0073 to 0.0183 and $K_{i,\text{T6P}}$ was also found to change between the two isoenzymes [41]. Next to these parameters, V_{max} increased from 6.25 to 15.75 mM s^{-1} , which is higher than values reported before in yeast glycolytic models [27,28]. Since the k_{cat} for Glk is much lower than for HXK [22] such increase in V_{max} was not expected.

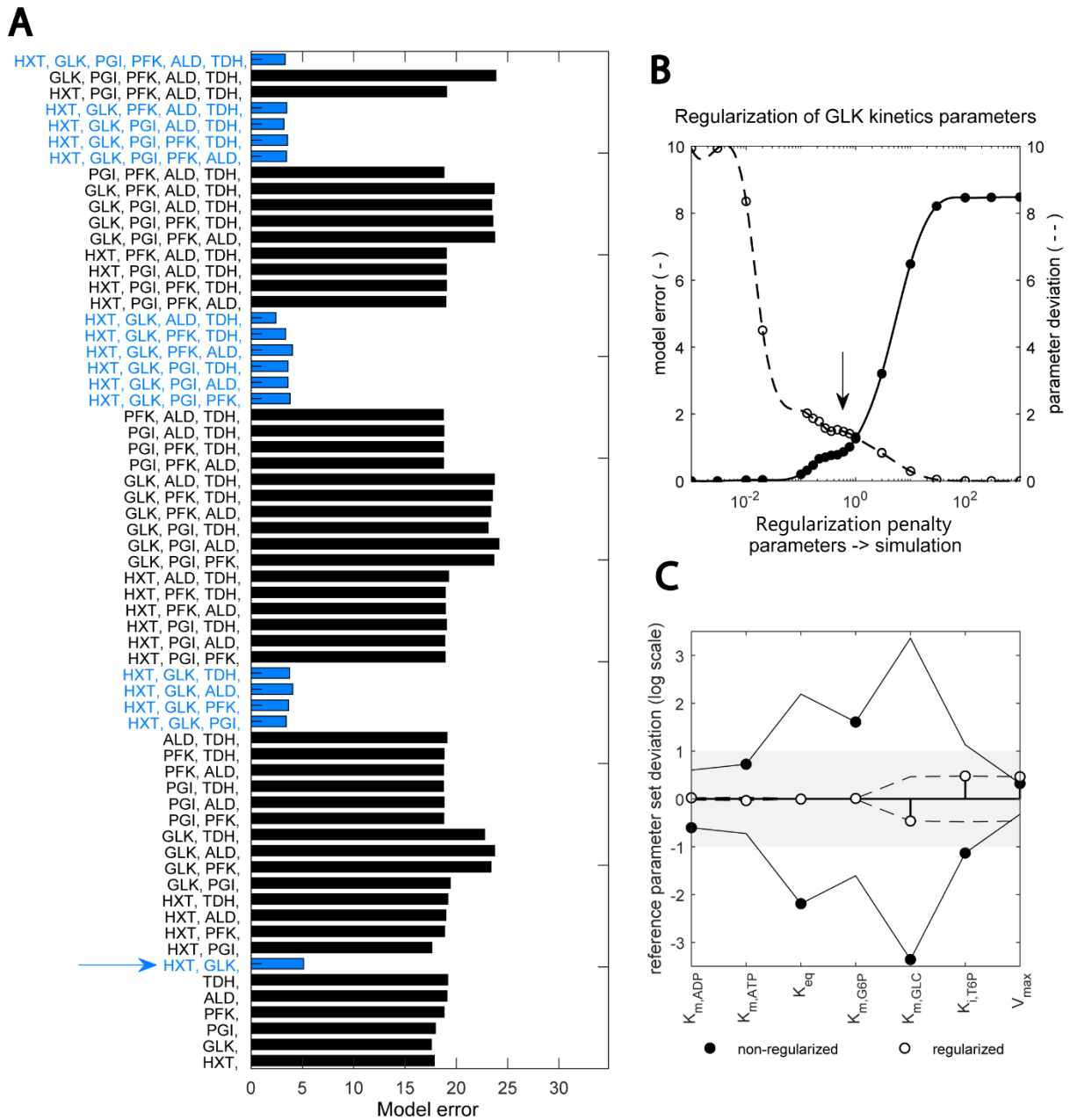


Figure 2.5. Two-step, scaled optimization approach results: (A) Fitting the data with different subsets of enzyme parameters. Bars show the error between simulation and best fit with the respective combination (upper x-axis). Blue bars highlight the combinations containing the two enzymes Hxt and Glk. Here, model error is defined as the normalized residual value between experimental and predicted data. (B) Implementation of a regularization factor on the estimation of Glk kinetic parameters. The dashed and continuous line show model and parameter error, respectively. The arrow indicates the chosen regularization factor. Parameters are regularized such that the data is still well reproduced (see appendix Figure A2.3 and A2.4). (C) Change in key Glk parameters identified upon regularization. The deviation between the estimated parameter and the initial value taken from [29] is shown in the y-axis (in logarithmic scale). Black and empty circles show the estimates prior and post regularization, when parameter dependencies are minimized. The x-axis shows specific parameters.

Outside glycolysis, changes to the model were implemented in the trehalose cycle and ATP maintenance reaction. Note, that the original model did not include glycogen metabolism, nor compartmentation of the trehalose cycle reactions. These reactions were added in this work, and trehalose cycle parameters re-estimated to account for the effect of the previously lumped reactions. Finally, the ATPase maximum reaction rate decreased to fit the adenosine nucleotide concentrations (ATP + ADP + AMP). This might be related to the fact that the initial model simulated the response to a GP of 20 g L⁻¹ of glucose [29], which is seen by the cell as a stress condition [9]. The final parameter set can be found in the appendix.

Table 2.1 Several parameters explain the adaptations in Hxt and Hxk isoenzymes. Changes in parameters in Hxt and Hxk kinetics that allow the Y3M1 model to fit the data. For the other parameters in these reactions, changes were below 5%.

Enzyme	Parameter	Units	Original model [29]	This work	Fold change	Literature
HXT	V _{max}	mM s ⁻¹	8.13	1.70	0.21	[27]: 3.67, [28]: 1.62.
	K _{m,GLC}	mM	1.01	0.90	0.90	[21]: 50-100 (low affinity HXT), 1-2 (high affinity HXT).
GLK/HXK	V _{max}	mM s ⁻¹	6.25	15.75	2.52	[27]: 3.75, [28]: 3.55-4.75, Kcat [22]: 10.2 (HXK1), 63.1 (HXK2), 0.07 (GLK).
	K _{m,GLC}	mM	0.35	0.11	0.31	[51]: 0.1 (HXK), 0.028 (GLK). [22]: 0.15 (HXK1), 0.2 (HXK2), 0.0106 (GLK).
	K _{i,T6P}	mM	0.0073	0.0183	2.51	[41]: 0.2 (HXK1), 0.04 (HXK2), 5 (GLK).

Glucose sensing influences hexose transporter kinetics during feast-famine cycles

Glucose uptake has been widely modelled as an equilibrium-driven passive transport reaction [22,27], where its kinetics are determined by isoenzyme-specific V_{max} and K_m parameters [21,50,52]. Here, we have found that these kinetics alone cannot explain the experimental data, for which a glucose sensing mechanism [23] needs to be active.

By sampling the parameter space and using passive transport reaction kinetics, we found that no combination of parameters could fit the data (Figure 2.6). Especially, none of the generated models could reproduce a net uptake reaction of almost zero at the end of the cycle (400 seconds) and reach the value of 0.72 mM s⁻¹ at 20 seconds, when the uptake rate reaches its maximum (Figure 2.6A). Since throughout the entire FF cycle the residual and maximum glucose concentration are 0.1 and 0.45 g L⁻¹, respectively, adjusting parameters to lower the effect of transmembrane glucose gradient for one also reduces for the other. Interestingly, the only way to reproduce the experimental uptake (Figure 2.6B) was by including a minimum glucose concentration term in Hxt kinetics (GLC_{ec,min} in equation 2.1). This term acted as a lower bound value above which glucose import occurs.

Suarez-Mendez et al. [13] already noticed a similar phenomenon when modelling glucose uptake dynamics. Here, we assumed that the threshold was an effect of glucose sensing under certain conditions [23]. Glucose sensing acts independently of glucose uptake [53] and is known to activate a cascade of reactions and ultimately lead to altered gene expression in yeast [54–56]. This could imply that, in line with [57], glucose sensing is observable under the FF condition, but not in the SP experiments in which residual glucose concentrations are markedly higher [9].

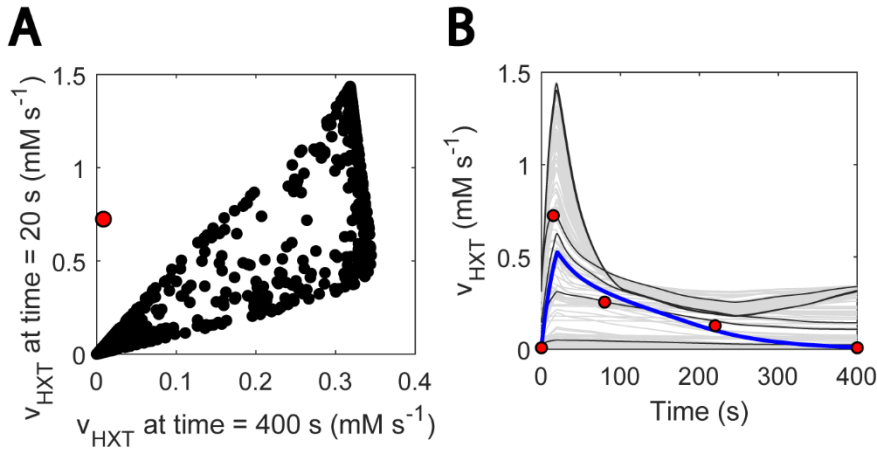


Figure 2.6. Glucose sensing is needed to explain Hxt kinetics (A) Glucose uptake rate at 20 seconds vs at 400 seconds. 20 seconds is the approximate point for the maximum reaction rate. Black data shows simulations generated with randomly generate parameter samples with passive transport kinetics, when no threshold value is considered. 1000 samples were run, within 3 orders of magnitude above and below the estimated parameters. Parameters were randomized for Hxt kinetics and external glucose concentration was fit to the experimental data. (B) Visualization of hexose transport rate during the cycle for the abovementioned models. The blue line corresponds to the simulation with the model considering glucose sensing. The grey and black coloured simulations are the ones with the generated models. Only 200 lines are displayed and some simulations are highlighted in black to ease visualization. The red dots point at the experimental data points. The effect of each parameter Hxt kinetic parameter can be found in appendix Glucose sensing.

$$v_{hxt} = v_{max} \cdot \frac{\left(GLC_{ec2} - \frac{GLC_{in}}{K_{eq}} \right)}{k_{M.GLCec} \cdot \left(1 + \frac{GLC_{ec2}}{K_{M.GLCec}} + \frac{GLC_{ic}}{K_{M.GLCic}} + 0.91 \cdot \frac{GLC_{ec2} \cdot GLC_{ic}}{K_{M.GLCec} \cdot K_{M.GLCic}} \right)},$$

where, $GLC_{ec2} = GLC_{ec} - GLC_{ec.min}$, if $GLC_{ec} > GLC_{ec.min}$

Equation 2.1. Kinetics used in the glucose transport reaction: The term in bold was added to account for the minimum glucose concentration for import to happen.

13C-labelled metabolite mass balances validate the model but suggest caveats in carbohydrate storage metabolism

Metabolic and flux profiles agreed between simulations and experimental data (Figure 2.4). Even though ¹³C isotope labelling was used in the flux estimation [26], these data have not been implemented in kinetic models yet. Here, we aimed at validating the model by implementing individual mass balances for each labelled metabolite (carbon structures) in the network. We found a considerable degree of agreement when simulating enrichment profiles. For the first 100 s of cycle, the percentage of enriched metabolite rose to about 80% for most metabolites (Fig 2.7A), to then decay as recirculation of unlabelled trehalose and glycogen became more prominent (Fig 2.7B-D).

Conversely, the model also showed limitations. Simulated enrichment of T6P decreased slower and glycolytic metabolites faster than expected during the late cycle, which could indicate that there is a surplus of glycogen recirculation in the model which was mostly unlabelled. This might be explained by the current glycogen metabolism kinetics, which were simplistic here. Small deviations from the experimental value can have a great impact on the late cycle stage, given that fluxes in the network are generally low. We initially aimed at representing glycogen synthesis and degradation as mass action or Michaelis-Menten kinetics, but unfortunately, this did not resemble the experimental reaction rates due to the high and relatively constant glycogen concentrations. Therefore, simplified phenomenological expressions were used (see appendix Rate equations). Besides glycogen metabolism, simulated enrichment of lower glycolysis metabolites was faster than expected, which could be attributed to the changes observed in other isoenzymes such as Tdh1, Tdh2 and Tdh3, which may have individual effects unaccounted for in this model.

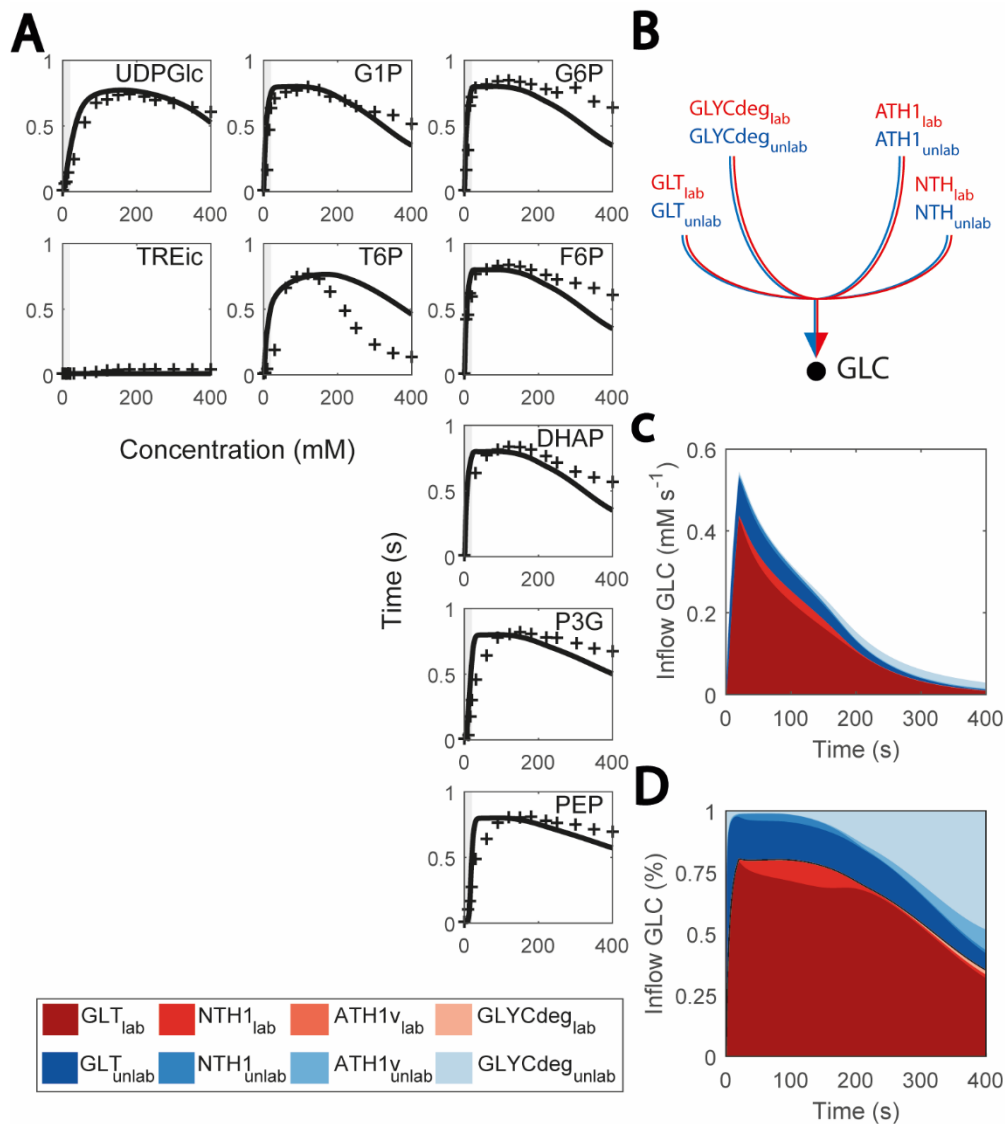


Figure 2.7. Predicted and observed ¹³C labelling enrichment during FF cycles (A) Enrichment of intracellular metabolite (%) vs time. Black lines consist of the simulations and black markers to the experimental data points. Feast phase is shaded in light grey, and famine phase has no shading. X-axis is cycle time, from 0 to 400 seconds and Y-axis is enrichment percentage, from 0 to 100%. (B) Diagram of inflow to cytosolic glucose. (C) Fluxes that positively contribute to the cytosolic glucose mass balance (mM s⁻¹) vs cycle time (s). Red coloured are labelled data, blue coloured, non-labelled. (D) Contribute of each flux to the cytosolic glucose mass balance (in %) vs cycle time (s). Red coloured are labelled data, blue coloured, non-labelled.

Identification of missing kinetic mechanisms

Another location with uncertainty is the trehalase reaction, which is carried out by an acid and neutral enzyme (Ath1p and Nth1p, respectively) [58,59] and whose *in vivo* fluxes were quantified in the FF condition in [26]. In the model simulations, Nth1p trehalase activity was reproduced, but only if cytosolic trehalose concentration was artificially low (Figure 2.8A-C) and redirected to the other compartments. Nonetheless, trehalose is expected to locate more in the cytosol than the vacuole [60]. This occurred as a result of Nth1 reaction being modelled as simple Michaelis-Menten kinetics (Figure 2.8A) [61]. To fit these kinetics, cytosolic concentrations were kept very low with a comparatively high increase during the cycle. To further doubt the current model understanding, the estimated $K_{m,TRE}$ decreased from 2.11 to 0.13 mM, but it was experimentally quantified to be 3-8 mM [62]. It is not known to us what this missing regulation could be. Post translational regulation acting on Nth1p could be a possible explanation [32,62], but new data on the state of the enzyme would be required to confirm this hypothesis.

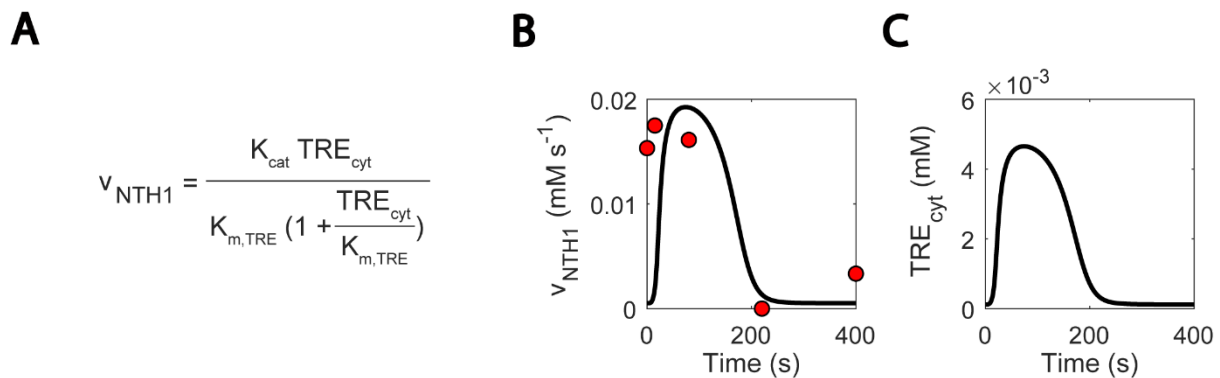


Figure 2.8. Missing regulation on Nth1p could explain excessively low simulated cytosolic trehalose concentrations (A) Nth1 reaction kinetics. (B) Nth1 reaction rate. (C) Cytosolic trehalose. Blank lines show simulations and red dots experimental data.

Conclusions and summary

In this work, we show how integrating experimental data from metabolomics, fluxomics and proteomics allowed to identify relevant mechanisms of metabolic adaptation to repetitive dynamic feast/famine conditions. Especially, testing different subsets of parameters for recalibration highlighted transporters and phosphorylation reactions as crucial for the adaptation. This *in silico* approach is comparable to the experimental approach of metabolic reverse engineering [63], but much faster and less laborious as no experiments with combinatorial genome modifications are required. The combinatorial approach can also be applied to other industrially relevant downscaling setups which are relevant to find out key parameter changes in a relatively simple manner and further optimize the bioprocess.

Furthermore, integrating ^{13}C labelling for the validation of model simulations calibrated with flux estimation reveals if the currently assumed mechanistic kinetics can sufficiently describe the intracellular flux and metabolome. Here, glucose uptake could not be explained by facilitated diffusion only (Equation 2.1), but required a minimal glucose threshold concentration (Figure 2.4). In addition, some reactions of the storage metabolism required non-mechanistic adjustments to reproduce the observed labelling enrichments.

Materials and methods

Strain and growth conditions

The haploid yeast *Saccharomyces cerevisiae* CEN PK 113-7D strain was grown at 30°C, pH 5, first in a batch phase and then in chemostat at dilution rate 0.1 h⁻¹ [13]. The repetitive feast/famine regime began after five residence times and consisted of 20/380 seconds-cycles in which a feed was added in the first 20 seconds. The concentration of this feed was 20 times higher than the one of the chemostat phase, to ensure that the culture would overall receive the same amount of glucose. Data was collected after 20 cycles. For further reference, see [13].

Experimental data sets used in this work

The experimental data sets used in this work consisted of metabolite concentrations measurements [13] and the respective calculated reaction rates [13]. Samples were collected more frequently during the feast than the famine phase, since network dynamics changed rapidly during the first. Extracellularly, concentrations were measured for carbohydrates glucose and trehalose. Intracellularly, concentrations were measured for carbohydrates involved in glycolysis, trehalose cycle, PPP, glycerol branch and the TCA cycle, and for adenosine nucleotides. Dynamic fluxes were estimated as piece-wise linear functions [64] using a consensus stoichiometric model for yeast [65]. Fluxes were estimated for glycolysis, carbohydrate storage metabolism (trehalose and glycogen cycles), PPP and the TCA cycle [26].

Model description

A kinetic model of yeast central carbon metabolism was adapted in this work [29]. The original model contained the reactions that compose glycolysis, glycerol branch, a simplified trehalose cycle. Reactions of the PPP, TCA cycle and uptake of glycolytic metabolites for biomass production were lumped as sink reactions (similar to [66]). An overview of the developed model can be seen in Figure 2.3. The following modifications were made to represent the complexity of carbon storage metabolism seen in the data and adapt the sink reactions of the TCA to the feast famine setup:

1. New reactions were added to represent a complete trehalose cycle and glycogen synthesis and degradation:
 - a. The α -glucoside transporter (Agt1p) mobilizes trehalose between the extracellular space and cytosol [32]. Its reaction rate was modelled using reversible uni-uni MM kinetics. Since the experimental data pointed at a decay in its activity during the cycle but it did not contain any information on possible inhibitors, an inhibitory effect of T6P was added as a proxy of an increasing flux through the trehalose cycle.
 - b. A vacuolar transport of trehalose was added to mobilize trehalose between cytosol and vacuole-like compartments. Even though trehalose can be compartmentalized in vesicles in the cytosol, the kinetics of the process are not known. Here it was assumed that reversible MM kinetics determine this process, as with Agt1p.
 - c. Acid trehalase (ATH1, EC 3.2.1.28) degrades trehalose to glucose. It acts in more acid environments than the cytosol such as the vacuole or the intracellular space [32], even though its location is still under debate. This reaction was modelled using irreversible MM kinetics. Similar to Agt1p, inhibition by T6P was added.
 - d. UDP-Glucose phosphorylase (UDPG, EC 2.7.7.9) carries out the reaction from G1P to UDP-glucose, which is later used as substrate for glycogen synthesis. This reaction was adapted from [61] and modelled using an ordered bi-bi mechanism.

- e. Glycogen synthesis was not modelled by enzymatic kinetics, but interpolated from the experimental data in this study, with an added UDP-glucose saturation factor.
 - f. Glycogen degradation was also interpolated from the experimental data in this study, with an added UDP-glucose saturation factor.
2. The sink reactions were optimized for chemostat growth [67] in the previous model. At a dilution rate of 0.1 h^{-1} the fluxes observed were higher than the ones seen under the FF regime. As a result, the flux simulated in FF towards the TCA cycle via the sink of pyruvate was over-estimated, resulting in a lesser flux towards the fermentative direction and more CO_2 being produced than measured. A factor was added to the reaction accounting for the pyruvate sink to reduce its flux and fit the CO_2 concentrations observed in the experiment.

In the following section, further details on model implementations are discussed.

System of ordinary differential equations

The model consists of a series of ordinary differential equation representing the mass balances for each metabolite in the model. The model contained three compartments: cytosol, vacuole, and extracellular space. The metabolites that are part of glycolysis, trehalose and glycogen cycles, glycerol branch and cofactors metabolism were located in the cytosol, trehalose could be compartmentalized in the vacuole or secreted to the extracellular space, and glucose was modelled extracellularly as well. Meanwhile the amount of carbon structure inside the cytosol depended on the inflow of glucose and outflow of the system, moiety conservations were used for cofactors as in [22]. The sum of adenosine and nicotinamide adenine nucleotides (ATP + ADP + AMP and NAD + NADH, respectively) was kept constant in the cell. The model mass balances can be seen in detail in appendix Ordinary differential equations.

Reaction rate equations

The reaction rate equations used in this model followed Michaelis Menten kinetics in most cases, but there were exceptions: Pfk kinetics are affected by multiple regulators and the alternance between tense and relaxed state [27], Pyk and Pdc follow Hill-type kinetics [28] and glucose transport occurs by facilitated diffusion (equilibrium constant equals 1). Additionally, multiple allosteric regulations occur in the network, both activation and (competitive) inhibition. Reactions were made reversible, except hydrolysis reactions, due to their remarkably negative Gibbs energy [68] and the sink reactions in the model. Reaction rates were expressed in (mM s^{-1}). The kinetic rate expressions can be seen in detail in appendix Rate equations.

Simulation setup

The simulations were performed in three steps aimed at resembling the experimental process that cells underwent in the experiments in [13]. The first step simulated a chemostat, which also served to confirm that the system remained in a physiological realistic steady state. The second step consisted of the feast famine cycles. 20 repetitive cycles were simulated in which glucose was fed for the first 20 seconds of the cycle without any outgoing flux. For the rest of the cycle, no glucose was fed, and the outgoing flux lasted until the same amount of volume increased in the first 20 seconds had been emptied, by approximately 260 seconds of cycle. Afterwards, both incoming and outgoing fluxes were kept at zero. After running for 20 cycles, the resulting simulation was compared to the experimental metabolite concentrations in reaction rates obtained in [13]. The third step concerned the simulation of the enrichment profiles reported in [26]. This extra simulation was run after the second step and 99% of the inflow of glucose was set to be fully ^{13}C labelled. All the simulations were carried with the abovementioned mechanistic model. Matlab version 9.3.0.713579, R2017b, and the ode15s solver

were used. The details of how simulations were constructed can be found in appendix Simulation setup.

Implementation of ¹³C-labeling data simulations

As described by Wahl [25], reactions of a metabolic network can only be correctly represented with mass isotopomeric models if there are no cleavage reactions present, because in the latter the position of the labelled carbon(s) is decisive to define the isotopomers of the following metabolites. In the interest of providing an accurate model without over-complicating it, the kinetic model is thus expanded to (uniformly) labelled carbon enrichment, instead of simulations of isotopic transients, as the simulation of the isotopic transients, requires determination of the distribution of the possible C-labelled atoms for every metabolite of the network and additionally accounting for the bidirectionality of reactions in the isotopomer balance equations, which is no longer as trivial as building an enrichment model [69].

For each carbon-based metabolite in the model, a mass balance was added to account for its respective ¹³C-labelled fraction. In this mass balance, the input and output reaction rates were the same than for the total metabolite concentration mass balance, but it was multiplied by the respective fraction of labelled metabolite. Whereas the metabolite total concentrations depend solely on the enzymatic rates, the metabolite labelled concentrations also depend on the fractions of other labelled metabolites (labelled concentration / total concentration) that the reactions use as substrate. Moreover, now the enzymatic fluxes need to be adjusted for reversible enzymatic reactions.

For mass balances equations of total metabolite concentrations, reversible enzymatic fluxes are defined with a positive value in one direction and negative in the reverse direction. However, to implement the mass balances equations of labelled metabolite concentrations, these are multiplied by metabolite's labelled fractions and so they need to be always positive. Thus, enzymatic fluxes that change directions during the simulation, are implemented as a forward and backwards flux. These are only used in the equations for labelled metabolite concentrations and are defined in the model with conditional statements. An example of the mass balance of labelled and unlabelled acetate can be seen below. Reaction reversibility is already accounted for in the calculation of the reaction rate:

$$\frac{d[ACE]}{dt} = +v_{PDC} - v_{ADH} - v_{sinkACE}$$

$$\frac{d[ACE^L]}{dt} = +PYR_f^L \cdot v_{PDC} - ACE_f^L \cdot v_{ADH} - ACE_f^L \cdot v_{sinkACE}$$

Where *L* refers to the labelled metabolite and *f*, the fraction of the total concentration. Enrichment simulations were performed after the 20 repetitive cycles were simulated. The experimental data consisted of percentage level of ¹³C enrichment over cycle time, obtained from [26].

Parameter values used in this work

The initial parameter values were obtained from the original model [29]. These parameter values had been fitted to experimental data (metabolomics and fluxomics) from a data at different steady states [67] and SRE [9]. A subset of the parameter values including enzymes Hxt and Glk, the ones involved in the trehalose cycle and ATPase kinetics were estimated in this work. The values of the kinetic rate expressions used in this work can be seen in appendix Parameter values.

Estimation of *in vivo* parameters

Some reactions in the model underwent changes during the feast famine cycles. For instance, the proportions of the isoenzymes Hxk/Glk changed. To account for its effect on kinetic parameters such

as K_m or k_{cat} , reaction parameters were estimated for HXT and HXK/GLK. Additionally, trehalose cycles parameters were estimated, since the final structure of the cycle was different than the initial, and the ATPase reaction rate constant needed to change as well. For initial parameter guesses, the initial parameter values from [29] were used. The nonlinear least-squares MATLAB solver `lsqnonlin` from the Optimization Toolbox, using an interior reflective Newton method [70], was used to estimate the parameters by minimizing the error between measured and simulated data during the transient experiment.

Design of the cost functions: combination of enzymes and weighting factors

Experimental quantification of isoenzymes pointed at the couple Hxk/Glk experiencing the biggest deviation prior and after the FF cycles, but minor changes were also confirmed for the other enzymes in glycolysis (Figure 2.2). Still, estimation of all the kinetic constants in glycolysis simultaneously was undesirable due to the appearance of parameter dependencies [48] which could lead to unphysiological parameter values. Therefore, to describe the changes in the experimental data with only the essential number of enzymes changing, the parameters were fitted to the data in multiple occasions. In each of those, a different selection of enzymes and cost function weighting factors was used.

- Selection of enzymes: multiple enzyme combinations were tested. These combinations contained the trehalose cycle and added different enzymes from glycolysis each time. The combination selected was the one that described experimental data properly while making physiological sense (such as including the changes in Hxk/Glk) and having the smallest number of enzymes possible. Simultaneously, random combinations of enzymes were also tested, to confirm results and give robustness to the method.
- Combination of weighting factors: it was not clear at first if it would be possible to describe all the experimental data simultaneously. For this purpose, each of the abovementioned enzyme combinations was run repeated times, each of them with a different set of weighting factors. The errors for every metabolite were normalized so that they would contribute with the same weight to the cost function. Additional weighting factors changed these weights in three orders of magnitude at most to account for differences in data error.

Design of the cost functions: regularization

Parameter dependencies could still appear for a selection of enzymes or within a single enzyme, even though less generalized than if all enzymes had been optimized together. To avoid this problem, parameters were estimated again after the previous round of data fit which was only based on selecting enzymes and cost function weights. This time L1-type regularization was implemented to force the parameter estimates closer to the initial parameter set, as long as experimental data could be properly fit, helping to identify the important parameter changes for a specific dataset [36,37]. In this way, only the necessary parameters needed to change to fit the FF data were made distinguishable. The regularization factor λ , defined by the trade-off between model error (the normalized deviation between model prediction and data) and parameter deviation from the reference parameter set, was applied to the cost function in the following manner:

$$error_{estimation} = error_{data} + error_{parameters}$$

$$error_{data} = \text{abs}(data_{simulated,normalized} - data_{experimental,normalized})$$

$$error_{parameters} = \lambda \cdot \text{abs}((parameters_{reference} - parameters_{estimated}))$$

Data availability

The raw data, scripts and presented model are available in the GitHub repository https://github.com/DavidLaoM/y3m2_ff. Python scripts and SMBL model format can be found in these respective GitHub repositories: https://github.com/DavidLaoM/y3m_py and https://github.com/DavidLaoM/y3m_xml.

References

1. Rao Z, Ma Z, Shen W, Fang H, Zhuge J, Wang X: **Engineered *Saccharomyces cerevisiae* that produces 1,3-propanediol from d-glucose.** *J Appl Microbiol* 2008, **105**:1768–1776.
2. Steen EJ, Chan R, Prasad N, Myers S, Petzold CJ, Redding A, Ouellet M, Keasling JD: **Metabolic engineering of *Saccharomyces cerevisiae* for the production of n-butanol.** *Microb Cell Factories* 2008, **7**:36.
3. Tippmann S, Scalcinati G, Siewers V, Nielsen J: **Production of farnesene and santalene by *Saccharomyces cerevisiae* using fed-batch cultivations with RQ -controlled feed: Production of Farnesene and Santalene.** *Biotechnol Bioeng* 2016, **113**:72–81.
4. Enfors S-O, Jahic M, Rozkov A, Xu B, Hecker M, Jürgen B, Krüger E, Schweder T, Hamer G, O’Beirne D, et al.: **Physiological responses to mixing in large scale bioreactors.** *J Biotechnol* 2001, **85**:175–185.
5. Haringa C, Tang W, Deshmukh AT, Xia J, Reuss M, Heijnen JJ, Mudde RF, Noorman HJ: **Euler-Lagrange computational fluid dynamics for (bio)reactor scale down: An analysis of organism lifelines.** *Eng Life Sci* 2016, **16**:652–663.
6. Theobald U, Mailinger W, Baltés M, Rizzi M, Reuss M: ***In vivo* analysis of metabolic dynamics in *Saccharomyces cerevisiae* : I. Experimental observations.** *Biotechnol Bioeng* 1997, **55**:305–316.
7. Mashego MR, van Gulik WM, Vinke JL, Visser D, Heijnen JJ: ***In vivo* kinetics with rapid perturbation experiments in *Saccharomyces cerevisiae* using a second-generation BioScope.** *Metab Eng* 2006, **8**:370–383.
8. Wu L, van Dam J, Schipper D, Kresnowati MTAP, Proell AM, Ras C, van Winden WA, van Gulik WM, Heijnen JJ: **Short-Term Metabolome Dynamics and Carbon, Electron, and ATP Balances in Chemostat-Grown *Saccharomyces cerevisiae* CEN.PK 113-7D following a Glucose Pulse.** *Appl Environ Microbiol* 2006, **72**:3566–3577.
9. van Heerden JH, Wortel MT, Bruggeman FJ, Heijnen JJ, Bollen YJM, Planque R, Hulshof J, O’Toole TG, Wahl SA, Teusink B: **Lost in Transition: Start-Up of Glycolysis Yields Subpopulations of Nongrowing Cells.** *Science* 2014, **343**:1245114–1245114.
10. Kresnowati MTAP, Suarez-Mendez CM, van Winden WA, van Gulik WM, Heijnen JJ: **Quantitative physiological study of the fast dynamics in the intracellular pH of *Saccharomyces cerevisiae* in response to glucose and ethanol pulses.** *Metab Eng* 2008, **10**:39–54.
11. Vaseghi S, Baumeister A, Rizzi M, Reuss M: ***In Vivo* Dynamics of the Pentose Phosphate Pathway in *Saccharomyces cerevisiae*.** *Metab Eng* 1999, **1**:128–140.
12. Visser D, van Zuylen GA, van Dam JC, Eman MR, Proll A: **Analysis of *in vivo* kinetics of glycolysis in aerobic *Saccharomyces cerevisiae* by application of glucose and ethanol pulses.** *Biotechnol Bioeng* 2004, **88**:12.
13. Suarez-Mendez C, Sousa A, Heijnen J, Wahl A: **Fast “Feast/Famine” Cycles for Studying Microbial Physiology Under Dynamic Conditions: A Case Study with *Saccharomyces cerevisiae*.** *Metabolites* 2014, **4**:347–372.

14. van Kleeff BHA, Kuenen JG, Heijnen JJ: **Heat Flux Measurements for the Fast Monitoring of Dynamic Responses to Glucose Additions by Yeasts That Were Subjected To Different Feeding Regimes in Continuous Culture.** *Biotechnol Prog* 1996, **12**:510–518.
15. Cruz AB, Hebly M, Duong G-H, Wahl SA, Pronk JT, Heijnen JJ, Daran-Lapujade P, van Gulik WM: **Similar temperature dependencies of glycolytic enzymes: an evolutionary adaptation to temperature dynamics?** *BMC Syst Biol* 2012, **6**:151.
16. Jöers A, Tenson T: **Growth resumption from stationary phase reveals memory in *Escherichia coli* cultures.** *Sci Rep* 2016, **6**:24055.
17. Brejning J, Jespersen L: **Protein expression during lag phase and growth initiation in *Saccharomyces cerevisiae*.** *Int J Food Microbiol* 2002, **75**:27–38.
18. Abulesz E-M, Lyberatos G: **Periodic operation of a continuous culture of Baker's yeast.** *Biotechnol Bioeng* 1989, **34**:741–749.
19. Crawford RA, Pavitt GD: **Translational regulation in response to stress in *Saccharomyces cerevisiae*.** *Yeast* 2019, **36**:5–21.
20. Elsemman IE, Rodriguez Prado A, Grigaitis P, Garcia Alborno M, Harman V, Holman SW, van Heerden J, Bruggeman FJ, Bisschops MMM, Sonnenschein N, et al.: **Whole-cell modeling in yeast predicts compartment-specific proteome constraints that drive metabolic strategies.** *Nat Commun* 2022, **13**:801.
21. Reifenberger E, Boles E, Ciriacy M: **Kinetic Characterization of Individual Hexose Transporters of *Saccharomyces Cerevisiae* and their Relation to the Triggering Mechanisms of Glucose Repression.** *Eur J Biochem* 1997, **245**:324–333.
22. Smallbone K, Messiha HL, Carroll KM, Winder CL, Malys N, Dunn WB, Murabito E, Swainston N, Dada JO, Khan F, et al.: **A model of yeast glycolysis based on a consistent kinetic characterisation of all its enzymes.** *FEBS Lett* 2013, **587**:2832–2841.
23. Youk H, van Oudenaarden A: **Growth landscape formed by perception and import of glucose in yeast.** *Nature* 2009, **462**:875–879.
24. Wiechert W, de Graaf AA: **Bidirectional reaction steps in metabolic networks: I. Modeling and simulation of carbon isotope labeling experiments.** *Biotechnol Bioeng* 1997, **55**:101–117.
25. Wahl S, Nöh K, Wiechert W: **¹³C labeling experiments at metabolic nonstationary conditions: An exploratory study.** *BMC Bioinformatics* 2008, **9**:152.
26. Suarez-Mendez CA, Ras C, Wahl SA: **Metabolic adjustment upon repetitive substrate perturbations using dynamic ¹³C-tracing in yeast.** *Microb Cell Factories* 2017, **16**.
27. Teusink B, Passarge J, Reijenga CA, Esgalhado E, van der Weijden CC, Schepper M, Walsh MC, Bakker BM, van Dam K, Westerhoff HV, et al.: **Can yeast glycolysis be understood in terms of *in vitro* kinetics of the constituent enzymes? Testing biochemistry: Do we understand yeast glycolysis?** *Eur J Biochem* 2000, **267**:5313–5329.
28. van Eunen K, Kiewiet JAL, Westerhoff HV, Bakker BM: **Testing Biochemistry Revisited: How *In Vivo* Metabolism Can Be Understood from *In Vitro* Enzyme Kinetics.** *PLoS Comput Biol* 2012, **8**:e1002483.

29. Lao-Martil D, Schmitz JPJ, Teusink B, van Riel NAW: *Glycolysis revisited: from steady state growth to glucose pulses*. *Systems Biology*; 2022.
30. François J, Parrou JL: **Reserve carbohydrates metabolism in the yeast *Saccharomyces cerevisiae***. *FEMS Microbiol Rev* 2001, **25**:125–145.
31. Wilson WA, Roach PJ, Montero M, Baroja-Fernández E, Muñoz FJ, Eydallin G, Viale AM, Pozueta-Romero J: **Regulation of glycogen metabolism in yeast and bacteria**. *FEMS Microbiol Rev* 2010, **34**:952–985.
32. Magalhães RSS, Popova B, Braus GH, Outeiro TF, Eleutherio ECA: **The trehalose protective mechanism during thermal stress in *Saccharomyces cerevisiae*: the roles of Ath1 and Agt1**. *FEMS Yeast Res* 2018, **18**.
33. Dengler L, Örd M, Schwab LM, Loog M, Ewald JC: **Regulation of trehalase activity by multi-site phosphorylation and 14-3-3 interaction**. *Sci Rep* 2021, **11**:962.
34. Villaverde AF, Fröhlich F, Weindl D, Hasenauer J, Banga JR: **Benchmarking optimization methods for parameter estimation in large kinetic models**. *Bioinformatics* 2019, **35**:830–838.
35. Kotte O, Heinemann M: **A divide-and-conquer approach to analyze underdetermined biochemical models**. *Bioinformatics* 2009, **25**:519–525.
36. Steiert B, Timmer J, Kreutz C: **L1 regularization facilitates detection of cell type-specific parameters in dynamical systems**. *Bioinforma Oxf Engl* 2016, **32**:i718–i726.
37. Dolejsch P, Hass H, Timmer J: **Extensions of ℓ_1 regularization increase detection specificity for cell-type specific parameters in dynamic models**. *BMC Bioinformatics* 2019, **20**:395.
38. van Riel NAW, Tiemann CA, Hilbers PAJ, Groen AK: **Metabolic Modeling Combined With Machine Learning Integrates Longitudinal Data and Identifies the Origin of LXR-Induced Hepatic Steatosis**. *Front Bioeng Biotechnol* 2020, **8**:536957.
39. Verhagen K, Eerden S, Wahl SA (Aljoscha): **Dataset proteomics: Analysis of change in protein expression in *Saccharomyces cerevisiae* upon shift from glucose chemostat to feast/famine regime**. 2022, doi:10.4121/19008833.
40. Kim D, Song J-Y, Hahn J-S: **Improvement of Glucose Uptake Rate and Production of Target Chemicals by Overexpressing Hexose Transporters and Transcriptional Activator Gcr1 in *Saccharomyces cerevisiae***. *Appl Environ Microbiol* 2015, **81**:8392–8401.
41. Blázquez MA, Lagunas R, Gancedo C, Gancedo JM: **Trehalose-6-phosphate, a new regulator of yeast glycolysis that inhibits hexokinases**. *FEBS Lett* 1993, **329**:51–54.
42. Liebermeister W, Noor E, Flamholz A, Davidi D, Bernhardt J, Milo R: **Visual account of protein investment in cellular functions**. *Proc Natl Acad Sci* 2014, **111**:8488–8493.
43. Van Leemputte F, Vanthienen W, Wijnants S, Van Zeebroeck G, Thevelein JM: **Aberrant Intracellular pH Regulation Limiting Glyceraldehyde-3-Phosphate Dehydrogenase Activity in the Glucose-Sensitive Yeast *tps1Δ* Mutant**. *mBio* 2020, **11**:e02199-20.
44. Wiemken A: **Trehalose in yeast, stress protectant rather than reserve carbohydrate**. *Antonie Van Leeuwenhoek* 1990, **58**:209–217.

45. Shima J, Takagi H: **Stress-tolerance of baker's-yeast (*Saccharomyces cerevisiae*) cells: stress-protective molecules and genes involved in stress tolerance.** *Biotechnol Appl Biochem* 2009, **53**:155–164.
46. Tran LM, Rizk ML, Liao JC: **Ensemble modeling of metabolic networks.** *Biophys J* 2008, **95**:5606–5617.
47. Oguz C, Watson LT, Baumann WT, Tyson JJ: **Predicting network modules of cell cycle regulators using relative protein abundance statistics.** *BMC Syst Biol* 2017, **11**:30.
48. Gábor A, Banga JR: **Robust and efficient parameter estimation in dynamic models of biological systems.** *BMC Syst Biol* 2015, **9**:74.
49. Raue A, Steiert B, Schelker M, Kreutz C, Maiwald T, Hass H, Vanlier J, Tönsing C, Adlung L, Engesser R, et al.: **Data2Dynamics: a modeling environment tailored to parameter estimation in dynamical systems.** *Bioinforma Oxf Engl* 2015, **31**:3558–3560.
50. Maier A, Völker B, Boles E, Fuhrmann GF: **Characterisation of glucose transport in *Saccharomyces cerevisiae* with plasma membrane vesicles (countertransport) and intact cells (initial uptake) with single Hxt1, Hxt2, Hxt3, Hxt4, Hxt6, Hxt7 or Gal2 transporters.** *FEMS Yeast Res* 2002, **2**:539–550.
51. Maitra PK: **A glucokinase from *Saccharomyces cerevisiae*.** *J Biol Chem* 1970, **245**:2423–2431.
52. Bosdriesz E, Wortel MT, Haanstra JR, Wagner MJ, de la Torre Cortés P, Teusink B: **Low affinity uniporter carrier proteins can increase net substrate uptake rate by reducing efflux.** *Sci Rep* 2018, **8**:5576.
53. Forsberg H, Ljungdahl PO: **Sensors of extracellular nutrients in *Saccharomyces cerevisiae*.** *Curr Genet* 2001, **40**:91–109.
54. Ravussin E: **Cellular sensors of feast and famine.** *J Clin Invest* 2002, **109**:1537–1540.
55. Conrad M, Schothorst J, Kankipati HN, Van Zeebroeck G, Rubio-Teixeira M, Thevelein JM: **Nutrient sensing and signaling in the yeast *Saccharomyces cerevisiae*.** *FEMS Microbiol Rev* 2014, **38**:254–299.
56. Rødkaer SV, Faergeman NJ: **Glucose- and nitrogen sensing and regulatory mechanisms in *Saccharomyces cerevisiae*.** *FEMS Yeast Res* 2014, **14**:683–696.
57. Karhumaa K, Wu B, Kielland-Brandt MC: **Conditions with high intracellular glucose inhibit sensing through glucose sensor Snf3 in *Saccharomyces cerevisiae*.** *J Cell Biochem* 2010, **110**:920–925.
58. Lillie SH, Pringle JR: **Reserve carbohydrate metabolism in *Saccharomyces cerevisiae*: responses to nutrient limitation.** *J Bacteriol* 1980, **143**:1384–1394.
59. Garre E, Matallana E: **The three trehalases Nth1p, Nth2p and Ath1p participate in the mobilization of intracellular trehalose required for recovery from saline stress in *Saccharomyces cerevisiae*.** *Microbiol Read Engl* 2009, **155**:3092–3099.
60. Keller F, Schellenberg M, Wiemken A: **Localization of trehalase in vacuoles and of trehalose in the cytosol of yeast (*Saccharomyces cerevisiae*).** *Arch Microbiol* 1982, **131**:298–301.

61. Smallbone K, Malys N, Messiha HL, Wishart JA, Simeonidis E: **Building a Kinetic Model of Trehalose Biosynthesis in *Saccharomyces cerevisiae***. In *Methods in Enzymology*. . Elsevier; 2011:355–370.
62. Veisova D, Macakova E, Rezabkova L, Sulc M, Vacha P, Sychrova H, Obsil T, Obsilova V: **Role of individual phosphorylation sites for the 14-3-3-protein-dependent activation of yeast neutral trehalase Nth1**. *Biochem J* 2012, **443**:663–670.
63. Mans R, Daran J-MG, Pronk JT: **Under pressure: evolutionary engineering of yeast strains for improved performance in fuels and chemicals production**. *Curr Opin Biotechnol* 2018, **50**:47–56.
64. de Jonge L, Buijs NAA, Heijnen JJ, van Gulik WM, Abate A, Wahl SA: **Flux response of glycolysis and storage metabolism during rapid feast/famine conditions in *Penicillium chrysogenum* using dynamic ¹³C labeling**. *Biotechnol J* 2014, **9**:372–385.
65. Herrgård MJ, Swainston N, Dobson P, Dunn WB, Arga KY, Arvas M, Blüthgen N, Borger S, Costenoble R, Heinemann M, et al.: **A consensus yeast metabolic network reconstruction obtained from a community approach to systems biology**. *Nat Biotechnol* 2008, **26**:1155–1160.
66. Chassagnole C, Noisommit-Rizzi N, Schmid JW, Mauch K, Reuss M: **Dynamic modeling of the central carbon metabolism of *Escherichia coli***. *Biotechnol Bioeng* 2002, **79**:53–73.
67. Canelas AB, Ras C, ten Pierick A, van Gulik WM, Heijnen JJ: **An *in vivo* data-driven framework for classification and quantification of enzyme kinetics and determination of apparent thermodynamic data**. *Metab Eng* 2011, **13**:294–306.
68. Bar-Even A, Flamholz A, Noor E, Milo R: **Rethinking glycolysis: on the biochemical logic of metabolic pathways**. *Nat Chem Biol* 2012, **8**:509–517.
69. Wahl SA, Dauner M, Wiechert W: **New tools for mass isotopomer data evaluation in ¹³C flux analysis: Mass isotope correction, data consistency checking, and precursor relationships**. *Biotechnol Bioeng* 2004, **85**:259–268.
70. Coleman TF, Li Y: **A Reflective Newton Method for Minimizing a Quadratic Function Subject to Bounds on Some of the Variables**. *SIAM J Optim* 1996, **6**:1040–1058.
71. Mittenbühler K, Holzer H: **Purification and characterization of acid trehalase from the yeast *suc2* mutant**. *J Biol Chem* 1988, **263**:8537–8543.
72. Stambuk BU, Panek AD, Crowe JH, Crowe LM, de Araujo PS: **Expression of high-affinity trehalose–H⁺ symport in *Saccharomyces cerevisiae***. *Biochim Biophys Acta BBA - Gen Subj* 1998, **1379**:118–128.
73. Postma E, Verduyn C, Kuiper A, Scheffers WA, Van Dijken JP: **Substrate-accelerated death of *Saccharomyces cerevisiae* CBS 8066 under maltose stress**. *Yeast* 1990, **6**:149–158.
74. Martinoia E, Massonneau A, Frangne N: **Transport processes of solutes across the vacuolar membrane of higher plants**. *Plant Cell Physiol* 2000, **41**:1175–1186.

Appendix

Ordinary differential equations

Some mass balances were added or edited to those used in the original model [29]:

$$\frac{dGLCi}{dt} = -v_{GLK} + v_{GLT} + 2 v_{NTH1} + 2 v_{ATH1vac} + v_{glcDeg}$$

$$\frac{dUDPGlc}{dt} = v_{UGP} - v_{TPS1} - v_{glycSynth}$$

$$\frac{dTRE}{dt} = v_{TPS2} - v_{NTH1} - v_{AGT1} - v_{vacuoleT}$$

$$\frac{dTREec}{dt} = -\frac{Fout \cdot TREec}{Vbroth} + v_{AGT1} \cdot bmf \cdot C_X - v_{ATH1ec} \cdot bmf \cdot C_X$$

$$\frac{dTREvac}{dt} = -v_{ATH1vac} + v_{vacuoleT}$$

$$\frac{dGlycogen}{dt} = v_{glycSynth} - v_{glycDeg}$$

$$\frac{dETOHec}{dt} = v_{ETOHtransport} \cdot bmf \cdot C_X - ETOHec \cdot \frac{Fout}{Vbroth}$$

$$\frac{dGLYCec}{dt} = v_{GLYCEROLtransport} \cdot bmf \cdot C_X - GLYCec \cdot \frac{Fout}{Vbroth}$$

$$\frac{dGLCec}{dt} = GLCin \cdot \frac{Fin}{Vbroth} - GLCec \cdot \frac{Fout}{Vbroth} - v_{GLT} \cdot bmf \cdot C_X + v_{SUC} + 2 v_{ATH1ec} \cdot bmf \cdot C_X$$

Rate equations

The following reaction rates were added to those used in the original model [29]:

$$v_{ATH} = \frac{ATH \cdot K_{cat} \cdot TRE}{K_{M,TRE} \cdot \left(\frac{TRE}{K_{M,TRE}} + 1 \right)}$$

$$v_{AGT1} = \frac{AGT1 \cdot K_{cat} \cdot \left(TRE_{cyt} - \frac{TRE_{vac}}{K_{eq}} \right)}{K_{M,TRE} \cdot \left(\frac{TRE_{ec}}{K_{M,TRE}} + \frac{TRE_{cyt}}{K_{M,TRE}} + \frac{UDPGlc}{K_{M,UDPGlc}} + 1 \right)}$$

$$v_{vacuoleT} = \frac{V_{max} \cdot \left(TRE_{cyt} - \frac{TRE_{vac}}{K_{eq}} \right)}{K_{M,TRE} \cdot \left(\frac{TRE_{vac}}{K_{M,TRE}} + \frac{TRE_{cyt}}{K_{M,TRE}} + 1 \right)}$$

Glycogen synthesis and degradation were directly interpolated from the data, with the additions of a saturation component, to avoid that it becomes a constraint in the system, especially when fluxes were overall small.

$$v_{glyc,synthesis} = \frac{v_{glyc,synthesis,interpolated} \cdot UDPGlc}{UDPGlc + 1E^{-4}}$$

$$v_{glyc,degradation} = \frac{v_{glyc,degradation,interpolated} \cdot Glycogen}{Glycogen + 1E^{-4}}$$

Glucose sensing

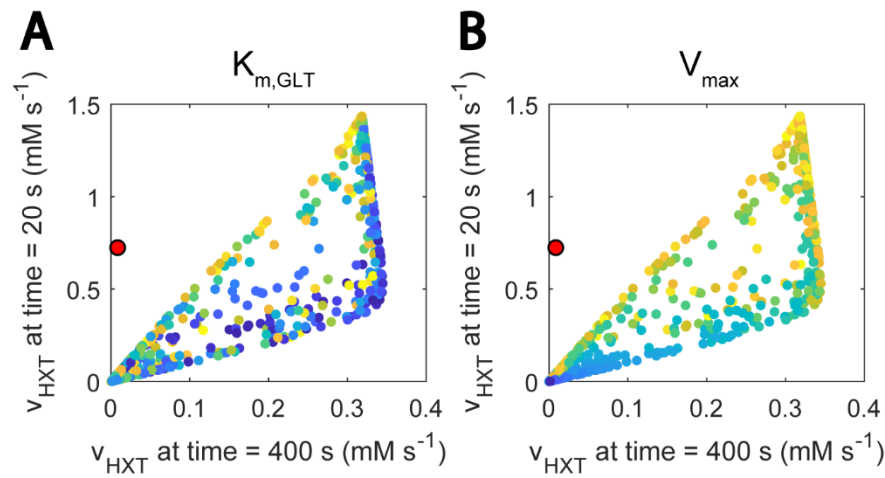


Figure A2.1. Glucose sensing is needed to explain Hxt kinetics: Individual parameter effect. Glucose uptake rate at 400 vs at 20 second. Blue and yellow colours show smaller and bigger parameter values. 1000 samples were run, within 3 orders of magnitude above and below the estimated parameters. Parameters were randomized for Hxt kinetics and external glucose concentration was fit to the experimental data. The red dot is the experimental data point.

Concentration and reaction rate model fit

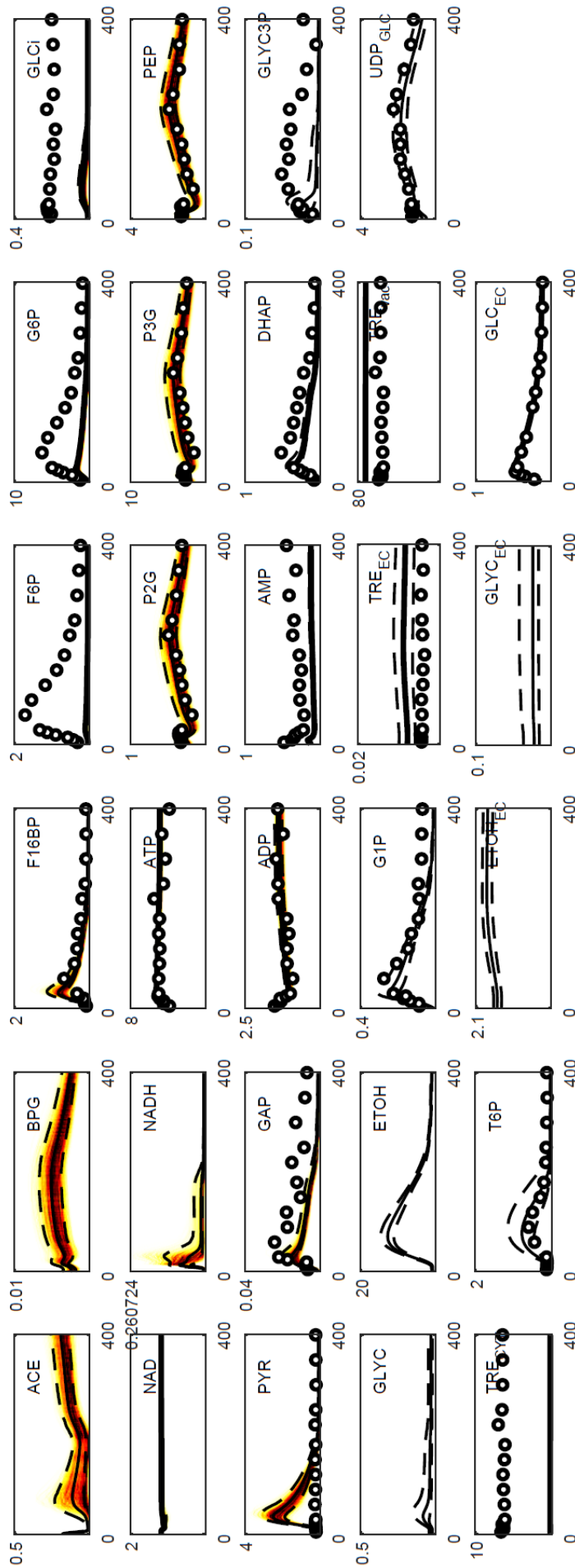


Figure A2.2. Simulation of metabolic concentrations is robust to parameter changes within 10% of their estimated value. Line plot of 10,000 model samples. Darker areas point at more dense regions. Models were sampled by adding random noise to all the parameters in the network, within a range of $\pm 10\%$ of the original parameter value.

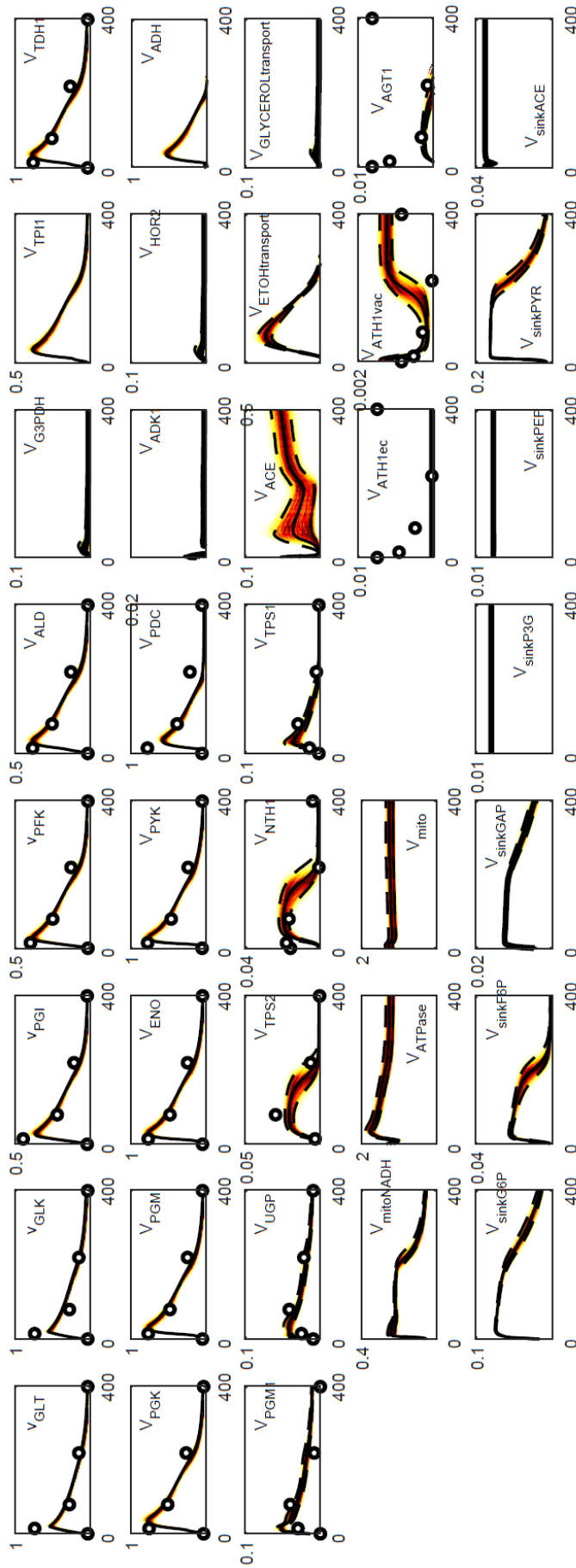


Figure A2.3 Simulation of reaction rates is robust to parameter changes within 10% of their estimated value. Line plot of 10.000 model samples. Darker areas point at more dense regions. Models were sampled by adding random noise to all the parameters in the network, within a range of $\pm 10\%$ of the original parameter value.

Parameter values

Several parameters from the original model were adjusted and others added:

Table A2.1. Re-estimated parameters.

Enzyme	Name	Original model [29]	This work	Reference	Units	Source
HXK	$K_{M,GLC}$	0.35	0.11	0.08	mM	[27]
HXK	$K_{i,T6P}$	0.01	0.0183	0.2	mM	[22]
HXK	K_{cat}	6.25	15.75	0.95	s^{-1}	[28]
GLT	$K_{M,Glc}$	1.01	0.90	1.1918	mM	[27]
GLT	V_{max}	8.13	1.70	0.734	$mM s^{-1}$	[28]
PGM1	K_{eq}	21.40	4.08	0.167		[61]
PGM1	$K_{M,G1P}$	0.07	0.1316	0.023	mM	[61]
PGM1	$K_{M,G6P}$	0.03	0.0154	0.05	mM	[61]
PGM1	K_{cat}	8.46	4.1018	100	s^{-1}	[61]
TPS2	$K_{M,T6P}$	0.37	0.2427	0.5	mM	[61]
TPS2	K_{cat}	28.41	20.752	81.45	s^{-1}	[61]
TPS2	$K_{M,Pi}$	0.70	0.6991	1	mM	This study
NTH1	$K_{M,TRE}$	2.11	0.13	2.99	mM	[61]
NTH1	K_{cat}	4.51	284.25	100	s^{-1}	[61]
TPS1	$K_{M,G6P}$	4.54	0.4422	3.8	mM	[61]
TPS1	$K_{M,UDPGlc}$	0.13	0.11	0.886	mM	[61]
TPS1	K_{cat}	9616.42	1.37E+04	1000	s^{-1}	[61]
TPS1	$K_{i,Pi}$	0.79	0.2863	1	mM	This study
TPS1	$K_{M,F6P}$	1.56	0.7116	1	mM	This study
UGP	K_{UTP}		0.9797	0.11	mM	[61]
UGP	$K_{i,UTP}$		0.2387	0.11	mM	[61]
UGP	K_{G1P}		0.1321	0.32	mM	[61]
UGP	$K_{i,UDPGlc}$		0.0163	0.035	mM	[61]

<i>UGP</i>	K_{cat}	1442.7	1000	s^{-1}	This work
<i>ATH1</i>	K_{TRE}	6.16E+03	4.7	mM	[71]
<i>ATH1</i>	K_{cat}	546.77	4.21E+05	s^{-1}	[71]
<i>ATH1</i>	$[ATH1]_{ec}$	0.0018		mM	This work
<i>ATH1</i>	$[ATH1]_{vac}$	0.000196		mM	This work
<i>AGT1</i>	$K_{TRE,ec}$	0.6846	4	mM	[72]
<i>AGT1</i>	K_{cat}	476.46	1.74E+04	s^{-1}	[73]
<i>AGT1</i>	$K_{TRE,ic}$	0.0855	4	mM	[72]
<i>AGT1</i>	K_{eq}	7.3	1000		This work
<i>AGT1</i>	$K_{i,UDPG}$	18.09	1	mM	This work
<i>AGT1</i>	$[AGT]$	6.67E-05		mM	This work
<i>vacT</i>	V_{max}	6.67E-05	1.00E-04	mM s^{-1}	This work
<i>vacT</i>	K_{TRE}	2.83	20	mM	[74]
<i>vacT</i>	K_{eq}	1	1		This work

In addition, several parameters were considered for the extracellular mass balances:

Table A2.2. Extracellular parameters. The missing values depend on the feeding (see appendix Simulation setup)

Parameter	Name	Value	Units
<i>Biomass concentration</i>	C_X	3.639	$g_{DW} L_{bioreactor}^{-1}$
<i>Biomass volume fraction</i>	bmf	0.002	$L_{bioreactor} g_{DW}^{-1}$
<i>Incoming flux</i>	Fin		$L_{bioreactor} s^{-1}$
<i>Outgoing flux</i>	$Fout$		$L_{bioreactor} s^{-1}$
<i>Broth volume</i>	$Vbroth$	3.894	$L_{bioreactor}$

Model fit

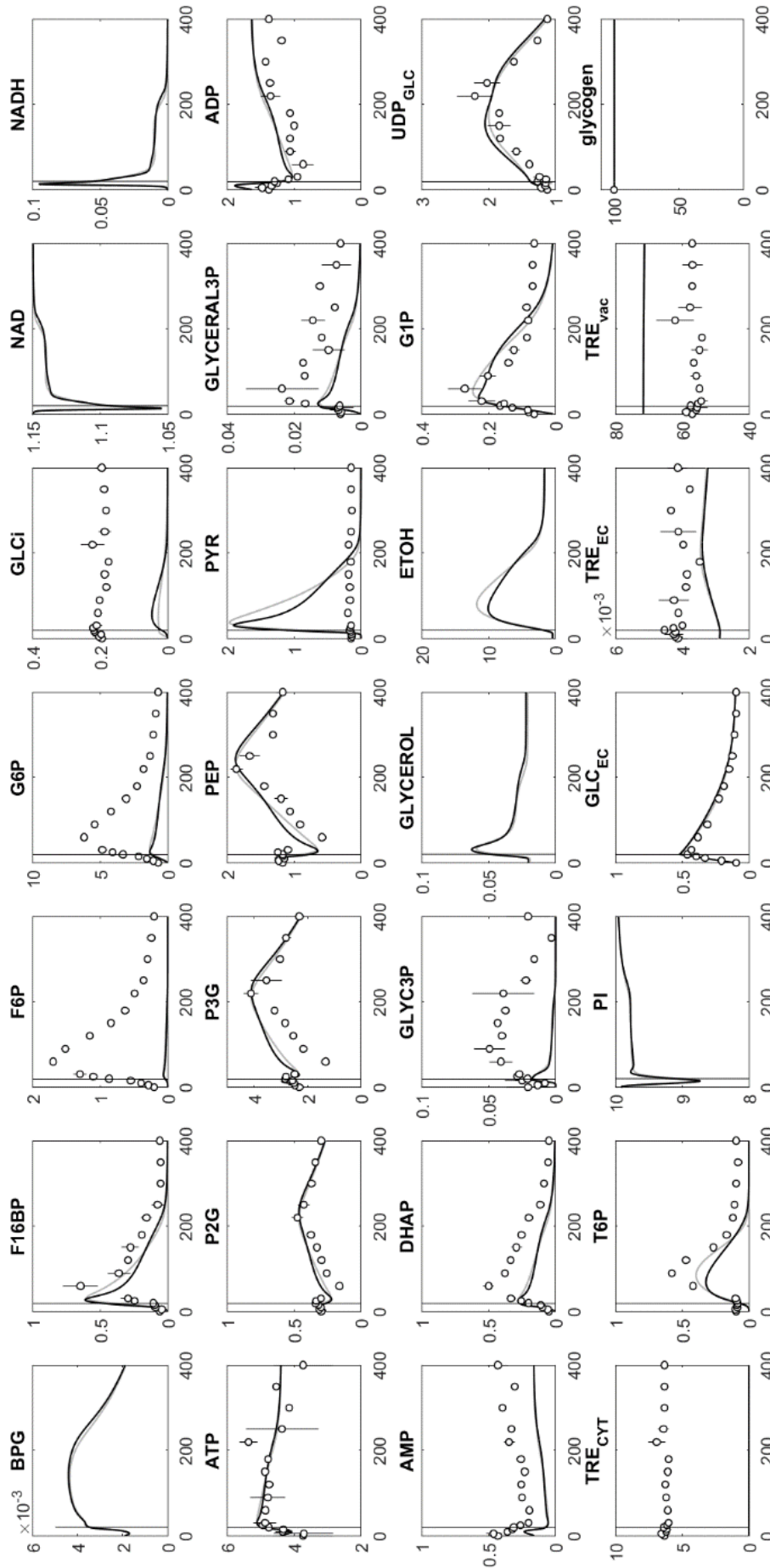


Figure A2.3. Metabolite concentrations (mM) over time (s). Model fit. (Grey) Non-regularized, (black) regularized and (black dots) experimental data. Intracellular trehalose was experimentally measured and a 9:1 distribution ratio was assumed for the vacuolar and cytosolic concentrations.

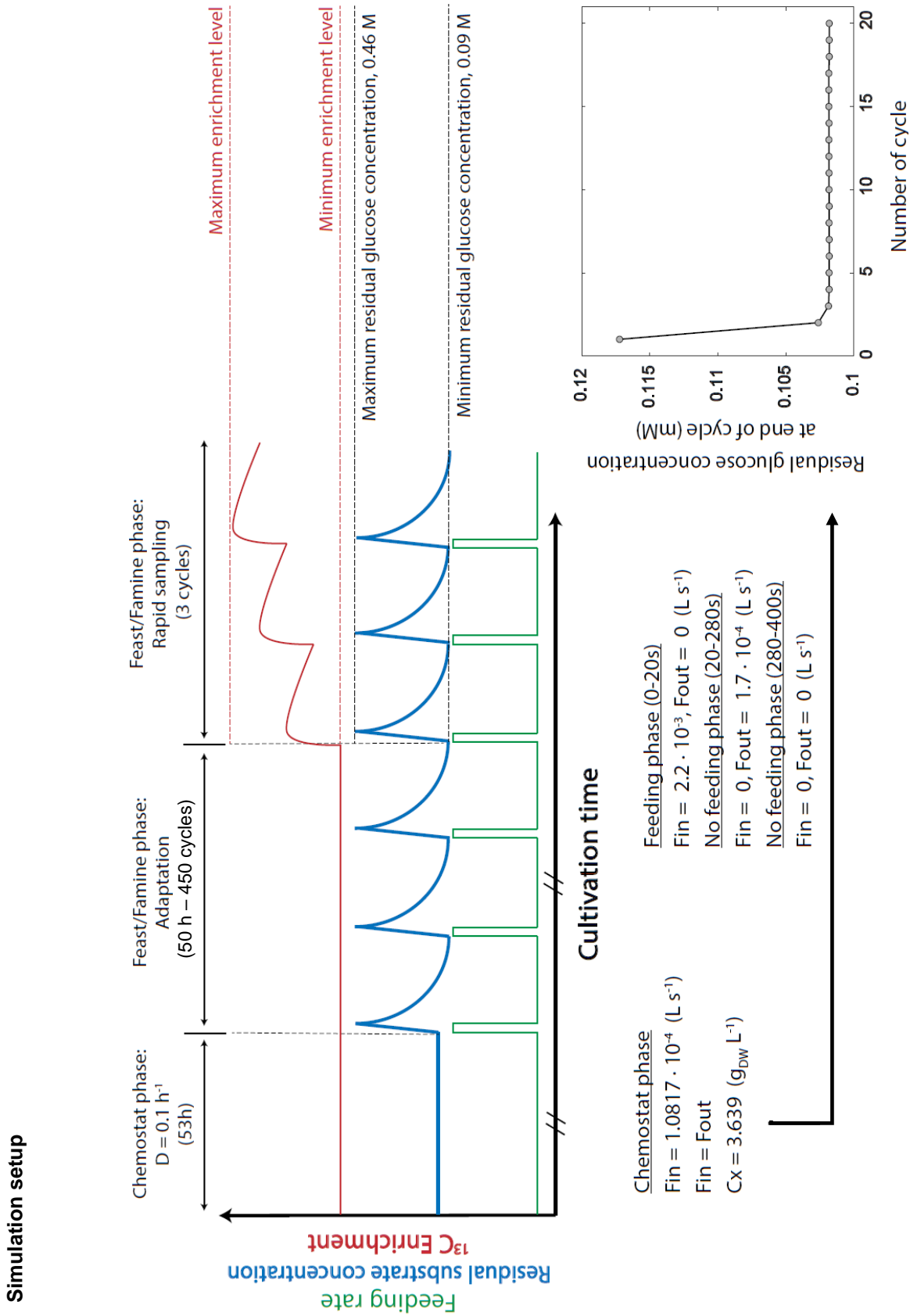


Figure A2.6. Graphical representation of the experimental setup for the repeated cycles. The parameter values shown where used in the model simulations.

3

Predicting metabolic adaptation under dynamic substrate conditions using a resource dependent kinetic model: A case study using *Saccharomyces cerevisiae*

K. J. A. Verhagen, S. A. Eerden, B. J. Sikkema and S. A. Wahl

Published in *Frontiers in Molecular Biosciences* (2022)

DOI: 10.3389/fmolb.2022.863470

Abstract

Exposed to changes in their environment, microorganisms will adapt their phenotype, including metabolism to ensure survival. To understand the adaptation principles, resource allocation based approaches were successfully applied to predict an optimal proteome allocation under (quasi) steady-state conditions. Nevertheless, for a general, dynamic environment, enzyme kinetics will have to be taken into account which were not included in the linear resource allocation models. To this end, a resource dependent kinetic model was developed and applied to the model organism *Saccharomyces cerevisiae* by combining published kinetic models and calibrating the model parameters to published proteomics and fluxomics datasets. Using this approach, we were able to predict specific proteomes at different dilution rates under chemostat conditions. Interestingly, the approach suggests that the occurrence of aerobic fermentation (Crabtree effect) in *S. cerevisiae* is not caused by space limitation in the total proteome, but rather an effect of constraints on the mitochondria. When exposing the approach to repetitive, dynamic substrate conditions, the proteome space was allocated differently. Less space was predicted to be available for non-essential enzymes (reserve space). This could indicate that the perceived 'overcapacity' present in experimentally measured proteomes may very likely serve a purpose in increasing the robustness of a cell to dynamic conditions. Especially, an increase of proteome space for the growth reaction as well as of the trehalose cycle was shown to be essential in providing robustness upon stronger substrate perturbations. The model predictions of proteome adaptation to dynamic conditions were additionally evaluated against respective experimentally measured proteomes, which highlighted the model's ability to accurately predict major proteome adaptation trends. This proof of principle for the approach can be extended to production organisms and applied for both understanding metabolic adaptation, and improving industrial process design.

Introduction

The ability of microorganisms to adapt to changing extracellular environmental conditions is essential for their survival and leads to metabolic robustness and competitive fitness [1,2]. Depending on the environmental conditions, different metabolic functions and/or flux distributions are needed that require a different proteome composition [3]. The proteome adaptation is triggered by not yet fully unraveled protein signaling cascades and further mechanisms [4]. An intuitive example of this adaptation is described for *Saccharomyces cerevisiae* (*S. cerevisiae*), when shifting from growth under minimal to rich medium conditions: Cells grown under rich nutrient conditions require a significantly smaller proteome fraction for biosynthesis genes [5–7] compared to cells grown in minimal medium, where amino acids and other biomass precursors are not present but have to be synthesized from glucose.

On the other hand, next to optimization of proteome resources, cells do maintain metabolic fitness and/or robustness [8]. Especially under substrate limiting conditions, cells seem to invest in proteins which may not be required yet, for example, to quickly utilize alternative substrates without delays in growth [9]. However, any additional increase in protein abundance also results in higher costs due to occupation of ribosomes, resource consumption and potentially additional protein misfolding. Different hypotheses have been formulated and respective models were developed to understand the optimization and trade-offs.

Constraint-based modelling approaches are essential to analyze putative properties of metabolic networks. The well-established and frequently used method for the analysis of (large genome-scale) metabolic networks is flux balance analysis (FBA) [10,11]. This method calculates feasible solutions under steady-state conditions, depending on a defined objective function (biomass or ATP maximization) [12]. However, this method cannot be applied to dynamic cultivation conditions and does not consider gene regulation nor protein expression. To overcome these limitations, dynamic flux balance analysis (dFBA) was developed to maximize biomass growth over time, with changing extracellular conditions [13]. To include the synthesis costs of proteins and ribosomes, resource balance analysis (RBA) was developed, allowing for the prediction of the optimal allocation of intracellular resources for steady-state growth [14]. Looking at cellular behavior in terms of resource allocation has also been used to explain overflow metabolism [15,16]. In this paradoxical phenomenon, cells use catabolic pathways with low ATP yields per substrate such as alcoholic fermentation when growing at high growth rates, even when a high-yield pathway like respiration is available. Following the current hypothesis, the answer is that these fermentative pathways are much cheaper in terms of proteome space cost, meaning that the ATP production rate per protein mass is larger [16].

Combining approaches from both dFBA and RBA, lead to conditional FBA (cFBA) [17,18], which combined both temporal changes in the extracellular environment with constraints on intracellular resource allocation. These powerful tools are able to reproduce and predict metabolic phenotypes beyond steady-state conditions and extend our understanding of microbial physiology. Nevertheless, short term dynamics require yet another mechanism: kinetics instead of quasi-steady state of the intracellular metabolites to capture the rapid intracellular changes of metabolites as well as kinetic regulation.

Experimentally, *S. cerevisiae* cultures show different metabolic responses to substrate perturbations depending on the cultivation condition. Especially, cell cultured under repetitive dynamic substrate conditions, the so-called ‘feast/famine’ regime showed a different response compared to cultures grown under steady-state limitation [19]. Ethanol production after a substrate pulse was observed for cultures originating from a chemostat [20], while no ethanol was observed for cells under a repetitive excess/limitation regime [21]. Furthermore, the intracellular response to substrate excess has

significantly different properties: While the ATP concentration dropped after a pulse originating from a chemostat culture [20], a rise was observed for a feast/famine culture. Moreover, the biomass yield of a feast/famine culture was lower than a chemostat culture. Lastly, chemostat-grown cells showed short and long-term accumulation of glycolytic intermediates after a substrate pulse, while this was not observed for feast/famine cultures. Storage synthesis and degradation leads to “wasting” of ATP (futile cycle) which was shown to rescue cellular metabolism, i.e. balance pathway capacities in case of sudden perturbations [22].

The observed differential metabolic response implies an adaptation during the prior dynamic growth condition. Similar differences in adaptations have been observed earlier – for example the lag phase before exponential growth [23,24], upon a change in substrate [25] and in the period just after switching to a different dilution rate in a chemostat [26].

There are three levels of metabolic regulation commonly assumed to be dominant [27]: (1) Allosteric regulation, in which enzyme activity is modified by non-covalent binding with other molecules. The response time of this type of regulation is almost instant [28], and it is often used for local fine-tuning in metabolism, thus it is unlikely to cause this adaptation effect. (2) Post-translational modifications (PTMs), in which enzyme activity is altered by addition of covalent attachments. The timescale of this response is a matter of seconds to minutes [29], and it is often part of short-term responses to stress situations (e.g. sudden changes in the environment).

(3) Translational regulation, influencing the composition of the proteome. This regulation has a response time of hours [30], which is in the same order of magnitude as the generation time, and thus the choices made at this level are important for the long-term strategy. It is also considered the most expensive regulatory level: degradation and synthesis of proteins requires significant amounts of ATP.

Recent studies showed that the amount of protein in a cell is limited due to macromolecular crowding and the kinetics of protein synthesis and degradation [31,32]. When all proteome space is occupied, increasing the concentration of one protein is only possible at the cost of another (Pareto frontier) [33].

We were curious to study the impact of short-term vs long-term adaptations to substrate perturbations encountered in natural and laboratory environments. Therefore, we developed a resource dependent kinetic model and exposed this to different dynamic environments to evaluate the impact of the allocation of proteins in the cellular proteome on the metabolic fitness of a yeast cell under short-term extracellular substrate dynamics.

Results

Construction of a proteome-dependent kinetic model

We wanted to construct a proteome dependent kinetic model, which was small, but still able to reproduce the main phenotypes observed for *S. cerevisiae*. Furthermore, it should be calibrated with available experimental data. We based the model on the kinetic model of yeast glycolysis [34] which we extended with reactions for the trehalose cycle, respiration pathway, as well as a growth reaction (see Figure 2.1). Each (lumped) reaction has been associated with a proteome fraction resulting in a proteome-dependent kinetic model of yeast central carbon metabolism and growth.

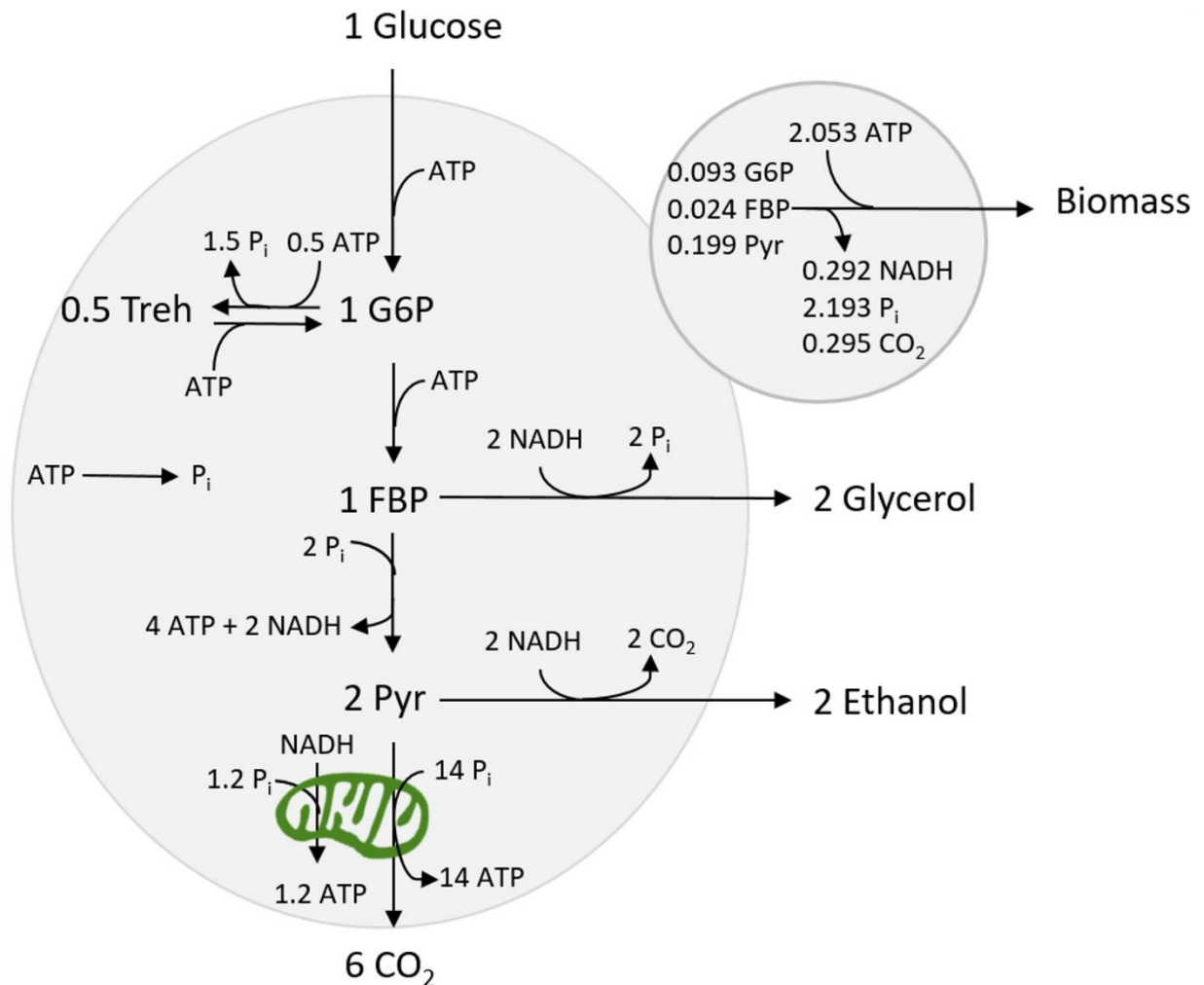


Figure 2.1. Map showing the metabolic network used in this model.

The Embden-Meyerhof glycolytic pathway has been implemented as three lumped reactions (uptake, upper and lower glycolysis) with three intermediates: G6P, FBP and pyruvate. The stoichiometry of the growth reaction was based on [35]. The NADPH requirement was assumed to be met by using the pentose phosphate pathway, which in sum (together with PGI) converts one G6P to six CO₂ and 12 NADPH. The required NADPH flux was balanced by a respective consumption of G6P. The ATP demand for growth has been derived from [36] taking into account that the demand was expressed as catabolized glucose amounts. Furthermore, the trehalose cycle was included as two lumped reactions, based on an existing kinetic model of the trehalose cycle [37] (see Appendix 1 for details).

Due to a lack of kinetic models of yeast TCA cycle and oxidative phosphorylation, the two respiratory reactions (from cytosolic NADH and pyruvate, v_{NDE} and v_{TCA} respectively) have been implemented using

general Michaelis-Menten kinetics. However, the two reactions are interdependent - both connect to the electron transport chain and consequently, the rate is determined by the same proteome fraction. A maximum value for the rate of the two reactions combined is defined, reflecting the capacity in the electron transport chain, limited by the provided proteome sector size (see Appendix 1).

The biomass reaction contains many, complex reactions and the kinetics of the full process currently cannot be derived from basic principles. Therefore, a holistic approach based on experimental observations was chosen, i.e. the growth rate has been found to correlate with the energy charge [38]. Here, the growth rate is described by a sigmoid function most sensitive within the range of an energy charge between 0.7 and 0.9 as observed for growing cells [38].

Calibration of model parameters using available experimental data

Especially, the specific activity for the defined pathways has a major impact on model predictions. To obtain realistic values, the specific enzyme activities (k_{cat}) were estimated from experimental omics data sets. In the proposed model, the $k_{cat,i}$ for each reaction i is defined as the max. reaction rate per fraction of proteome (mol/Cmol_x/h), where 100% proteome reflects 500 mg protein per g_x [39]. Hence, the maximum rate of the reaction i ($V_{max,i}$) with a given sector fraction φ_i is:

$$V_{max,i} = \varphi_i \cdot k_{cat,i}$$

From this, the enzymatic rate V_i is calculated by multiplying the $V_{max,i}$ with the function $f_i(\vec{c})$ describing the effects on enzymatic rate due to substrate and product concentrations, as well as effects by allosteric activators and inhibitors (see Appendix 1 for specification of $f_i(\vec{c})$ for each reaction):

$$V_i = V_{max,i} \cdot f_i(\vec{c})$$

The k_{cat} parameters have been estimated by combining the proteome and fluxome measurements under batch conditions. The proteome fractions were taken from [5] using *S. cerevisiae* grown at batch conditions with defined glucose minimal medium and aligned according to the protein classification in the KEGG database. Specifically, grouping all proteins with the KEGG BRITE label “Genetic Information Processing” and all proteins with the “Metabolism” label that were not classified as “Central Carbon Metabolism” or “Energy Metabolism” being assigned to the “growth protein sector”, assuming that their size is growth rate-dependent in minimal medium. Furthermore, for the calculations, it was assumed that the whole proteome sector of cells grown under substrate excess at the maximal growth rate was used.

The corresponding flux distribution, i.e. under batch conditions was obtained from [40] with the exception of fluxes for the trehalose cycle - these were obtained from the feast/famine experiments conducted by [41]. For both trehalose synthesis and degradation, the maximum value of the flux reached in one feast/famine cycle was used, which was $5.10 \cdot 10^{-3}$ mol/Cmol_x/h for trehalose synthesis and $4.09 \cdot 10^{-3}$ mol/Cmol_x/h for the degradation of trehalose. The k_{cat} value for maintenance was set to 0.0155 mol/Cmol_x/h, which is the maintenance requirement measured at near-zero growth rates [42].

To obtain the k_{cat} parameters, a parameter optimization was performed, estimating the parameters which produced the smallest deviation between the simulated and experimental fluxes [40], using the batch proteome composition taken from [5] (see Appendix 2 for details). Using this approach, the proteome dependent kinetic model was able to largely reproduce the experimental flux distribution (Table 2.1) and this k_{cat} calibration was used in all further calculations.

Table 2.1. Comparison of the predicted fluxes of a chemostat experiment at a dilution rate of 0.4 h⁻¹ with the experimental flux distribution of Heyland et al. [40]. Upt, uptake; UGlc, upper glycolysis; LGlc, lower glycolysis; Ferm, fermentation; Esnk, electron sink/glycerol pathway; Resp, respiration; Trsn, trehalose synthesis; Trdg, trehalose degradation; Grwt, growth.

	Upt	Uglc	LGlc	Ferm	Esnk	Resp	Trsn	Trdg	Grwt
Predicted flux (mol/Cmol_x/h)	0.504	0.4669	0.8251	0.7391	0.0898	0.0719	0.0072	0.0072	0.4
Experimental flux (mol/Cmol_x/h)	0.4753	0.4373	0.8745	0.7272	0.0428	0.0808	0.0051	0.0041	0.4
Deviation	+6%	+7%	-6%	+2%	+110%	-11%	+41%	+76%	0%

Prediction of the steady-state growth phenotype under carbon limited steady-state conditions

S. cerevisiae is a Crabtree-positive yeast, thus fermentation is observed next to oxidative phosphorylation at substrate uptake rates above an observed ‘critical’ rate [43]. The ability of the model to reproduce the Crabtree effect is assessed by optimizing proteomes for dilution rates in the range from 0.05 h⁻¹ to 0.4 h⁻¹. The proteome optimization was started at the dilution rate of 0.4 h⁻¹ using the experimental batch proteome as starting value. The most competitive proteome out of 1000 randomly generated proteome allocations was selected using minimization of the residual substrate concentration as objective function. Subsequently, this procedure was repeated for the next, lower dilution rate. The optimal proteome allocation of the previous dilution rate was used as starting value. To validate the model, the predicted fluxes and metabolite concentrations were compared with a flux and metabolome dataset (Suarez-Mendez et al., 2016) at different dilution rates at chemostat conditions. This comparison of predicted and measured fluxes and metabolite concentrations can be found in Appendix 3, in figures A2.2 and A2.3 respectively.

The experimental data for ethanol production and oxygen consumption in Figure 2.2 shows that the ethanol production starts at a dilution rate of 0.28 h⁻¹ [44,45]. Above this critical dilution rate the oxygen consumption rate decreases, while ethanol production keeps increasing. Ethanol production is first predicted by the model for a dilution rate of 0.25 h⁻¹, which is a lower rate compared to the experimental data. Furthermore, there is no decrease in the oxygen consumption rate above a dilution rate of 0.28 h⁻¹ for the optimized proteomes, which was observed in experimental studies [45]. From the model this can be explained by the proteome specific ATP production ‘cost’: Respiration has a higher yield compared to fermentation (Table 2.2). Hence, reducing the size of the respiration proteome sector will not be predicted by the model as it is not beneficial. The predicted plateau originates from a constraint that was introduced manually (12 % of the proteome for respiration) to reflect the maximum oxygen consumption rate measured by [44] after long-term evolution. The continuous increase in ethanol production rate can then be explained by the increasing need for ATP with increasing growth rate while respiration is at its maximum.

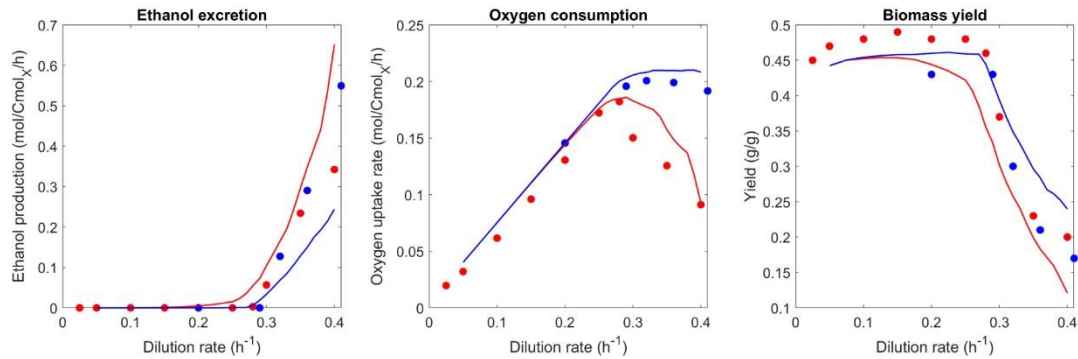


Figure 2.2. Comparison of predicted and observed phenotypic rates (ethanol excretion, oxygen uptake rate, and biomass yield) at different dilution rates. Blue represents the best proteome out of 1,000 randomly generated proteomes; red represents the best proteome out of 100 randomly generated proteomes (limited evolution with adaptation from the batch proteome). For the experimental data similarly—red represents data from Van Hoek et al. [45] (seven generations at steady-state starting from batch), and blue represents a respiration-adapted culture [44].

TABLE 2.2. Comparison of the proteome-specific ATP yield for fermentation and respiration obtained by Nilsson and Nielsen (2016) and this study. Values of this study were derived from simulations performed at a growth rate of 0.4 h^{-1} .

	Fermentation ($\text{mol}_{\text{ATP}}/\text{g}_{\text{prot}}/\text{h}$)	Respiration ($\text{mol}_{\text{ATP}}/\text{g}_{\text{prot}}/\text{h}$)
Nilsson and Nielsen [16]	0.40	0.21
This study	0.18	0.20

This result conflicts with the discussed dataset of [45] as well as model predictions of [16], which was partly based on this experimental dataset. This mismatch and conclusions will be discussed in more detail later. Notably, there is also experimental evidence from previous studies that the predicted plateau is reasonable. It was shown that the respiratory repression observed by [45] could be negated upon long-term adaptation [43,44,46] and a stable maximum oxygen uptake rate above a dilution rate of 0.28 h^{-1} was found.

To test the hypothesis of short- vs long-term evolution, the proteome optimization approach was performed with a reduced number of generated proteomes and compared to the experimental data of [45] (Figure 2.2, red line). With a high number of generated proteomes for the optimization the experimental findings of long-term chemostats could be reproduced. From these predictions we hypothesize that cells not exposed to long-term glucose-limited conditions did not yet reach the ‘optimal’ proteome allocation and respective metabolic phenotype. This set number of 1000 simulations was chosen as after this amount of simulations only very limited further optimization of the objective function was observed. As such, 1000 simulations was concluded as sufficient to reach the optimum. Work on adapted glucose-grown cultures, at which point glucose repression on respiration disappears, are cultivated for at least 50 generations at the same dilution rate (Barford et al., 1979). Work by van Hoek et al. (1998), describing the Crabtree effect with its typical glucose repression of respiration, cultivated cultures at the same dilution rate for 7 generations. Therefore, a set number of 100 simulations was chosen to reflect this state of limited adaptation of the proteome from batch growth conditions.

Looking into the global trends in the fully evolved proteome allocation at different dilution rates (Figure 2.3, see Appendix 4 for sensitivity analysis), an increase with dilution rate can be seen for nearly all sectors leading to unused space (in the following called overcapacity sector, last panel). The

overcapacity sector accounts for the fraction of the proteome which remains unused within the optimized proteomes. Before discussing specific trends, the high dilution rates will be highlighted. Even close to the maximal growth rate, the model predicts a small overcapacity sector. Nevertheless, please note that batch and very high dilution rate might still have different optimization criteria, in the model here minimal substrate concentration was applied as objective function. Because of the optimization approach some robustness is required this was not further tuned as the fraction is rather small (7%) and does not change trends. Additionally, the algorithm samples from an enumerated number of randomly generated proteomes and therefore requires some buffer for robustness.

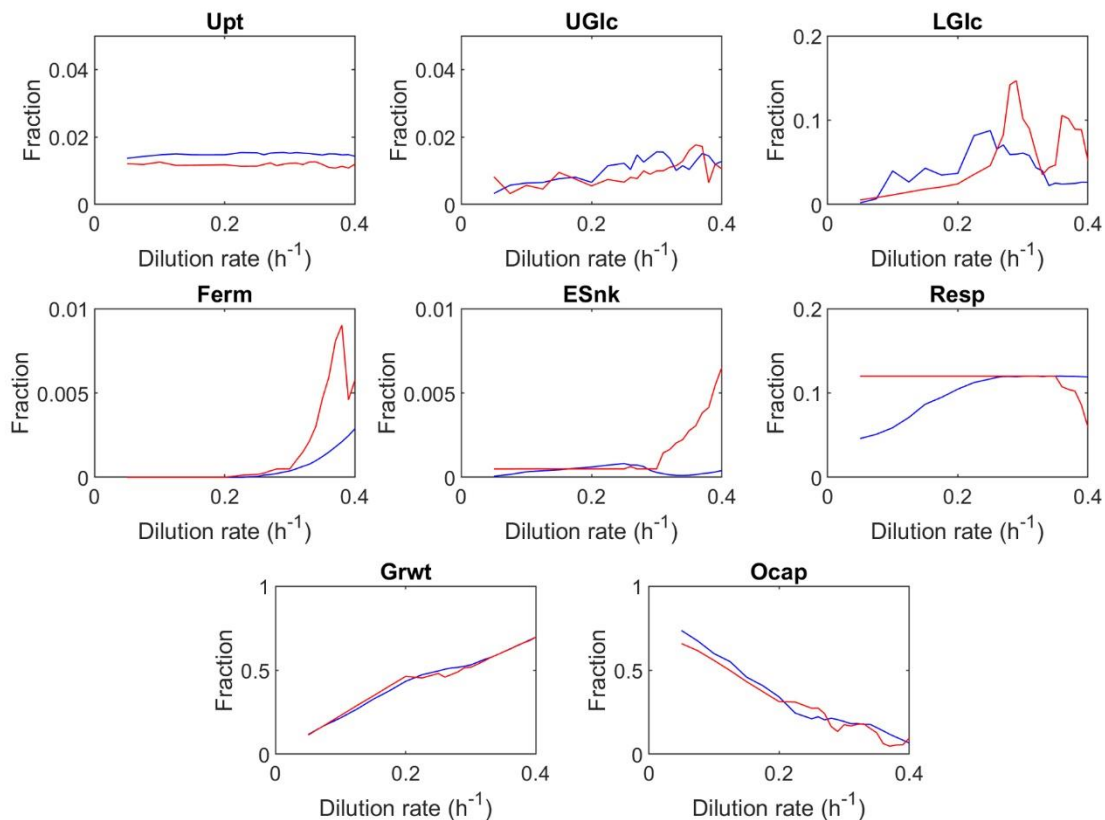


Figure 2.3. Predicted proteome fractions at steady-state as a function of the dilution rate. Blue represents the best proteome out of 1,000 randomly generated proteomes; red represents the best proteome out of 100 randomly generated proteomes. The values shown are averaged over 40 optimization runs, and the single results are displayed in the appendix Figure A2.4. Upt, uptake; UGlc, upper glycolysis; LGlc, lower glycolysis; Ferm, fermentation; ESnk, electron sink/glycerol pathway; Resp, respiration; Grwt, growth; Ocap, overcapacity. The trehalose sector was decreased to zero in all instances of the overcapacity simulation, and therefore not shown in the figure.

A major difference between this model and earlier studies [16] is that the proteome space limit is not reached at the critical growth rate ($D = 0.28 \text{ h}^{-1}$). At the critical dilution rate ($D = 0.28 \text{ h}^{-1}$), the overcapacity sector still has a significant fraction (21 %). As briefly discussed earlier, [16] postulated that the Crabtree effect could be explained by the catalytic efficiency of the fermentation and respiration pathways expressed as ATP per amount of protein used in the pathway (Table 2.2). To estimate these catalytic efficiencies, [16] used the fluxes and specific enzyme activities for fermentation and respiration, under the assumption that all enzymes operate at half of their maximum specific activity [16], whereas in this model, the estimation of the catalytic efficiency is based upon proteome and fluxome dataset, using dynamic saturation of enzymes. The estimation proposed by [16]

subsequently produced a proteome composition in which the mass of all respiration proteins is 19 times larger than the protein mass of all glycolysis enzymes [16], while from proteome measurements it was observed that the mass of all respiration proteins are 0.3 times the size of the mass of all glycolysis proteins [5,47]. This large difference in proteome allocation between glycolysis and respiration causes the catalytic efficiency of fermentation to be overestimated. The conclusion that the proteome is fully allocated after the critical growth rate is reached, leads to the prediction that the 'optimal' endpoint of proteome allocation is reached, which cannot explain datasets by [43,44]. Additional modelling studies by [47] suggest that the decrease in oxygen consumption at higher growth rates observed by [45] is not caused by a limitation in proteome capacity, but rather by a maximum rate of mitochondria biogenesis, where long-term adaptation could overcome the described glucose repression of respiration.

Prediction of proteome allocation under dynamic conditions

The proteome compositions especially at low dilution rates were characterized by a significant overcapacity sector. The kinetic proteome allocation approach could not yet answer, why the cells maintained such an excess proteome. As discussed earlier, hypothesis for a proteome overcapacity are competitiveness and robustness including towards dynamic environmental conditions. Overcapacity could enable faster substrate uptake rates and enable a competitive advantage and outcompete slower consuming microbes [48]. Furthermore, excess capacity could enable a robust, balanced functioning of pathways like glycolysis [22] under dynamic substrate conditions.

To test these hypotheses, we studied the predicted proteome allocation under different repetitive substrate feeding regimes using the proteome dependent kinetic model, using the minimization of the time-weighted residual substrate concentration as objective function. With this approach, we were able to select for competitive proteomes with fast substrate uptake rates. As reference dynamic condition an experimentally explored feeding regime was chosen, i.e. a cycle length of 400 seconds of which 20 seconds were used to feed the culture ($D = 2 \text{ h}^{-1}$), leading to the average dilution rate of $D = 0.1 \text{ h}^{-1}$ over the complete cycle [19].

Proteome allocations and respective metabolic phenotypes were then compared to the steady-state at the same (average) growth rate. First, we studied the maximum, minimum and average enzyme saturation (V/V_{\max}) during dynamic conditions compared to the enzyme saturation under chemostat conditions (Table 2.3). Under dynamic conditions, the maximal enzyme saturation is much higher (up to 92 % for the respiration reaction) compared to chemostat conditions (77% for respiration). Nevertheless, the average enzyme saturation over the whole cycle is actually lower compared to the reference chemostat state (for respiration 25% compared to 77% at steady-state). This indicates that the proteome optimization to some extent focuses on the 'peak' flux, especially for the large sectors of respiration and growth, indicating high usage of the available flux capacity, while on average leaving a large overcapacity over the whole cycle. This enables a rapid consumption of substrate as soon as it becomes available, which was the optimization criteria.

Table 2.3. Enzyme saturation, i.e., v/v_{\max} under dynamic feeding conditions compared to steady-state (both at a dilution rate of $D = 0.1 \text{ h}^{-1}$). For dynamic conditions, v/v_{\max} is calculated at the maximum rate during the cycle and the minimum as well as the average over the cycle. Upt, uptake; UGlc, upper glycolysis; LGlc, lower glycolysis; Ferm, fermentation; Esnk, electron sink/glycerol pathway; Resp, respiration; TrSn, trehalose synthesis; TrDg, trehalose degradation; Grwt, growth.

	Upt	UGlc	LGlc	Ferm	Esnk	Resp	TrSn	TrDg	Grwt
Max V/V_{\max} ratio under FF	6%	19%	8%	25%	46%	92%	79%	11%	100%
Min V/V_{\max} ratio under FF	<1%	<1%	<1%	<1%	<1%	1%	<1%	4%	<1%
Average V/V_{\max} ratio under FF	1%	3%	1%	4%	7%	25%	10%	7%	24%
V/V_{\max} ratio under chemostat	<1%	2%	6%	-	13%	77%	-	-	74%

We were now curious to see how the perturbation strength would influence the proteome allocation. Therefore, the length of the feeding period was varied at the same average dilution rate, resulting in different substrate perturbation intensities. The respective predicted proteome allocations were calculated and compared (Figure 2.4) for the different ratios of feeding time over cycle time (TF/TC). TF/TC values were chosen as log2 increments from the experimentally used TF/TC value of 1/20 [19].

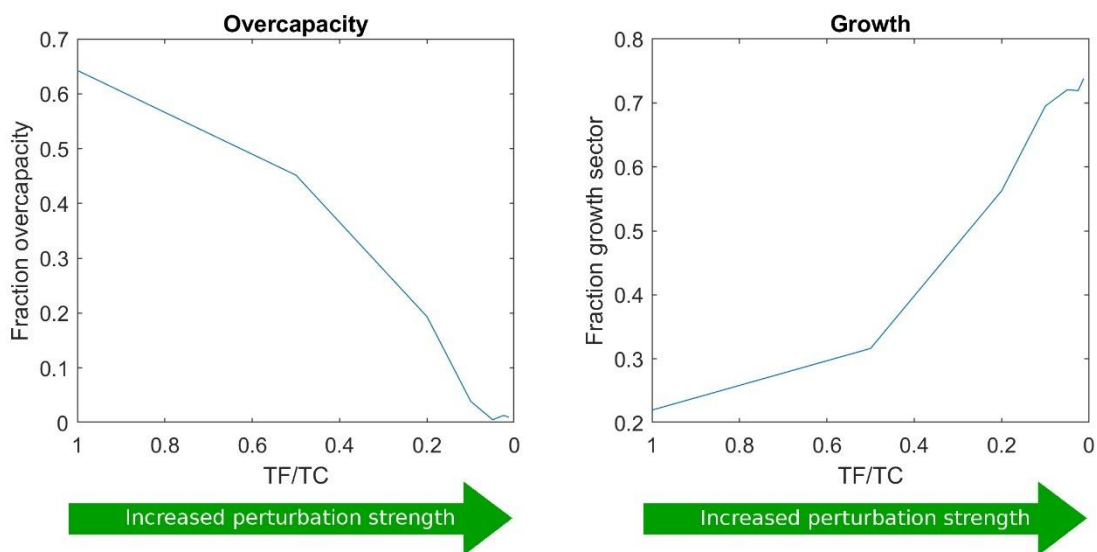


Figure 2.4. Proteome allocation as a function of the ratio of feeding time over cycle time (TF/TC). Further proteome sector fractions are shown in Appendix 5.

Especially, the growth sector fraction increased with the perturbation intensity, suggesting that this strategy was the most effective measure to survive the higher substrate concentration variations (from faster feeding) and consequently high flux dynamics. The growth reaction seemed to act as an efficient and fast sink for substrate and ATP. However, in reality the growth sector does not consist of a single reaction and may not be able to provide a rapid response upon glucose influx. For this reason, two other scenarios were additionally evaluated: 1) the regulation of the trehalose cycle upon repeated substrate pulses and 2) the regulation of the ratio between upper and lower glycolysis (see Appendix 6).

Impact of the proteome fraction for the trehalose cycle

The trehalose cycle has been described to function as ‘safety valve’ upon large changes in glycolytic flux [22,49–51]. Under dynamic conditions in yeast, it was found that a significant amount of imported glucose was recycled through the trehalose cycle, especially during periods of high flux changes [41]. To evaluate the effect of storage metabolism activity under dynamic conditions the reference condition ($D=0.1 \text{ h}^{-1}$, $TF/TC = 0.05$, [19]), was further analyzed. We varied the trehalose sector size between 0 and 1% (Figure 2.5) and compared the response of metabolism using FBP and P_i as indicators. A balanced metabolic response will lead to repetitive cycles in FBP and P_i . Such repetitive response was observed for proteomes with a trehalose sector larger than 0.1%. Increasing the trehalose sector above 0.1% leads to reduced fluctuations in G6P/FBP and P_i , suggesting a more robust metabolic response. Simulated changes in FBP and P_i are in line with results from previous work by van Heerden et al. [22].

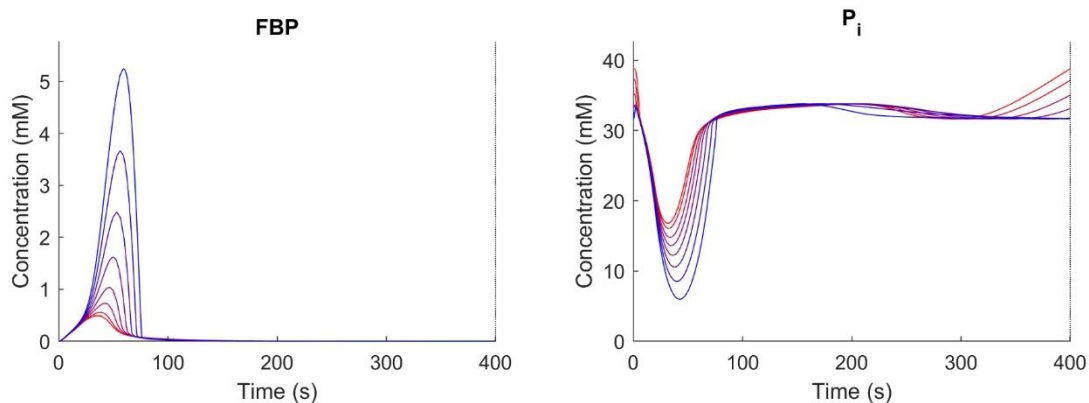


Figure 2.5. Concentration time course over repetitive cycles ($D = 0.1 \text{ h}^{-1}$, $TF/TC = 0.05$) for different trehalose sector fractions (blue = 0.1 red 1%). Shown are FBP and P_i as representative metabolites. For trehalose sector fractions $<0.1\%$, no stable cycles were obtained.

Comparison of the model predictions to experimental proteomes

To evaluate the prediction accuracy and trends of the predicted proteomes under dynamic conditions, the simulated proteome adaptation from chemostat to feast/famine conditions was compared with the experimentally measured proteome fold changes between chemostat and feast/famine conditions [52] (Figure 2.6). Proteins of trehalose/glycogen storage, ribosomes, and oxidative phosphorylation were used as proxies for the storage, growth and respiration sectors respectively (proteins categorized in the same way as calibration approach, see Methods).

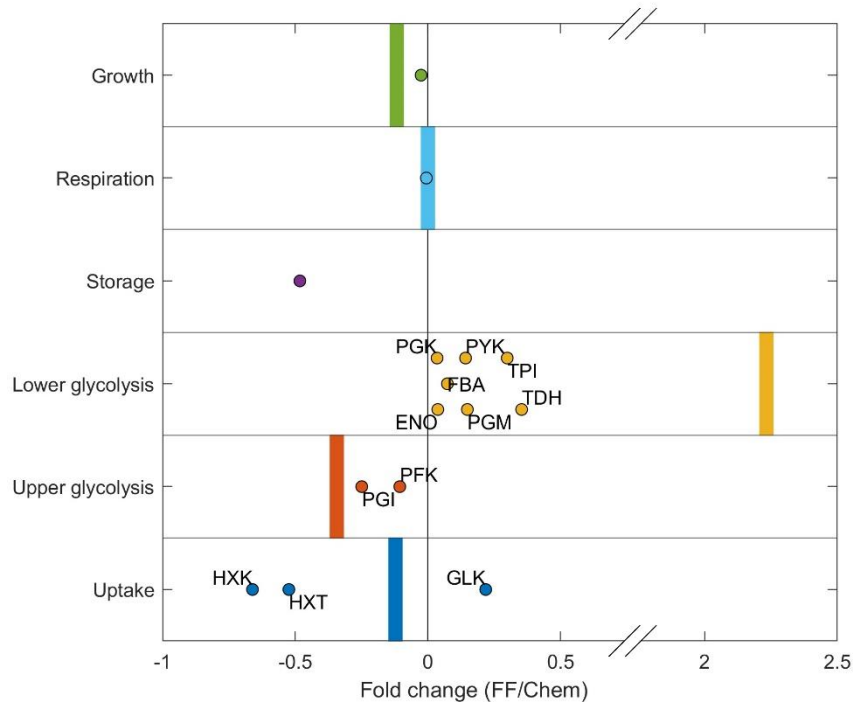


Figure 2.6. Protein concentration fold change from chemostat to feast/famine cultivation. The experimental fold change individual proteins are displayed as dots. Proteins of trehalose/glycogen storage, ribosomes, and oxidative phosphorylation were used as proxies for the storage, growth, and respiration sectors, respectively. Simulation fold changes for each sector are shown as vertical bars. The simulated storage sector for steady-state conditions was 0 and increased under simulated feast/famine conditions. As such, no fold change could be calculated, and therefore this fold change is not shown.

The model predicted the experimentally observed changes in upper and lower glycolysis (Figure 2.6). The enzyme Tdh catalyzes the glyceraldehyde dehydrogenase reaction (TDH), which forms ATP using Pi. However, if upper and lower glycolysis are imbalanced during high fluxes, this reaction becomes a bottleneck, leading to the accumulation of FBP and subsequently to an imbalanced metabolism. Therefore, it was expected that that Tdh had to be upregulated under substrate fluctuating conditions to facilitate balanced intermediates, which was reflected in both the model predictions as well as in the experimental dataset. The predicted change in lower glycolysis is larger than in the experimental data. This is likely caused by the fact that simulated proteomes for chemostat conditions contain no overcapacity in the lower glycolysis sector, whereas experimental proteomes under chemostat conditions do appear to contain more overcapacity in this proteome sector. As such, the fold change between measured and simulated values is higher. Furthermore, the model reproduced the average change observed for the uptake sector, although it should be noted that effects of individual iso-enzymes (especially with regard to HXK/GLK, which catalyze the first step of glycolysis) was not taken into account in the current model.

Significant deviations between experimental and predicted fractions were observed for the storage sector. This was significantly decreased experimentally, while the resource dependent kinetic model predicted an increase. Experimentally, a decrease of 28%, from 0.25% to 0.2% of the proteome, was observed, while in the model an increase to 0.2% of the proteome was predicted. Possible reasons for this difference in sector size could be: (1) The synthesis of trehalose has additional functions in the cell which are not represented in the model – it is described that trehalose plays an important role in different stress responses, including severe substrate limitation at low dilution rates (see also Figure A2.3). (2) The measured and predicted proteomes do not include post-translational modifications which are known to significantly affect the k_{cat} 's of enzymes in the trehalose cycle [53], nor changes that could occur during cell-cycle progression.

Furthermore, there could also be a bias from the experimental setup - the differences in trehalose sector, combined with the observed increase of the lower glycolysis sector compared to experimental conditions, suggests that the experimental chemostat proteome is potentially already primed for dynamic environments, and as such is more robust than the predicted optimized chemostat proteomes.

Conclusions & Outlook

In this work, we developed a proteome-dependent kinetic modelling framework that predicts the optimal proteome composition for defined extracellular dynamic conditions. The approach could reproduce observed complex metabolic phenomena, such as the Crabtree effect, including long-term adjustments under chemostat conditions.

Analysis of the predicted proteomes showed that under substrate limiting conditions (i.e. low dilution rates) with close to constant extracellular concentrations, a significant part of the optimized proteome is not required (thus lot of overcapacity). With increasing substrate availability and/or concentration fluctuations, this overcapacity is shown to decrease. Cells optimized for steady-state conditions were not able to survive these substrate perturbations. This suggests that in reality, where conditions are never as ideal and 'optimal' as presented in the model simulations, cells already possess proteome adjustments to create a more robust metabolism, allowing them to cope effectively with external perturbations such as substrate gradients.

Such adjustments to perturbations were found when comparing steady-state and feast/famine condition predictions. The approach generated a stable phenotype and the predicted changes in proteome allocation, i.e. downregulation of uptake and upper glycolysis sectors, upregulation of the lower glycolysis sector, were also found experimentally. This complex, and strongly kinetics dependent prediction highlights the relevance of kinetic properties also for the regulation of protein expression. Nevertheless, to achieve this prediction, some constraints, which had to be derived from experimental observations, had to be included: the maximum mitochondrial fraction and the glucose repression on fermentation. These boundaries seemed to be only stretched after very long-term evolution, as was observed by [43]. Following this observation, the model was used to predict the proteome composition and metabolic behavior of cells at different stages of adaptation, able to simulate differences in cultivation history. Thus, the modelling approach was able to cover a large range of conditions and evolution outcomes, which could be specifically relevant for the prediction of production processes regimes running over a long time span.

Materials & Methods

Proteome-dependent kinetic yeast model

The proteome-dependent kinetic yeast model is based on a system of ordinary differential equations (ODEs) that describe the mass balances of all intra- and extra-cellular metabolites. This system of ODEs is solved with the `ode15s` function in MATLAB2020b, for which the absolute tolerance is set to $1e-4$ and all variables are constrained to be higher than zero with the "NonNegative" setting. A detailed description of the final proteome-dependent kinetic yeast model used is given in the Appendix 1.

To predict which proteome composition is the most competitive for defined environmental conditions, a Monte-Carlo approach is used. The metabolic behavior of 1000 random proteomes, generated around a seed proteome, is compared based on an objective function. Under steady-state conditions, the minimization of the residual substrate concentration was used as objective function. Under dynamic conditions, the minimization of a time-weighted average substrate concentration was used, to promote fast consumption of available substrate, therefore selecting for competitive proteomes:

$$\frac{\int_0^{t_{cycle}} c_s \cdot t \, dt}{\int_0^{t_{cycle}} t \, dt}$$

Subsequently, it is determined whether the solution is balanced. If the objective function is optimized and the solution is balanced, the objective function and the seed proteome are updated. In the next iteration, the proteome is then generated around this new seed proteome, with a maximum deviation of 25% per sector.

Proteome allocation to model sectors

All proteins from experimental datasets are sorted in the same nine protein sectors that are used in the model, to allow for direct comparison of the experimental proteomes and the optimized proteomes. The proteins are categorized per sector based on either the protein name or the description in the KEGG database [54,55] (Appendix 7). The whole dataset is sorted with the MATLAB2020b functions 'strcmp' and 'contains', which are used to search the dataset for specific names or keywords to group the proteins by.

Parameter optimization

The proteome cost parameters are estimated by optimization with the MATLAB2020b function `fmincon`. For all parameter optimizations, a multi-start approach is used. This approach minimizes the risk of reaching a local minimum in the solution space by starting the optimization from different initial guesses. The tolerance of the function is set to $1e-12$ for all optimizations. For the estimation of the k_{cat} parameters, the difference between the experimental and simulated fluxes is minimized. Additional weight in the objective function was applied for the growth rate, as k_{cat} parameters have to be rejected if the maximum growth rate is not reached.

Overcapacity simulations

The amount of overcapacity in the yeast proteome is determined by introducing a tenth protein sector. This new protein sector does not have a function for the cells, and hence, only takes up space in the proteome. Therefore, the fraction of the proteome that can be allocated into the extra sector without altering the metabolic fluxes is defined as overcapacity. The overcapacity is estimated for each sector separately, to minimize the changes in each step. The sectors are sorted in decreasing order, and then optimized for overcapacity in this order. The amount of overcapacity in each sector is determined in a step-wise approach. Per iteration, one percent of the specific protein sector is removed and allocated into the extra sector. Subsequently, the fluxes of the adapted proteome are compared to the reference fluxes, and only if the change in the fluxes remains within the boundaries, the seed proteome is

updated. This new seed proteome is then used for the next iteration, in which the sector size is again decreased by 1%. By decreasing the sector size by 1% of the current size, the step size is reduced with each iteration. If the flux profile deviates more than the threshold value, the adapted proteome allocation is rejected. The fluxes are evaluated based the following criterium: The average value of the uptake and growth fluxes should not deviate more than 1% from the reference flux, to ensure that the same substrate uptake and growth rates are achieved.

Data Availability Statement

The dataset on proteome fold changes between chemostat and feast/famine conditions, analyzed in this study, can be found in the 4TU.ResearchData repository <https://doi.org/10.4121/19008833>. The codes used for this publication can be found at <https://doi.org/10.4121/19074791>.

References

1. Chubukov V, Gerosa L, Kochanowski K, Sauer U: **Coordination of microbial metabolism**. *Nat Rev Microbiol* 2014, **12**:327–340.
2. Gerosa L, Sauer U: **Regulation and control of metabolic fluxes in microbes**. *Curr Opin Biotechnol* 2011, **22**:566–575.
3. Litsios A, Ortega ÁD, Wit EC, Heinemann M: **Metabolic-flux dependent regulation of microbial physiology**. *Curr Opin Microbiol* 2018, **42**:71–78.
4. Zhao Q, Stettner AI, Reznik E, Paschalidis ICh, Segrè D: **Mapping the landscape of metabolic goals of a cell**. *Genome Biol* 2016, **17**:109.
5. de Godoy LMF, Olsen JV, Cox J, Nielsen ML, Hubner NC, Fröhlich F, Walther TC, Mann M: **Comprehensive mass-spectrometry-based proteome quantification of haploid versus diploid yeast**. *Nature* 2008, **455**:1251–1254.
6. Liebermeister W, Noor E, Flamholz A, Davidi D, Bernhardt J, Milo R: **Visual account of protein investment in cellular functions**. *Proc Natl Acad Sci* 2014, **111**:8488–8493.
7. Nagaraj N, Alexander Kulak N, Cox J, Neuhauser N, Mayr K, Hoerning O, Vorm O, Mann M: **System-wide Perturbation Analysis with Nearly Complete Coverage of the Yeast Proteome by Single-shot Ultra HPLC Runs on a Bench Top Orbitrap**. *Mol Cell Proteomics* 2012, **11**:M111.013722.
8. Basan M: **Resource allocation and metabolism: the search for governing principles**. *Curr Opin Microbiol* 2018, **45**:77–83.
9. Dekel E, Alon U: **Optimality and evolutionary tuning of the expression level of a protein**. *Nature* 2005, **436**:588–592.
10. Orth JD, Thiele I, Palsson BØ: **What is flux balance analysis?** *Nat Biotechnol* 2010, **28**:245–248.
11. Varma A, Palsson BO: **Stoichiometric flux balance models quantitatively predict growth and metabolic by-product secretion in wild-type *Escherichia coli* W3110**. *Appl Environ Microbiol* 1994, **60**:3724–3731.
12. Schuetz R, Kuepfer L, Sauer U: **Systematic evaluation of objective functions for predicting intracellular fluxes in *Escherichia coli***. *Mol Syst Biol* 2007, **3**:119.
13. Mahadevan R, Edwards JS, Doyle FJ: **Dynamic Flux Balance Analysis of Diauxic Growth in *Escherichia coli***. *Biophys J* 2002, **83**:1331–1340.
14. Goelzer A, Muntel J, Chubukov V, Jules M, Prestel E, Nölker R, Mariadassou M, Aymerich S, Hecker M, Noirot P, et al.: **Quantitative prediction of genome-wide resource allocation in bacteria**. *Metab Eng* 2015, **32**:232–243.
15. Basan M, Hui S, Okano H, Zhang Z, Shen Y, Williamson JR, Hwa T: **Overflow metabolism in *Escherichia coli* results from efficient proteome allocation**. *Nature* 2015, **528**:99–104.
16. Nilsson A, Nielsen J: **Metabolic Trade-offs in Yeast are Caused by F1F0-ATP synthase**. *Sci Rep* 2016, **6**.

17. Reimers A-M, Knoop H, Bockmayr A, Steuer R: **Cellular trade-offs and optimal resource allocation during cyanobacterial diurnal growth.** *Proc Natl Acad Sci* 2017, **114**:E6457–E6465.
18. Rügen M, Bockmayr A, Steuer R: **Elucidating temporal resource allocation and diurnal dynamics in phototrophic metabolism using conditional FBA.** *Sci Rep* 2015, **5**.
19. Suarez-Mendez C, Sousa A, Heijnen J, Wahl A: **Fast “Feast/Famine” Cycles for Studying Microbial Physiology Under Dynamic Conditions: A Case Study with *Saccharomyces cerevisiae*.** *Metabolites* 2014, **4**:347–372.
20. Wu L, van Dam J, Schipper D, Kresnowati MTAP, Proell AM, Ras C, van Winden WA, van Gulik WM, Heijnen JJ: **Short-Term Metabolome Dynamics and Carbon, Electron, and ATP Balances in Chemostat-Grown *Saccharomyces cerevisiae* CEN.PK 113-7D following a Glucose Pulse.** *Appl Environ Microbiol* 2006, **72**:3566–3577.
21. Suarez-Mendez CA: **Dynamics of Storage Carbohydrates Metabolism in *Saccharomyces cerevisiae*.** 2015, doi:10.4233/UUID:2504BD76-9811-4D3C-A66B-3AAE7FBB40B5.
22. van Heerden JH, Wortel MT, Bruggeman FJ, Heijnen JJ, Bollen YJM, Planque R, Hulshof J, O’Toole TG, Wahl SA, Teusink B: **Lost in Transition: Start-Up of Glycolysis Yields Subpopulations of Nongrowing Cells.** *Science* 2014, **343**:1245114–1245114.
23. Brejning J, Jespersen L: **Protein expression during lag phase and growth initiation in *Saccharomyces cerevisiae*.** *Int J Food Microbiol* 2002, **75**:27–38.
24. Jöers A, Tenson T: **Growth resumption from stationary phase reveals memory in *Escherichia coli* cultures.** *Sci Rep* 2016, **6**:24055.
25. Chu D, Barnes DJ: **The lag-phase during diauxic growth is a trade-off between fast adaptation and high growth rate.** *Sci Rep* 2016, **6**:25191.
26. Abulesz E-M, Lyberatos G: **Periodic operation of a continuous culture of Baker’s yeast.** *Biotechnol Bioeng* 1989, **34**:741–749.
27. Wegner A, Meiser J, Weindl D, Hiller K: **How metabolites modulate metabolic flux.** *Curr Opin Biotechnol* 2015, **34**:16–22.
28. Pincus D, Resnekov O, Reynolds KA: **An evolution-based strategy for engineering allosteric regulation.** *Phys Biol* 2017, **14**:025002.
29. Karim MdR, Kawanago H, Kadowaki M: **A quick signal of starvation induced autophagy: Transcription versus post-translational modification of LC3.** *Anal Biochem* 2014, **465**:28–34.
30. Cohen AA, Geva-Zatorsky N, Eden E, Frenkel-Morgenstern M, Issaeva I, Sigal A, Milo R, Cohen-Saidon C, Liron Y, Kam Z, et al.: **Dynamic Proteomics of Individual Cancer Cells in Response to a Drug.** *Science* 2008, **322**:1511–1516.
31. Molenaar D, van Berlo R, de Ridder D, Teusink B: **Shifts in growth strategies reflect tradeoffs in cellular economics.** *Mol Syst Biol* 2009, **5**:323.
32. Vazquez A, Beg QK, deMenezes MA, Ernst J, Bar-Joseph Z, Barabási A-L, Boros LG, Oltvai ZN: **Impact of the solvent capacity constraint on *E. coli* metabolism.** *BMC Syst Biol* 2008, **2**:7.

33. Mori M, Marinari E, De Martino A: **A yield-cost tradeoff governs *Escherichia coli*'s decision between fermentation and respiration in carbon-limited growth.** *Npj Syst Biol Appl* 2019, **5**.
34. Teusink B, Passarge J, Reijenga CA, Esgalhado E, Van Der Weijden CC, Schepper M, Walsh MC, Bakker BM, Van Dam K, Westerhoff H V., et al.: **Can yeast glycolysis be understood terms of *in vitro* kinetics of the constituent enzymes? Testing biochemistry.** *Eur J Biochem* 2000, **267**:5313–5329.
35. Suarez-Mendez CA, Hanemaaijer M, ten Pierick A, Wolters JC, Heijnen JJ, Wahl SA: **Interaction of storage carbohydrates and other cyclic fluxes with central metabolism: A quantitative approach by non-stationary ¹³C metabolic flux analysis.** *Metab Eng Commun* 2016, **3**:52–63.
36. Della-Bianca BE, de Hulster E, Pronk JT, van Maris AJA, Gombert AK: **Physiology of the fuel ethanol strain *Saccharomyces cerevisiae* PE-2 at low pH indicates a context-dependent performance relevant for industrial applications.** *FEMS Yeast Res* 2014, **14**:1196–1205.
37. Smallbone K, Malys N, Messiha HL, Wishart JA, Simeonidis E: *Building a kinetic model of trehalose biosynthesis in Saccharomyces cerevisiae.* Elsevier Inc.; 2011.
38. Boer VM, Crutchfield CA, Bradley PH, Botstein D, Rabinowitz JD: **Growth-limiting Intracellular Metabolites in Yeast Growing under Diverse Nutrient Limitations.** *Mol Biol Cell* 2010, **21**:198–211.
39. Ertugay N, Hamamci H: **Continuous cultivation of bakers' yeast: Change in cell composition at different dilution rates and effect of heat stress on trehalose level.** *Folia Microbiol (Praha)* 1997, **42**:463–467.
40. Heyland J, Fu J, Blank LM: **Correlation between TCA cycle flux and glucose uptake rate during respiro-fermentative growth of *Saccharomyces cerevisiae*.** *Microbiology* 2009, **155**:3827–3837.
41. Suarez-Mendez CA, Ras C, Wahl SA: **Metabolic adjustment upon repetitive substrate perturbations using dynamic ¹³C-tracing in yeast.** *Microb Cell Factories* 2017, **16**.
42. Vos T, Hakkaart XDV, Hulster EAF, Maris AJA, Pronk JT, Daran-Lapujade P: **Maintenance-energy requirements and robustness of *Saccharomyces cerevisiae* at aerobic near-zero specific growth rates.** *Microb Cell Factories* 2016, **15**:1–20.
43. Barford JP, Hall RJ: **An Examination of the Crabtree Effect in *Saccharomyces cerevisiae*: the Role of Respiratory Adaptation.** *J Gen Microbiol* 1979, **114**:267–275.
44. Rieger M, Käppeli O, Fiechter A: **The Role Of Limited Respiration In The Incomplete Oxidation Of Glucose By *Saccharomyces Cerevisiae*.** *Microbiology* 1983, **129**:653–661.
45. Van Hoek P, Van Dijken JP, Pronk JT: **Effect of Specific Growth Rate on Fermentative Capacity of Baker's Yeast.** *Appl Environ Microbiol* 1998, **64**:4226–4233.
46. Postma E, Verduyn C, Scheffers WA, Van Dijken JP: **Enzymic analysis of the crabtree effect in glucose-limited chemostat cultures of *Saccharomyces cerevisiae*.** *Appl Environ Microbiol* 1989, **55**:468–477.
47. Elsemman IE, Rodriguez Prado A, Grigaitis P, Garcia Albornoz M, Harman V, Holman SW, van Heerden J, Bruggeman FJ, Bisschops MMM, Sonnenschein N, et al.: **Whole-cell modeling in yeast**

- predicts compartment-specific proteome constraints that drive metabolic strategies.** *Nat Commun* 2022, **13**:801.
48. Jannasch HW: **Enrichments of aquatic bacteria in continuous culture.** *Arch Für Mikrobiol* 1967, **59**:165–173.
 49. Blomberg A: **Metabolic surprises in *Saccharomyces cerevisiae* during adaptation to saline conditions: questions, some answers and a model.** *FEMS Microbiol Lett* 2000, **182**:1–8.
 50. Thevelein JM, Hohmann S: **Trehalose synthase: guard to the gate of glycolysis in yeast?** *Trends Biochem Sci* 1995, **20**:3–10.
 51. Vicente RL, Spina L, Gómez JPL, Dejean S, Parrou J-L, François JM: **Trehalose-6-phosphate promotes fermentation and glucose repression in *Saccharomyces cerevisiae*.** *Microb Cell* 2018, **5**:444–459.
 52. Verhagen K, Eerden S, Wahl SA (Aljoscha): **Dataset proteomics: Analysis of change in protein expression in *Saccharomyces cerevisiae* upon shift from glucose chemostat to feast/famine regime.** 2022, doi:10.4121/19008833.
 53. Sengupta S, Chaudhuri P, Lahiri S, Dutta T, Banerjee S, Majhi R, Ghosh AK: **Possible regulation of trehalose metabolism by methylation in *Saccharomyces cerevisiae*.** *J Cell Physiol* 2011, **226**:158–164.
 54. Goffeau A, Barrell BG, Bussey H, Davis RW, Dujon B, Feldmann H, Galibert F, Hoheisel JD, Jacq C, Johnston M, et al.: **Life with 6000 Genes.** *Science* 1996, **274**:546–567.
 55. Kanehisa M, Sato Y, Kawashima M, Furumichi M, Tanabe M: **KEGG as a reference resource for gene and protein annotation.** *Nucleic Acids Res* 2016, **44**:D457–D462.
 56. Pronk JT, Steensma HY, Van Dijken JP: **Pyruvate Metabolism in *Saccharomyces cerevisiae*.** *Yeast* 1996, **12**:1607–1633.
 57. de Vries S, Grivell LA: **Purification and characterization of a rotenone-insensitive NADH: Q6 oxidoreductase from mitochondria of *Saccharomyces cerevisiae*.** *Eur J Biochem* 1988, **176**:377–384.
 58. Illmer P, Erlebach C, Schinner F: **A practicable and accurate method to differentiate between intra- and extracellular water of microbial cells.** *FEMS Microbiol Lett* 1999, **178**:135–139.
 59. Lamprecht I, Schaarschmidt B, Welge G: **Microcalorimetric investigation of the metabolism of yeasts - V. Influence of ploidy on growth and metabolism.** *Radiat Environ Biophys* 1976, **13**:57–61.

Appendix

1 Model structure

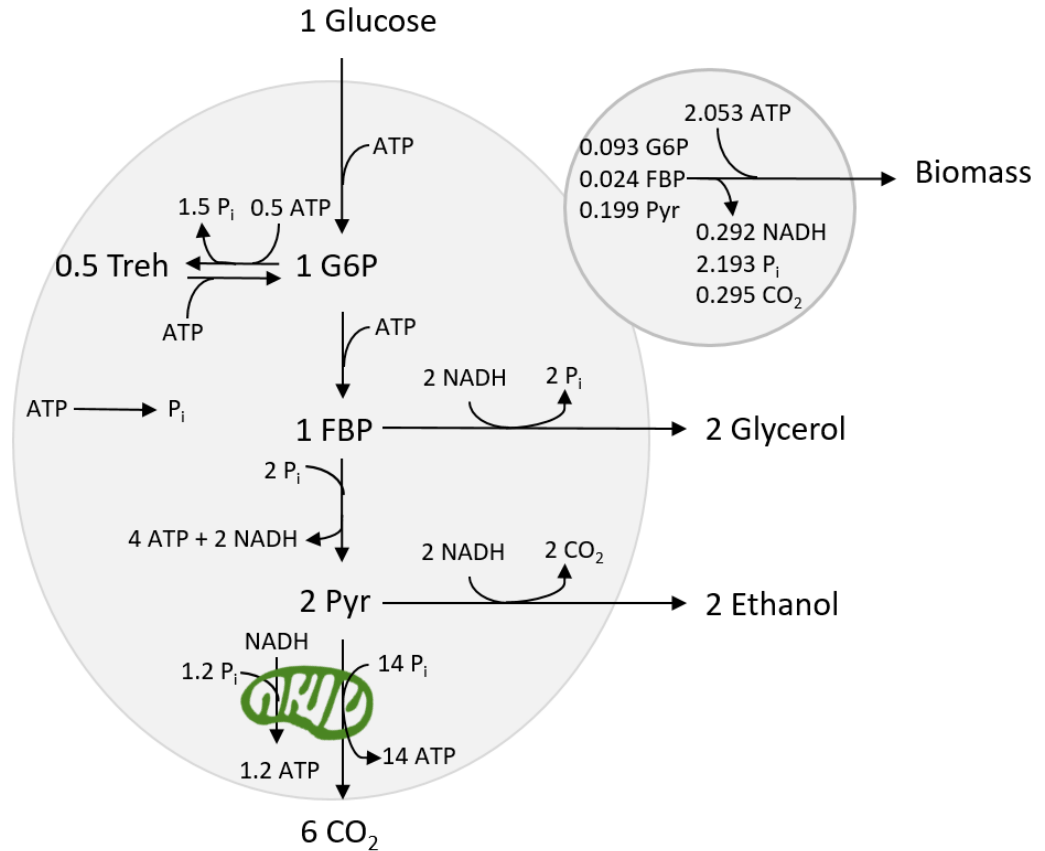


Figure A2.1. Map showing the metabolic network used in this model.

First, we tag glucose, ethanol, glycerol and biomass with the label EC, and the other compounds with the label IC, then the system of equations becomes:

$$\begin{cases} \frac{dc_{EC}}{dt} = D_{(t)} \cdot (c_{EC,in} - c_{EC}) + S_{EC} \cdot v \cdot c_x \\ \frac{dc_{IC}}{dt} = S_{IC} \cdot v \cdot \rho_x \end{cases}$$

In this model, 4 variables are user supplied:

- ϕ : an 9-dimensional proteome allocation vector (should add up to one)
- D_{avg} : the average dilution rate (for batch, set to 0)
- t_{cycle} : the length of a feast-famine cycle
- t_{feed} : the length of the feed phase of the feast-famine cycle (for chemostat, set equal to t_{cycle})

To compensate D for the feast/famine operation, $D_{(t)}$ is defined as followed:

$$D_{(t)} = \begin{cases} D_{avg} \cdot \frac{t_{cycle}}{t_{feed}} & \text{in the feed phase} \\ 0 & \text{outside feed phase} \end{cases}$$

The concentrations of ADP and NAD are calculated as followed:

$$c_{ADP} = c_{AxP} - c_{ATP} \quad \text{with } c_{AxP}$$

$$c_{NAD} = c_{NADx} - c_{NADH} \quad \text{with } c_{NADx}$$

2 Stoichiometry

Table A2.1. The stoichiometric matrix S of the metabolic model

	Upt	UGlc	LGlc	Ferm	Esnk	TCA	NDE	TrSn	TrDg	Grwt	Mtn
Glucose	-1	0	0	0	0	0	0	0	0	0	0
Biomass	0	0	0	0	0	0	0	0	0	1	0
Ethanol	0	0	0	1	0	0	0	0	0	0	0
Glycerol	0	0	0	0	1	0	0	0	0	0	0
ATP	-1	-1	2	0	0	7/5	1.2	-1	-2	-2.0531	-1
NADH	0	0	1	-1	-1	0	-1	0	0	0.2916	0
P _i	0	0	-1	0	1	-7/5	-1.2	3	0	2.1930	1
G6P	1	-1	0	0	0	0	0	-2	2	-0.0927	0
FBP	0	1	-0.5	0	-0.5	0	0	0	0	-0.0236	0
PYR	0	0	1	-1	0	-1/5	0	0	0	-0.1992	0
Treh	0	0	0	0	0	0	0	1	-1	0	0
(CO ₂)*	0	0	0	1	0	3/5	0	0	0	0.2954	0

* CO₂ is not simulated in the ODE system, but this stoichiometry was used for calculating q_{CO_2}

Flux vector as used in ODE system:

$$v = \begin{pmatrix} v_{upt} \\ v_{uglc} \\ v_{lglc} \\ v_{ferm} \\ v_{esnk} \\ v_{TCA} \\ v_{NDE} \\ v_{trsn} \\ v_{trdg} \\ \mu \\ v_{mtn} \end{pmatrix}$$

3 Rate equations

1 Uptake

$$v_{upt} = \varphi_{upt} \cdot k_{cat,upt} \cdot \frac{C_{Glc}}{K_{m,upt,Glc} + C_{Glc}} \cdot \frac{C_{ATP}}{K_{m,upt,ATP} + C_{ATP}}$$

The value of φ_{upt} is capped to φ_{upt}^{max} , to reflect the limited space for proteins on the membrane. Any proteome allocated to this sector above this value is ignored.

2 Upper glycolysis

$$v_{uglc} = \varphi_{uglc} \cdot k_{cat,uglc} \cdot \frac{C_{G6P}}{K_{m,uglc,G6P} + C_{G6P}} \cdot \frac{C_{ATP}}{K_{m,uglc,ATP} + C_{ATP}} \cdot \frac{K_{i,uglc,ATP}^{n_{uglc,ATP}}}{K_{i,uglc,ATP}^{n_{uglc,ATP}} + C_{ATP}^{n_{uglc,ATP}}}$$

3 Lower glycolysis

$$v_{lglc} = \varphi_{lglc} \cdot k_{cat,lglc} \cdot \frac{C_{FBP}}{K_{m,lglc,FBP} + C_{FBP}} \cdot \frac{C_{ADP}}{K_{m,lglc,ADP} + C_{ADP}} \cdot \frac{C_{P_i}}{K_{m,lglc,P_i} + C_{P_i}} \cdot \frac{C_{NADH}}{C_{NADH}}$$

4 Fermentation

$$v_{ferm} = \varphi_{ferm} \cdot k_{cat,ferm} \cdot \frac{C_{PYR}^{n_{ferm,PYR}}}{K_{m,ferm,PYR}^{n_{ferm,PYR}} + C_{PYR}^{n_{ferm,PYR}}} \cdot \frac{C_{NADH}^{n_{ferm,NADH}}}{K_{m,ferm,NADH}^{n_{ferm,NADH}} + C_{NADH}^{n_{ferm,NADH}}}$$

To regulate the activation of fermentation, a critical glucose concentration is set, equal to the residual glucose concentration at a dilution rate of 0.28 h^{-1} (0.057 mM).

5 Glycerol electron sink

$$v_{esnk} = \varphi_{esnk} \cdot k_{cat,esnk} \cdot \frac{C_{FBP}}{K_{m,esnk,FBP} + C_{FBP}} \cdot \frac{C_{NADH}}{K_{m,esnk,NADH} + C_{NADH}}$$

6 Respiration (pyruvate-dependent and NADH-dependent)

$$v_{TCA} = \varphi_{resp} \cdot k_{cat,resp} \cdot \frac{C_{PYR}}{K_{m,resp,PYR} + C_{PYR}} \cdot \frac{C_{ADP}^{n_{resp,ADP}}}{K_{m,resp,ADP}^{n_{resp,ADP}} + C_{ADP}^{n_{resp,ADP}}} \cdot \frac{C_{P_i}^{n_{resp,P_i}}}{K_{m,resp,P_i}^{n_{resp,P_i}} + C_{P_i}^{n_{resp,P_i}}}$$

$$v_{NDE} = \varphi_{resp} \cdot k_{cat,resp} \cdot \frac{C_{NADH}}{K_{m,resp,NADH} + C_{NADH}} \cdot \frac{C_{ADP}^{n_{resp,ADP}}}{K_{m,resp,ADP}^{n_{resp,ADP}} + C_{ADP}^{n_{resp,ADP}}} \cdot \frac{C_{P_i}^{n_{resp,P_i}}}{K_{m,resp,P_i}^{n_{resp,P_i}} + C_{P_i}^{n_{resp,P_i}}}$$

If $v_{TCA} + v_{NDE} > \varphi_{resp} \cdot k_{cat,resp}$ (if ETC capacity is exceeded)

Then $v_{NDE} = \varphi_{resp} \cdot k_{cat,resp} - v_{TCA}$ (TCA cycle gets priority, rest of φ_{resp} is used by NDE (mitochondrial external NADH dehydrogenase)).

The value of φ_{resp} is capped to φ_{resp}^{max} , to reflect the limited space for proteins on the membrane. Any proteome allocated to this sector above this value is ignored.

7 Trehalose synthesis

$$v_{trsn} = \varphi_{treh} \cdot k_{cat,trsn} \cdot \frac{C_{G6P}^{n_{treh,G6P}}}{K_{m,trsn,G6P}^{n_{treh,G6P}} + C_{G6P}^{n_{treh,G6P}}} \cdot \frac{C_{ATP}}{K_{m,trsn,ATP} + C_{ATP}}$$

UTP of the original model [37] has been replaced by ATP assuming thermodynamic equilibrium between these pools, i.e. it is assumed that the phosphorylation ratio of the uridylate and adenylate pools is quasi-constant, and that the adenylate pool is about 3.5 times as big as the uridylate pool [35].

8 Trehalose degradation

$$v_{trsn} = \varphi_{treh} \cdot k_{cat,trdg} \cdot \frac{c_{treh}}{K_{m,trdg,treh} + c_{treh}} \cdot \frac{c_{ATP}}{K_{m,trdg,ATP} + c_{ATP}}$$

9 Growth

$$\begin{aligned} \mu = \varphi_{grwt} \cdot k_{cat,grwt} \cdot & \frac{c_{ATP}^{n_{grwt,ATP}}}{K_{m,grwt,ATP}^{n_{grwt,ATP}} + c_{ATP}^{n_{grwt,ATP}}} \cdot \frac{c_{G6P}^{n_{grwt,G6P}}}{K_{m,grwt,G6P}^{n_{grwt,G6P}} + c_{G6P}^{n_{grwt,G6P}}} \\ & \cdot \frac{c_{FBP}^{n_{grwt,FBP}}}{K_{m,grwt,FBP}^{n_{grwt,FBP}} + c_{FBP}^{n_{grwt,FBP}}} \cdot \frac{c_{PYR}^{n_{grwt,PYR}}}{K_{m,grwt,PYR}^{n_{grwt,PYR}} + c_{PYR}^{n_{grwt,PYR}}} \cdot \frac{c_{NAD}^{n_{grwt,NAD}}}{K_{m,grwt,NAD}^{n_{grwt,NAD}} + c_{NAD}^{n_{grwt,NAD}}} \end{aligned}$$

10 Maintenance

$$v_{mtn} = k_{cat,mtn} \cdot \frac{c_{ATP}}{K_{m,mtn,ATP} + c_{ATP}}$$

4 Used parameter values

Table A2.2. Estimated k_{cat} parameters without multiplication ($k_{cat,i}$), multiplication factors and the final k_{cat} parameters estimated for each protein sector based on the proteome and fluxome of yeast in batch conditions [5,40].

Parameter	Value ($\text{mol}\cdot\text{Cmol}_x^{-1}\cdot\text{h}^{-1}$)	Origin
$K_{cat,upt}$	567.03	Fitted to proteome data of [5] and flux distribution of [40]
$K_{cat,uglc}$	223.07	Fitted to proteome data of [5] and flux distribution of [40]
$K_{cat,lglc}$	127.84	Fitted to proteome data of [5] and flux distribution of [40]
$K_{cat,ferm}$	229.1	Fitted to proteome data of [5] and flux distribution of [40]
$K_{cat,esnk}$	30.721	Fitted to proteome data of [5] and flux distribution of [40]
$K_{cat,resp}$	3.501	Fitted to proteome data of [5] and flux distribution of [40]
$K_{cat,trsn}$	5.919	Fitted to proteome data of [5] and flux distribution of [41]
$K_{cat,trdg}$	7.812	Fitted to proteome data of [5] and flux distribution of [41]
$K_{cat,grwt}$	0.578	Fitted to proteome data of [5] and flux distribution of [40]
$K_{cat,mtn}$	0.0155	[42]

Table A2.3. The values for the K_M as used in the model.

Parameter	Value	Origin
$K_{M,upt,S}$	$10.286 \text{ mol}\cdot\text{m}^{-3}$	Fitted to model of [34], multiplied by 10 to set residual glucose to realistic value in Crabtree experiment
$K_{M,upt,ATP}$	$0.4186 \text{ mol}\cdot\text{m}^{-3}$	Fitted to model of [34]
$K_{M,uglc,G6P}$	$1.9811 \text{ mol}\cdot\text{m}^{-3}$	Fitted to model of [34]
$K_{M,uglc,ATP}$	$0.1564 \text{ mol}\cdot\text{m}^{-3}$	Fitted to model of [34]
$K_{i,uglc,ATP}$	$1.68 \text{ mol}\cdot\text{m}^{-3}$	Fitted to model of [34]
$K_{M,lglc,FBP}$	$0.736 \text{ mol}\cdot\text{m}^{-3}$	Fitted to model of [34]
$K_{M,lglc,ADP}$	$0.27 \text{ mol}\cdot\text{m}^{-3}$	Fitted to model of [34]
$K_{M,lglc,Pi}$	$4.78 \text{ mol}\cdot\text{m}^{-3}$	Fitted to model of [34]
$K_{M,ferm,PYR}$	$0.866 \text{ mol}\cdot\text{m}^{-3}$	Fitted to model of [34]
$K_{M,ferm,NADH}$	$0.01\cdot C_{NADx}$	Arbitrarily chosen (much smaller than <i>in vivo</i> concentration)
$K_{M,esnk,FBP}$	$0.1648 \text{ mol}\cdot\text{m}^{-3}$	Fitted to model of [34]
$K_{M,esnk,NADH}$	$0.0352 \text{ mol}\cdot\text{m}^{-3}$	Fitted to model of [34]
$K_{M,mtn,ATP}$	$0.01\cdot C_{AxP}$	Arbitrarily chosen (ATP cannot be used if it is depleted)
$K_{M,resp,PYR}$	$0.8 \text{ mol}\cdot\text{m}^{-3}$	K_m of isolated mitochondria for pyruvate [56]
$K_{M,resp,NADH}$	$0.03 \text{ mol}\cdot\text{m}^{-3}$	NDI kinetics, [57], assuming that NDE has same K_M
$K_{M,resp,ADP}$	$0.01\cdot C_{AxP}$	Arbitrarily chosen (much smaller than <i>in vivo</i> concentration)
$K_{M,resp,Pi}$	$0.05 \text{ mol}\cdot\text{m}^{-3}$	Arbitrarily chosen (much smaller than <i>in vivo</i> concentration)
$K_{M,trsn,G6P}$	$0.973 \text{ mol}\cdot\text{m}^{-3}$	Fitted to model of [37]
$K_{M,trsn,ATP}$	$0.255 \text{ mol}\cdot\text{m}^{-3}$	Fitted to model of [37]
$K_{M,trdg,Treh}$	$5 \text{ mol}\cdot\text{m}^{-3}$	Fitted to model of [37]
$K_{M,trdg,ATP}$	$0.4186 \text{ mol}\cdot\text{m}^{-3}$	Fitted to model of [37]
$K_{M,grwt,ATP}$	$0.75\cdot C_{AxP}$	Arbitrarily chosen so that μ is sensitive in energy charges around 0.8
$K_{M,grwt,G6P}$	$0.35 \text{ mol}\cdot\text{m}^{-3}$	Arbitrarily chosen (much smaller than <i>in vivo</i> concentration)

$K_{M,grwt,FBP}$	$0.02 \text{ mol}\cdot\text{m}^{-3}$	Arbitrarily chosen (much smaller than <i>in vivo</i> concentration)
$K_{M,grwt,PYR}$	$0.2 \text{ mol}\cdot\text{m}^{-3}$	Arbitrarily chosen (much smaller than <i>in vivo</i> concentration)
$K_{M,grwt,NAD}$	$0.01 \cdot C_{NADx}$	Arbitrarily chosen (much smaller than <i>in vivo</i> concentration)

Table A2.4. Miscellaneous parameter values used in the model.

Parameter	Value	Origin
$C_{Glc,in}$	$41.67 \text{ mol}\cdot\text{m}^{-3}$ (7.5 g/l)	[19]
$C_{x,in}$	0	Sterile medium
$C_{EtOH,in}$	0	No ethanol in medium
$C_{glyc,in}$	0	No glycerol in medium
ρ_x	$26656 \text{ mol}_x\cdot\text{m}^{-3}$	Derived from [58] and [59] assuming 1 mol biomass weighs 24.6 g _x
C_{AxP}	$8.28 \text{ mol}\cdot\text{m}^{-3}$	[19]
C_{NADx}	$1.46 \text{ mol}\cdot\text{m}^{-3}$	[19]
$n_{uglc,ATP}$	2	Fitted to model of [34]
$n_{treh,G6P}$	1.58	Fitted to model of [37]
$n_{ferm,PYR}$	1.9	Fitted to model of [34]
$n_{ferm,NADH}$	25	Arbitrarily chosen (large value for sharp sigmoid)
$n_{resp,ADP}$	25	Arbitrarily chosen (large value for sharp sigmoid)
$n_{resp,Pi}$	25	Arbitrarily chosen (large value for sharp sigmoid)
$n_{grwt,ATP}$	25	Arbitrarily chosen so that μ is sensitive in energy charges around 0.8 (assuming that the “safety valves” have not been triggered)
$n_{grwt,G6P}$	10	Arbitrarily chosen (large value for sharp sigmoid)
$n_{grwt,FBP}$	10	Arbitrarily chosen (large value for sharp sigmoid)
$n_{grwt,PYR}$	10	Arbitrarily chosen (large value for sharp sigmoid)
$n_{grwt,NAD}$	25	Arbitrarily chosen (large value for sharp sigmoid)
φ_{upt}^{max}	0.016	Arbitrarily chosen, as twice the uptake sector in the proteome data from [5]
φ_{resp}^{max}	0.12	Arbitrarily chosen to match the oxygen consumption of [45]

5 Objective function

Under steady-state conditions, the minimization of the residual substrate concentration was used as objective function. Under dynamic conditions, the minimization of a time-weighted average substrate concentration was used, to promote fast consumption of available substrate, therefore selecting for competitive proteomes:

$$\frac{\int_0^{t_{cycle}} c_s \cdot t \, dt}{\int_0^{t_{cycle}} t \, dt}$$

6 Comparison of predicted flux distribution to experimental flux distribution

The k_{cat} parameters were calculated by estimating the fluxes that were obtained at half-saturation conditions with the experimental batch proteome [5]. This is done with a proteome model in which all k_{cat} parameters equal one. Subsequently, the factor between these fluxes and the experimental flux distribution of [40] is defined as the k_{cat} parameter for the corresponding reaction.

When the obtained parameters are used to simulate a chemostat experiment at a dilution rate of 0.4 h^{-1} the cells reach an unstable state because the flux capacity is not sufficient. This was assumed to be a result of both the conditions under which the parameters were estimated and the possibility of reserve flux capacity in the actual yeast proteome. The concentrations used for the estimation might be too low, as it is likely that the cells operate closer to saturation conditions when growing at the maximum growth rate. To correct the flux capacity and to enable accurate reproduction of the flux distribution of [40], the estimated k_{cat} parameters are increased with specific factors (Appendix 1), except for the k_{cat} for maintenance. These factors are found with a multi-start optimization aimed at minimizing the difference between the simulated fluxes and the flux distribution of [40]. The result of simulating a chemostat experiment at a dilution rate of 0.4 h^{-1} with the new k_{cat} parameters shows that the model can now successfully simulate an experiment with the experimental proteome allocation.

7 Comparison of steady state model with experimental data at different dilution rates

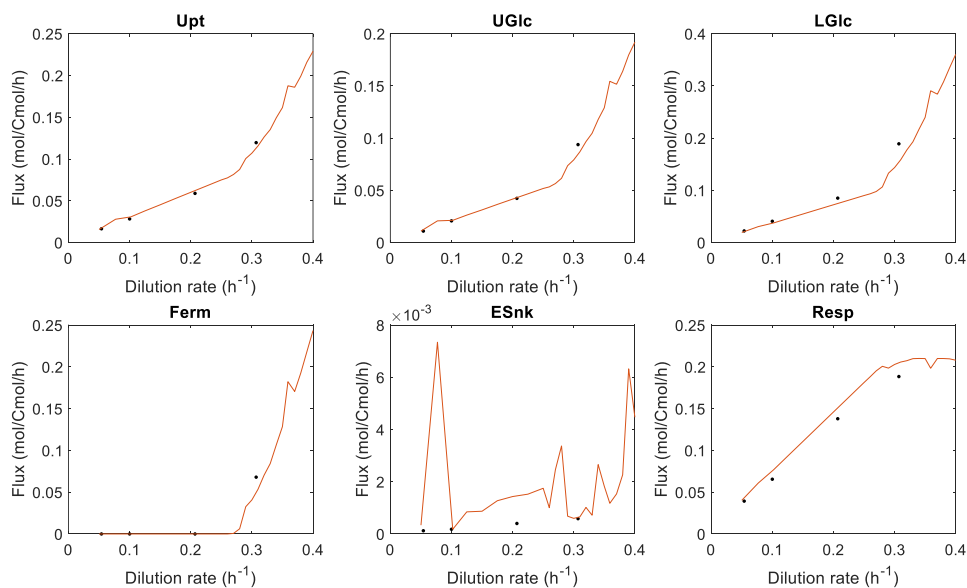


Figure A2.2. Comparison of simulated steady-state fluxes at different dilution rates (orange line) with experimental data from [35] (black points). Upt, uptake; UGlc, upper glycolysis; LGlc, lower glycolysis; Ferm, fermentation; ESnk, electron sink/glycerol pathway; Resp, respiration

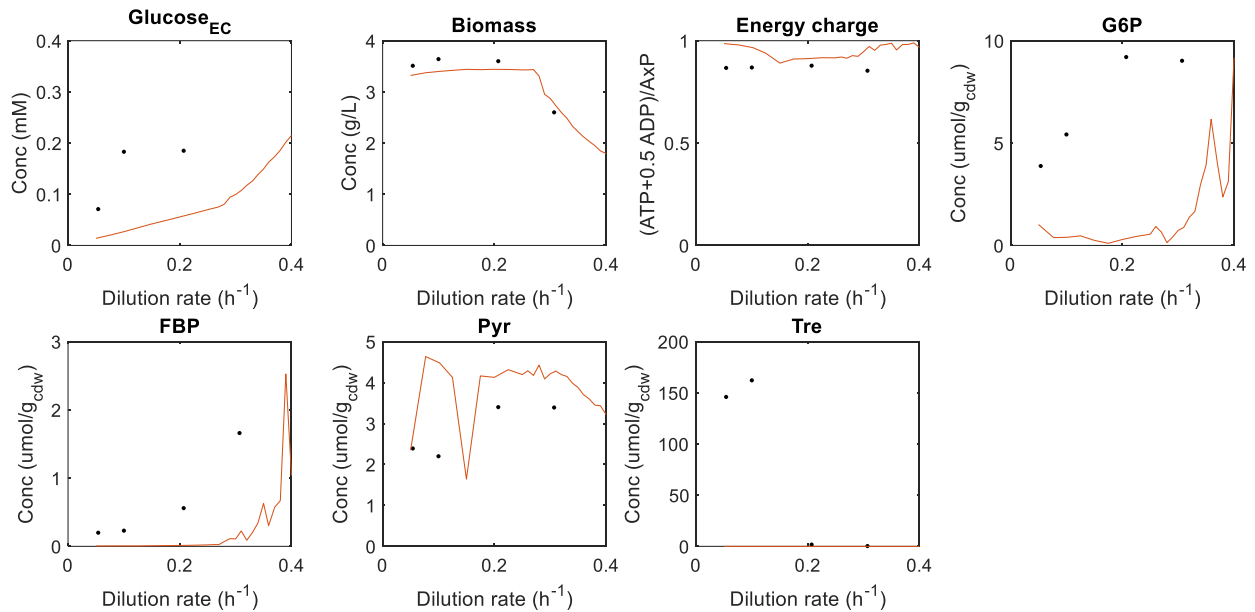


Figure A2.3. Comparison of simulated steady-state fluxes at different dilution rates (orange line) with experimental data from [35] (black points).

8 Sensitivity analysis of steady state model at different dilution rates

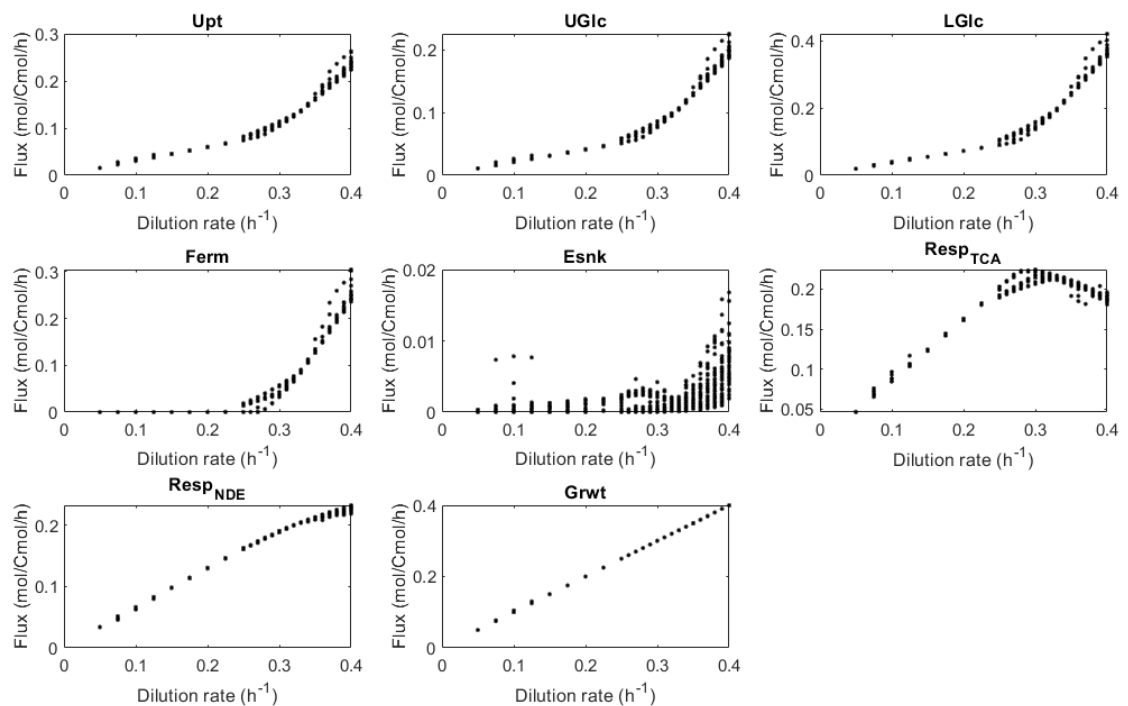


Figure A2.4. Sensitivity analysis of fluxes through each sector at different steady-state dilution rates. Per dilution rate, 40 simulations were evaluated. Especially around the critical dilution rate of 0.28 h⁻¹, when the Crabtree effect occurs, variability with respect to respiration and fermentation is present, but overall limited variability is present in the fluxes of optimized proteomes.

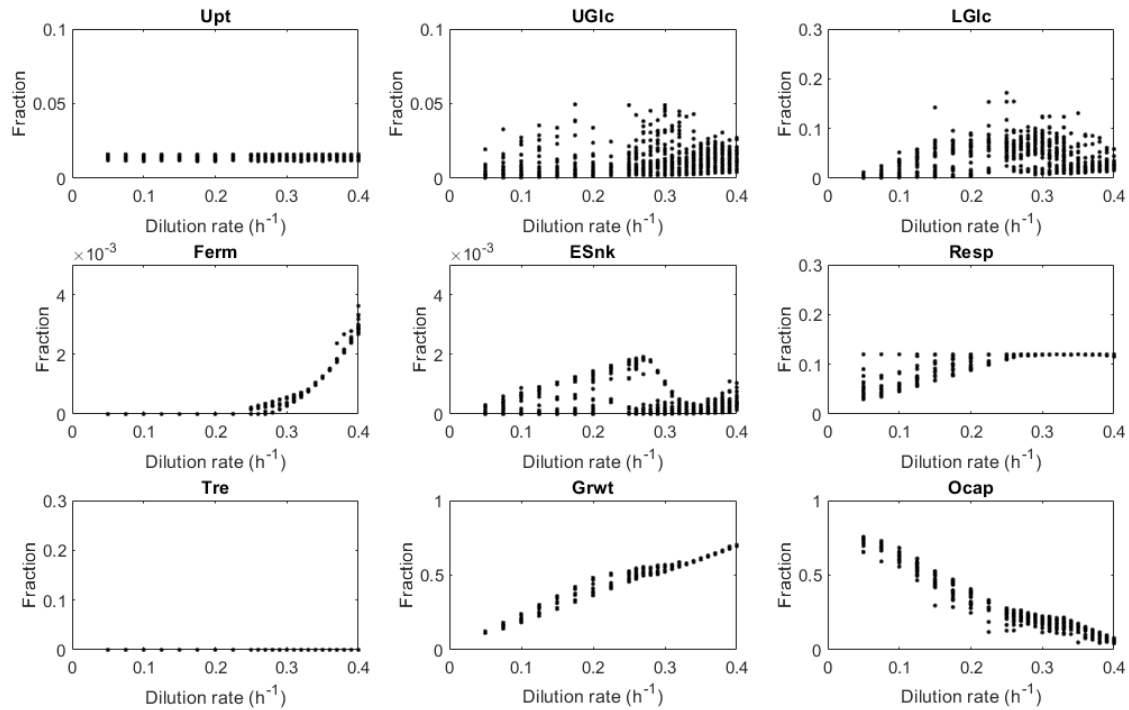


Figure A2.5. Sensitivity analysis of fluxes through each sector at different steady-state dilution rates. Per dilution rate, 40 simulations were evaluated. High variability is especially present in the lower glycolysis and respiration sectors, significantly affecting the amount of overcapacity present. This high variability does however not appear to have a large impact on the fluxes (Figure A2.4)

9 Optimized proteome sector sizes at increasing feast/famine perturbation strength

Table A2.5. The optimized proteome sector sizes at increasing perturbation strength. The perturbation strength is expressed as the feeding time over the cycle time (TF/TC); a TF/TC of 1 is equal to chemostat, 0.05 is equal to an experimental pulse perturbation strength of a feast/famine cycle [19]. Upt = Uptake, UGlc = Upper Glycolysis, LGlc = Lower Glycolysis, Ferm = Fermentation, ESnk = Electron sink/glycerol pathway, Resp = Respiration, TrSn = Trehalose synthesis, TrDg = Trehalose degradation, Grwt = Growth, Strc = Structural sector, Ocap = Overcapacity

TF/TC	Upt	UGlc	LGlc	ESnk	Ferm	Resp	Tre	Growth	Strc	Ocap
1	0.0139	0.0035	0.004	0	0.0002	0.0535	0	0.2199	0.0625	0.6425
0.5	0.0154	0.0063	0.023	0.0005	0.0002	0.1141	0.002	0.3162	0.0708	0.4516
0.2	0.016	0.0023	0.0384	0.0002	0.0006	0.12	0.0045	0.5627	0.0618	0.1934
0.1	0.016	0.0061	0.0573	0.0031	0.0005	0.12	0.001	0.6951	0.0618	0.0391
0.05	0.016	0.0091	0.0585	0.0089	0.001	0.12	0.0013	0.7205	0.0592	0.0055
0.025	0.0136	0.0092	0.0471	0.0143	0.0006	0.12	0.0008	0.7193	0.0618	0.0134
0.0125	0.0134	0.009	0.0395	0.0063	0.0007	0.1197	0.0014	0.7379	0.0618	0.0102

10 The ratio of upper over lower glycolysis and its effect on the stability of the glycolytic pathway

The phosphate 'deadlock', described by [22] to be dependent on the intracellular concentrations of Pi and FBP, is hypothesized (next to the trehalose cycle) to be additionally regulated by adaption within glycolysis. Specifically, the ratio between the capacity of upper vs lower glycolysis is considered. By increasing the capacity of lower glycolysis over upper glycolysis, the ATP supply should be restored more quickly, without complete depletion of Pi. This effect was demonstrated by changing the size of the lower glycolysis sector in a proteome, optimized for feast/famine conditions (Figure S6). Using the energy charge, it is observed that proteomes larger lower glycolysis sector have are able to maintain a higher energy charge throughout the cycle, however, it appears that the effect on the stability of glycolysis, as indicated by G6P, FBP and Pi, is limited.

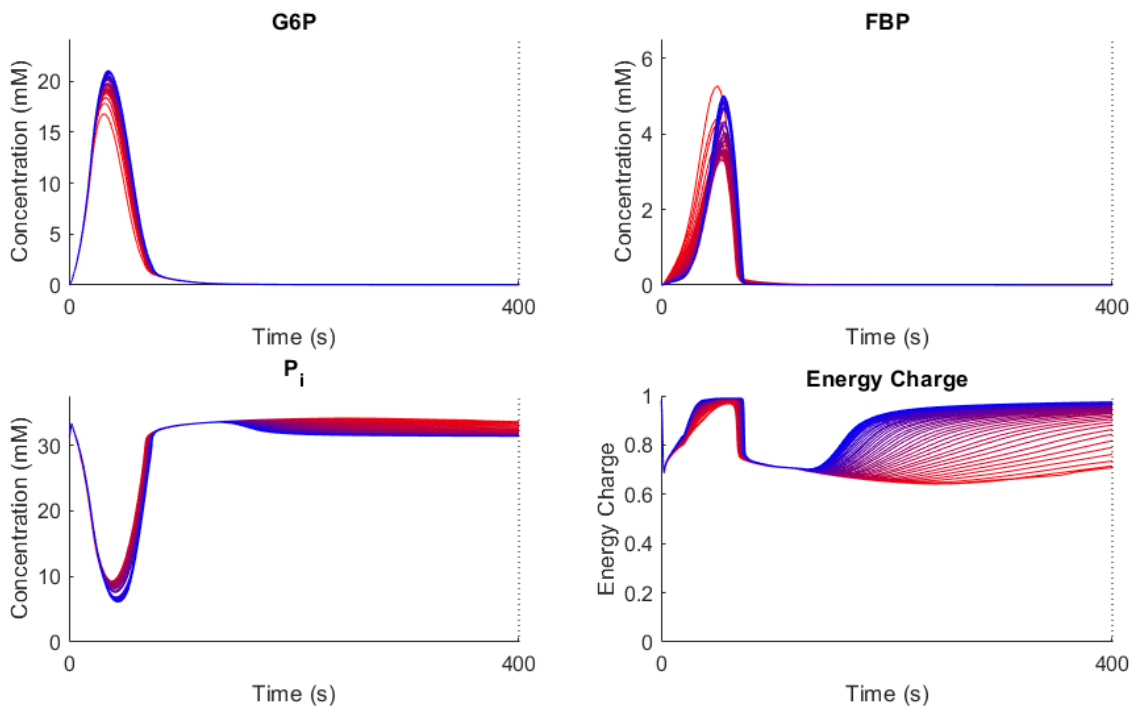


Figure A2.6. The extra- and intracellular metabolite profiles of proteomes with a upper glycolysis/lower glycolysis ratio between 1/10 (blue) to 1/100 (red).

11 Protein categorisation

The proteome datasets are sorted in the same nine sectors that are used in the proteome-dependent kinetic model. The complete datasets are sorted based on protein names and keywords with the use of MATLAB 2020b. First, specific proteins are sorted out based on their protein name. Secondly, the remaining proteins are sorted based on keywords are sorted based on the KEGG Pathway names, the GOMF names and the GOMB names [54,55].

Table A2.6. Proteins and proteins groups from KEGG sorted to their respective protein sectors defined in the model.

Sector	Proteins/Protein groups
Upt	HXK, GLK, HXT
UGlc	PGI, FBP, PFK
LGlc	FBA, TPI, TDH, PGK, GPM, ENO, PYK, PCK
Ferm	PDC, ADH
ESnk	GPD, HOR, RHR
Resp	PYC, PDA, PDB, PDX, LPD, CIT, MDH, ACO, MLS, ICL, IDH, IDP, SDH, LCS, FUM, KGD, LPD, LAT, ALD, ACS, TCA Cycle, Oxidative phosphorylation
Treh	PGM, TPS, GSY, NTH, ATH, GPH
Grwt	Genetic Information Processing, Amino acid metabolism, Metabolism of other amino acids, Lipid metabolism, Metabolism of cofactors and vitamins, biosynthesis, Nucleotide metabolism, Cytoskeleton, Biosynthesis, Transcription, Cell cycle, DNA, Metabolism, Pentose Phosphate pathway, Ribosome, RNA, SNARE, Proteasome, Cytoskeleton, Structural, Cell wall, Translation, Biogenesis, Reproduction, Assembly, Golgi
Struc	HSP, HRI, PKR, PERK, GCN2, YBH, RCK, RQC, RCN, LSM, PIL, TMA, RDL, RTN, PST, STM, Not Included in Pathway or Brite, Environmental Information Processing, Cellular Processes, Signaling, Protein kinases, Protein phosphatases, Peptidases, Glycosyltransferases, Protein families: signaling and cellular processes, Organismal Systems, Stress, maintenance

4

A dive into yeast's sugar diet – Comparing the metabolic response of glucose, fructose, sucrose & maltose under dynamic feast/famine conditions

K. J. A. Verhagen, I.H. Pardijs, H.M. van Klaveren and S. A. Wahl

Abstract

The impact of substrate gradients on the microbial physiology has been studied for glucose but not other common carbohydrates that partly have different transport mechanisms that could trigger a different intracellular response. Here we show a comprehensive comparison of four different sugars, glucose, fructose, sucrose and maltose. Both mono-saccharides are transported via facilitated diffusion by transporters of the HXT family. For the disaccharides, maltose and sucrose follow different mechanisms. Maltose is transported by active transport and hydrolyzed intracellularly, while sucrose is hydrolyzed extracellularly and the resulting monosaccharides are imported. To explore the impact of the carbon source and the impact of large-scale gradients, steady-state and dynamic feast/famine cultivation conditions were compared with regards to physiology, the intracellular metabolome as well as the proteome, generating a comprehensive dataset for future modelling efforts.

Especially, gradients of maltose lead to a significant decrease in biomass yield while *Saccharomyces cerevisiae* could cope well with gradients in glucose, fructose and sucrose. Although the physiology was very comparable for these sugars, the intracellular metabolome as well as proteome responded differently. Especially, the concentration of upper glycolytic enzymes decreased for glucose and maltose, while an increase was observed for sucrose and fructose when exposed to gradients. Nevertheless, for all conditions a surprising stable energy-charge was observed between 0.78 and 0.89, which is significantly different to results from single-pulse experiments or limitation to excess shifts where for example maltose-accelerated death was observed. These differences highlight the importance to study metabolism under close-to large-scale conditions to obtain representative physiology and kinetics.

Introduction

While glucose is commonly used as only carbon source for research at lab-scale, this is rarely the case in large-scale industrial processes. Under industrial conditions, more complex feedstocks are utilized, that are derived from plant material. Clearly, a more complex feedstock with several carbon sources will lead to a different metabolic response compared to glucose. Four substrates will be considered in this chapter: the mono-saccharides glucose and fructose, and the di-saccharides sucrose and maltose. These substrates were selected based on the (1) different transport mechanisms, i.e. passive and active (2) slightly different entry points and (3) different signaling pathway responses. With these differences, glycolysis is expected to be perturbed in different ways: On the one hand different substrate stimulus as transport will determine the pulse strength, on the other hand differential regulatory expression of glycolytic enzymes.

The two mono-saccharides with the composition $C_6H_{12}O_6$, glucose and fructose are very similar substrates. Both are imported into the cell by one of the Hxt transporters, with Hxt1, Hxt3 and Hxt7 being the most relevant [1–3]. Intracellularly, both glucose and fructose are further metabolized by the phosphorylation through hexokinase to G6P and F6P respectively. Here, for both, Hxk2 is the major paralog for this reaction. Glucose can also be converted by glucokinase (Glk1) [4]. Under low substrate conditions, a high affinity for the sugars is observed for the transport of glucose ($K_M = 1.5$ mM) and fructose ($K_M = 6$ mM) into the cell. Consequently, slightly higher residual substrate concentrations were observed for *S. cerevisiae* grown in chemostat on fructose compared to glucose due to this difference in affinity, however similar yields of biomass were obtained [5]. Under high substrate concentrations, a low-affinity uptake system is in place, with $K_M = 20$ mM and $K_M = 40$ mM for glucose and fructose respectively [4].

The catabolism of the disaccharides has several differences in terms of uptake steps. For sucrose, the first step is the hydrolysis of sucrose to equimolar amounts of glucose and fructose, catalyzed by invertase [6] (see Figure 4.1). Invertase is encoded by genes from the *SUC* family, with *SUC2* the most common one. The invertase enzyme encoded by *SUC2* can occur in two locations. The glycosylated variant is in the periplasmic space, where it can hydrolyze extracellular sucrose to glucose and fructose. The non-glycosylated version of invertase remains in the cytoplasm of the cell. Strains that do not have an active *SUC2* gene are still able to consume sucrose at a basal level. This is most likely through maltases, encoded for by the *MAL*-gene family, which are also in the cytoplasm. Transport of sucrose into the cytoplasm is facilitated by active transport through Agt1 or maltose permeases [7–9].

Maltose is a disaccharide consisting of two 1,4- α interlinked glucose molecules [10]. In contrast to glucose and fructose, maltose is transported by an active transport mechanism, the maltose-proton symporter. Then, maltose is hydrolyzed intracellularly to two glucose molecules by α -glucosidase or 'maltase' [11,12] (see Figure 4.1). The difference in uptake results in a net loss of 1 ATP per mol maltose compared to a mol of glucose, as the proton needs to be exported again at the expense of ATP. Weusthuis et al. [13] reported a 25% decrease in biomass yield of *Saccharomyces cerevisiae* when grown anaerobically on maltose compared to glucose. However, aerobically, this effect is minor [14].

S. cerevisiae has been reported to be (hyper-)sensitive to sudden changes in the extracellular maltose concentration [15]. This phenomenon, also known as 'maltose accelerated death', was described as the unrestricted uptake of maltose, resulting in accumulation of glucose and protons and eventually cell death [16]. This phenomenon was observed for extracellular maltose concentrations larger than 50 mM [15].

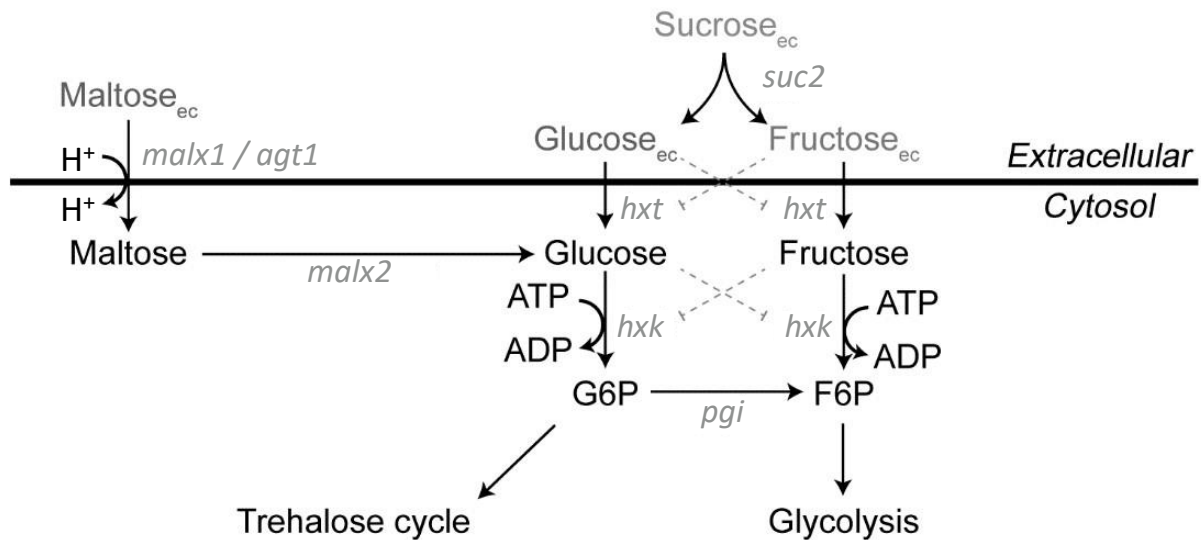


Figure 4.1. Schematic overview of the uptake of glucose, fructose and maltose, as well as the extracellular hydrolysis of sucrose in *S. cerevisiae*, coupled to reactions and pathways in central carbon metabolism. Here *malx1* represents *mal11*, *mal21*, *mal31*, *mal41* and *mal61*; *malx2* represents *mal12*, *mal22*, *mal32*, *mal42* and *mal62*.

Regulatory mechanisms in *S. cerevisiae*

Metabolism is regulated at different cellular levels, which have significantly different response times. Allosteric activation or inhibition of the enzyme reaction, or post-translational modification are very fast mechanisms which can react to sudden changes in environmental conditions. In contrast, adjustment of the enzyme concentration by gene expression (regulation) requires much more time. This gene regulation mechanism is controlled via multiple regulatory pathways [17–22]. In these pathways, the nutrients are both substrate and signal molecule, activating the first steps of the signalling pathways. In general, glucose is a preferred substrate in yeast, controlling not only its own use, but also the consumption of other carbon sources. This process, called glucose repression, results in a preferential consumption of glucose over other present saccharides, such as sucrose, fructose, or maltose [19,21–24].

Apart from repression of the consumption of other substrates, cell growth is also regulated by glucose sensing via protein kinase A (PKA) in many *S. cerevisiae* strains. Particularly, PKA is described to regulate the expression of proteins involved in biomass synthesis, such as ribosomes [18,19,22,25]. A major signalling cascade leading to the activation of PKA is controlled by cyclic AMP (cAMP), the Gpr1/Gpa2 and Ras proteins [17–19,26]. The Gpr1p-Gpa2p signalling system is stimulated by the presence of different substrates, and in turn affects the activity of adenylyl cyclase. As these proteins have different affinities for each sugar, a different response from this signalling system is expected. Especially, there is a higher affinity for sucrose compared to glucose, and the system is basically insensitive to the presence of fructose [27].

The signalling response of cAMP in *S. cerevisiae* upon a switch from ethanol to different sugar carbon sources showed a similar response for glucose and sucrose, while for maltose no significant cAMP response was found. For fructose, a lower response, half the size of glucose and sucrose was observed [28]. This also indicates that these different sugar substrates produce very different responses compared to each other. The exact mechanism linking this signalling cascade to cell growth in response to sugar levels however is still unknown [18,19]. Additionally, CEN.PK113-7D, the strain used in this study, lacks the ability to produce cAMP [29]. The mechanism through which PKA is activated in this strain is therefore still unknown.

Results & Discussion

In this work, we used metabolomics and proteomics, as well as dynamic flux estimations to analyze the effect of different substrate transport mechanisms and substrate signaling pathways under dynamic conditions with four different sugars as substrates: glucose, fructose, sucrose, and maltose. Especially we determined: 1) Average metabolic rates and yields under both steady-state and feast/famine conditions, 2) the dynamic metabolic response during a feast/famine cycle, and 3) the changes in the proteome composition after adaptation to feast/famine conditions. Specifically, the chemostat was sampled after 5 residence times (50 h), to ensure that a steady-state was achieved. Similarly, the feast/famine cycle was sampled after 5 residence times (corresponding to 50 h or ~450 400s cycles). A schematic overview of this is shown in Figure 4.2.

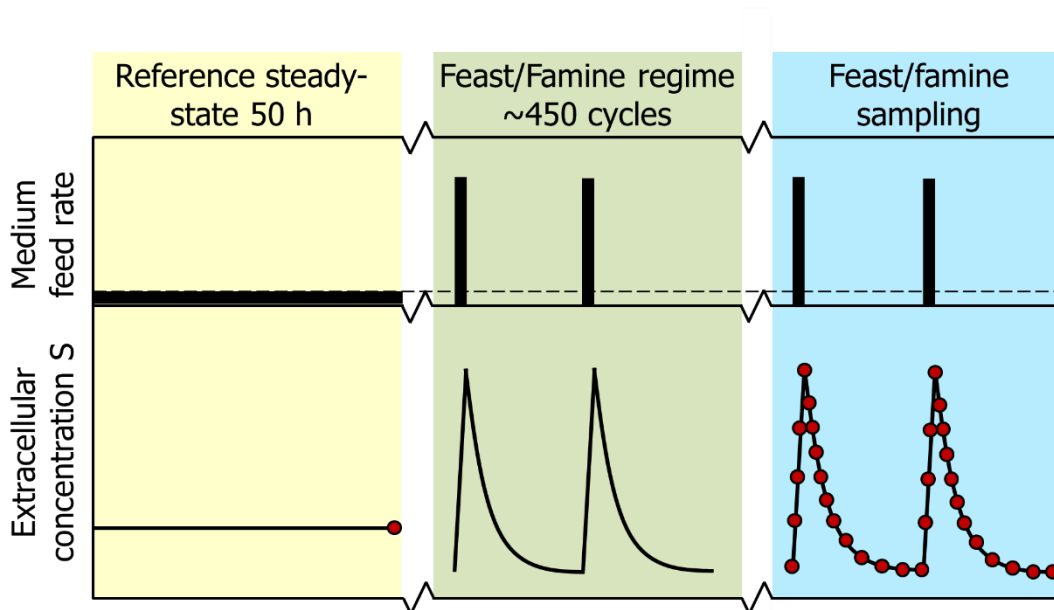


Figure 4.2. Profile of the experimental feeding regime. After a chemostat phase (reference steady-state) of 50 h, a block-wise feed is applied in a 400 s cycle at the same average substrate supply and dilution rate for another 50 h (adapted from [13]). At the top, a schematic overview of the feed rate during chemostat and feast/famine regimes is shown. At the bottom, the resulting extracellular substrate concentration profile in the fermentation broth is shown. Sampling time points are shown as red dots.

All cellular responses were compared with respect to differences in feeding condition (steady-state vs. feast/famine) and used sugar sources. The results are structured by analyzing (1) the extracellular environment, (2) the average phenotype and then (3) metabolic and proteomic responses. Note that all cultures and conditions were performed with the same amount of substrate (in terms of moles of carbon) and water per time, resulting in the same growth rate for all conditions and carbon sources.

Substrate in the extracellular environment

The extracellular sugar concentrations were measured under both steady-state and feast/famine (FF) conditions after 5 residence times, allowing the cells to adapt to the imposed feeding regime (see Figure 4.2). For the monosaccharides, a significant difference can be observed: for fructose a much higher residual sugar concentration under both the steady-state ($Frc/Glc = 4.7$ fold) and the feast/famine ($Frc/Glc = 5.8$ fold) condition are observed. This difference in residual sugar concentration can be explained by differences of the affinities of hexose transporters which are much higher for glucose ($K_M = 1.5$ mM) compared to fructose ($K_M = 6$ mM) [4]. As a consequence, the relative changes in concentration during the feast famine cycle were lower under fructose conditions ($max/min Frc = 1.8$ compared to $max/min Glc = 4.9$), which may result in a milder intracellular metabolic response.

For the disaccharides, the transport mechanisms are very different. Using sucrose feeding, it can be observed that the fed sucrose is immediately converted into glucose and fructose by invertase leading to a residual sucrose concentration of less than 0.01 mM. Comparable to the respective monosaccharide cultivations, the difference in affinity for glucose was higher, i.e. at steady-state, the residual fructose concentration was 1.5 fold higher than glucose.

Strikingly, while the residual glucose concentration at the end of the cycle with sucrose feeding was very similar to conditions with glucose as only substrate, the residual fructose concentration was far lower compared to conditions with only fructose. This indicates that the affinity for fructose increased under conditions with sucrose as substrate. While this may be explained by a lower transport rate (about half), this effect was not found for glucose.

With maltose as substrate, no extracellular hydrolysis was observed. Rather, the extracellular maltose concentration appeared to follow a similar profile as under glucose conditions. Furthermore, similar to the glucose conditions, a higher affinity for maltose under feast/famine condition compared to the steady-state was visible. Similar (glucose equivalent) residual sugar concentrations were observed under both steady state ($Mal_{glc,eq}/Glc = 1.1$) and feast/famine ($Mal/Glc = 0.8$) conditions. Relative changes however were observed to be slightly larger under maltose conditions ($max/min Mal = 6.2$ compared to $max/min Glc = 4.9$). However, a faster decrease was observed for the glucose concentration during feast/famine cycles, with substrate uptake reaching zero after 350 s, while maltose was still decreasing at that timepoint. This indicates that the initial glucose uptake rate was higher compared to the maltose uptake.

Uptake rate estimation

While steady-state uptake rates were very comparable between the different sugars (see Table 4.1), a very different picture is observed for the dynamic uptake rates during the feast/famine cycles (Figure 4.3).

To quantitatively compare the transport of sugars into the cell under feast/famine conditions, a piecewise affine (PWA) rate approximation was calculated based on the concentration measurements. The timepoints 0, 15, 80, 220 and 400 s were used as breakpoints [30,31]. Furthermore, the first and last timepoints were coupled to reflect the cyclic nature of the imposed feeding regime (see Figure 4.3). The breakpoints were manually selected as they resulted in the lowest sum of residual squares (SSR) over all different conditions.

For the monosaccharides, clear differences in the uptake rate dynamics were observed. As expected, based on the lower affinity (higher K_M), the fructose uptake rate changed less pronounced compared to the glucose uptake rate during the cycle. The maximum for glucose was $1.46 \mu\text{mol}_{glc,eq}/\text{g}_{cdw}/\text{s}$ compared to $0.80 \mu\text{mol}_{glc,eq}/\text{g}_{cdw}/\text{s}$ for fructose, nearly a two-fold difference. On the other hand,

fructose was consumed over the whole cycle, while the glucose uptake was basically stopped after 360 s.

Under sucrose conditions, a very high invertase rate was observed, i.e. there was no residual sucrose measured during any time point of the cycle. This was different for the invertase products, glucose and fructose, here a peak uptake rate of $0.45 \mu\text{mol}_{\text{glc,eq}}/\text{g}_{\text{cdw}}/\text{s}$ was observed which dropped to $0.25 \mu\text{mol}_{\text{glc,eq}}/\text{g}_{\text{cdw}}/\text{s}$ at the end of the cycle. These rates did thus not follow the profiles of the respective monomer cultivations, where the uptake dropped to zero towards the end of the cycle, indicating that the presence of sucrose has a significant effect on the overall sugar transport into the cell.

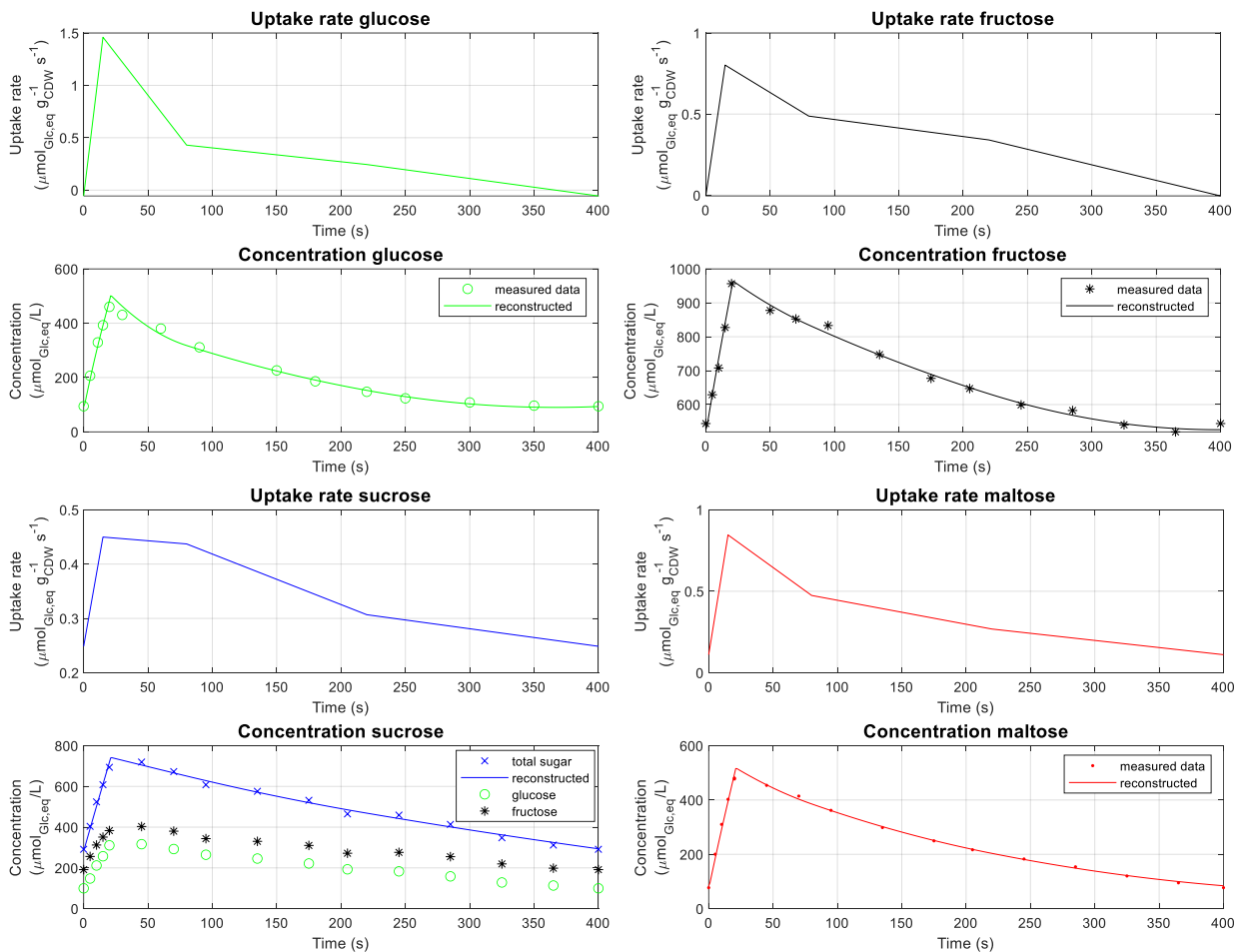


Figure 4.3. Estimation of the sugar uptake rates in $\mu\text{mol}/\text{g}_{\text{cdw}}/\text{s}$ (in glucose equivalents, i.e. 1 mol maltose = 2 mol glucose equivalents) and measured extracellular sugar concentrations over one 400s cycle during four different cultivation conditions: Glucose, fructose, sucrose and maltose as substrates. The estimation of the uptake rates is based on a piece-wise linear function approximation. Due to the cyclic nature of the feast/famine regime, the first point of the cycle at 0 s corresponds to the last point at 400 s.

Surprisingly, the maltose uptake rate, which is catalyzed by an active proton symport, was lower compared to glucose (diffusion). The maximum reached was $0.85 \mu\text{mol}_{\text{glc,eq}}/\text{g}_{\text{cdw}}/\text{s}$, only about 60% of the glucose uptake maximum. Additionally, maltose transport continued up until the end of the cycle, maintaining a minimum uptake rate of $0.11 \mu\text{mol}_{\text{glc,eq}}/\text{g}_{\text{cdw}}/\text{s}$.

Average biomass specific rates and yields

Under steady state conditions, a growth rate of 0.1 h^{-1} was achieved for all different sugars. In table 4.1, the rates and yields under steady-state and feast/famine conditions have been summarized for each of the four substrates. At this growth rate, no significant differences were observed between the different sugars at steady-state.

Looking into the differences between steady-state and feast/famine feeding, small differences are observed for most sugars. Under glucose conditions there is a small decrease in biomass yield (-3 %), with only minor differences in overall rates. Comparable to glucose, there were only slight decreases in biomass yield under fructose and sucrose conditions. For maltose however, a more significant decrease in biomass yield (-8%) and an increase in respiratory activity (+13%) were observed for feast/famine conditions as compared to steady-state. This decrease in yield, coupled with an increase in respiration, indicates that more ATP may be consumed in a futile cycle or stress response. It has been reported that a culture grown under maltose-limited conditions was unable to cope with a pulse of maltose (Postma et al., 1989). This phenomenon, called maltose-accelerated death, results in a significant accumulation of maltose inside the cell, which, when converted into glucose, can no longer be processed by hexokinase, due to insufficient capacity, leading to a high intracellular osmotic pressure. In addition, the cell is acidified by the large influx of protons due to the unregulated maltose transport. These two factors subsequently lead to cell death [15].

Putatively, in the case of a maltose feast/famine regime a large part of the imported maltose is directly funneled through the trehalose cycle to prevent this phenomenon from occurring. Additionally, the transport seems less active compared to continuously limited conditions. This topic will be further discussed during the analysis of the intracellular metabolomics and proteomics.

Table 4.1. Reconciled average biomass specific rates and yields for steady-state and feast/famine conditions with different sugars as substrate. Standard deviation was calculated from three biological replicates. The relative changes between steady-state and feast/famine conditions are given in the last column.

Glucose			
Rate/Yield	Steady-state	Feast/Famine (averaged over cycle)	Change (%)
$-q_s$ (mCmol · g _X ⁻¹ · h ⁻¹)	6.89 ± 0.21	7.06 ± 0.07	2
μ (h ⁻¹)	0.101 ± 0.0002	0.100 ± 0.0006	0
$-q_{O_2}$ (mmol · g _X ⁻¹ · h ⁻¹)	2.67 ± 0.21	2.70 ± 0.04	1
q_{CO_2} (mCmol · g _X ⁻¹ · h ⁻¹)	2.85 ± 0.21	2.80 ± 0.05	-2
C_X (g _X · L ⁻¹)	3.64 ± 0.16	3.46 ± 0.17	-4
$Y_{X/S}$ (g _X /g _S)	0.49	0.47	-3
Fructose			
Rate/Yield	Steady-state	Feast/Famine (averaged over cycle)	Change (%)
$-q_s$ (mCmol · g _X ⁻¹ · h ⁻¹)	6.84 ± 0.12	7.07 ± 0.18	3
μ (h ⁻¹)	0.104 ± 0.0007	0.098 ± 0.0009	0
$-q_{O_2}$ (mmol · g _X ⁻¹ · h ⁻¹)	2.75 ± 0.14	2.58 ± 0.16	-6
q_{CO_2} (mCmol · g _X ⁻¹ · h ⁻¹)	3.12 ± 0.09	3.01 ± 0.15	-4
C_X (g _X · L ⁻¹)	3.63 ± 0.07	3.51 ± 0.04	-3
$Y_{X/S}$ (g _X /g _S)	0.49	0.47	-3
Sucrose			
Rate/Yield	Steady-state	Feast/Famine (averaged over cycle)	Change (%)
$-q_s$ (mCmol · g _X ⁻¹ · h ⁻¹)	7.00 ± 0.09	7.23 ± 0.22	3
μ (h ⁻¹)	0.101 ± 0.0004	0.100 ± 0.0003	0
$-q_{O_2}$ (mmol · g _X ⁻¹ · h ⁻¹)	2.77 ± 0.14	2.81 ± 0.10	1
q_{CO_2} (mCmol · g _X ⁻¹ · h ⁻¹)	3.05 ± 0.13	3.11 ± 0.08	2
C_X (g _X · L ⁻¹)	3.55 ± 0.11	3.45 ± 0.02	-3
$Y_{X/S}$ (g _X /g _S)	0.50	0.48	-3
Maltose			
Rate/Yield	Steady-state	Feast/Famine (averaged over cycle)	Change (%)
$-q_s$ (mCmol · g _X ⁻¹ · h ⁻¹)	6.99 ± 0.06	7.61 ± 0.04	9
μ (h ⁻¹)	0.099 ± 0.0008	0.100 ± 0.0005	0
$-q_{O_2}$ (mmol · g _X ⁻¹ · h ⁻¹)	2.87 ± 0.13	3.24 ± 0.08	13
q_{CO_2} (mCmol · g _X ⁻¹ · h ⁻¹)	3.12 ± 0.12	3.58 ± 0.11	15
C_X (g _X · L ⁻¹)	3.57 ± 0.07	3.27 ± 0.03	-8
$Y_{X/S}$ (g _X /g _S)	0.48	0.44	-8

Intracellular metabolite dynamics

Based on the observed changes in the uptake rate dynamics for the different sugars (Table 2), differences in intracellular metabolite concentrations in time were expected. To this end, metabolites of the central carbon metabolism were quantified for both steady-state and feast/famine conditions for the different sugar substrates.

Glycolysis and trehalose cycle

With glucose as substrate, the concentrations of metabolites of the upper glycolysis, such as glucose-6-phosphate (G6P), increased rapidly, reaching its maximum concentration 60 s after the start of the cycle, delayed compared to the maximum extracellular glucose concentration at 20 s [32] (see Table 4.2 and Figure 4.4). Similarly, a peak was observed for fructose-1,6-bisphosphate (FBP) at 60 s, which then decreased following G6P. In the lower glycolysis, 3PG showed a minor increase during the first 20 seconds after the pulse, followed by a sharp decrease until 60 s, at which point it increased again. This behavior is inverse to the profile of FBP, and can be explained by the allosteric activation by FBP of the last (rate-limiting) step of the lower glycolysis, pyruvate kinase [33]. Towards the end of the cycle, after 220 s, the 3-phosphoglycerate (3PG) concentration decreased again, likely caused by the fact that glucose uptake was significantly decreased after this point.

Table 4.2. Comparison of selected metabolic concentrations and fluxes during feast/famine conditions for the different sugars. Peaks are defined as the highest concentration measurement during a cycle.

Glucose			
Metabolite	Max/min ratio	Time peak concentration (s)	Fold change average FF vs SS
Extracellular glucose	4.88	20	1.12
G6P	8.65	60	1.05
FBP	14.66	60	0.59
3PG	2.14	220	0.88
Energy charge	1.13	60	0.98
Uptake flux	313	15	1.02
Fructose			
Metabolite	Max/min ratio	Time peak concentration (s)	Fold change average FF vs SS
Extracellular fructose	1.76	20	0.79
G6P	1.72	71	0.57
FBP	3.86	71	0.62
3PG	1.34	5	1.04
Energy charge	1.07	50	1.03
Uptake flux	172	15	1.03
Sucrose			
Metabolite	Max/min ratio	Time peak concentration (s)	Fold change average FF vs SS
Extracellular total sugar/glucose/fructose	2.47 / 3.17 / 2.10	20	0.72 / 0.75 / 0.70
G6P	1.48	70	0.88
FBP	2.17	70	0.72
3PG	1.45	5	1.11
Energy charge	1.05	70	0.98
Uptake flux	1.80	15	1.03

Maltose				
Metabolite	Max/min ratio	Time peak concentration (s)	Fold change average FF vs SS	
Extracellular maltose	6.23	20	1.16	
G6P	3.44	99	1.05	
FBP	7.73	99	0.59	
3PG	1.61	10	0.88	
Energy charge	1.15	71	0.97	
Uptake flux	7.63	15	1.09	

As was already indicated before from the extracellular sugar profile for fructose conditions, the relative change in concentration (1.76) is much smaller than for the glucose condition (4.9). The reduced perturbation is also reflected in the intracellular metabolic response, i.e. the glycolytic response to fructose having only around a quarter the magnitude compared to glucose (see table 2). This same effect is also propagated into the trehalose cycle and pentose phosphate pathway (see Appendix).

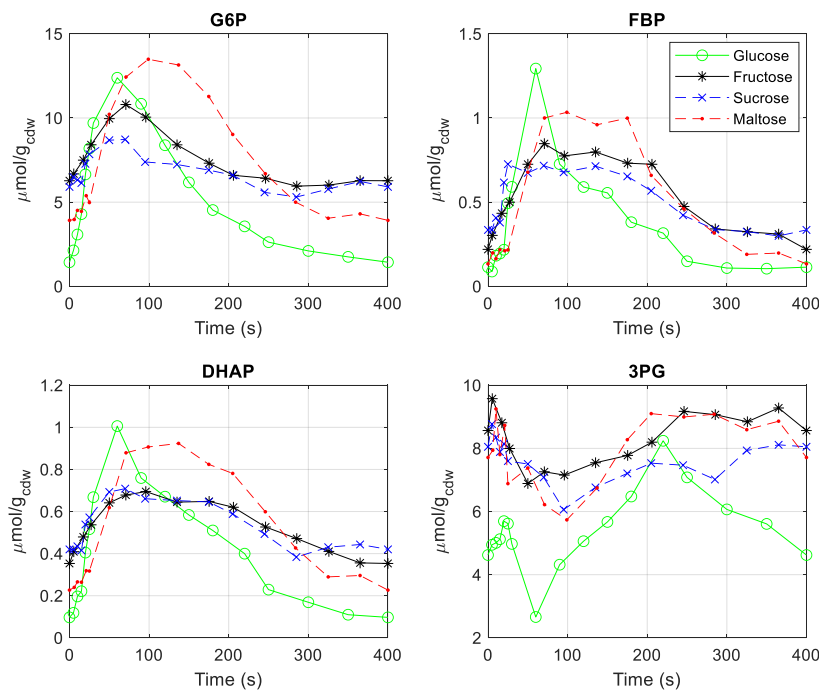


Figure 4.4. Concentration measurements of intracellular glycolytic metabolites during a 400s feast/famine cycle for glucose (green), fructose (black), sucrose (blue) and maltose (red) as substrate. Dashed lines indicate disaccharide sugars, full lines indicate monosaccharide sugars.

Similarly, for the disaccharide sucrose with lower maximal uptake rates, the magnitude of the metabolic response was smaller compared to glucose conditions. For example, in G6P a ~50% increase was observed, compared to a ~750% increase under glucose conditions. The reduced dynamics were then also observed in the pentose phosphate pathway (see Appendix) and the trehalose cycle, suggesting a reduced glucose recycling through this cycle. Interestingly, for lower glycolysis, i.e. downstream of FBP, larger changes in metabolite concentrations were observed, possible due to the missing release of inorganic phosphate (Pi) from within the trehalose cycle.

Interestingly, a significant delay of 30 s in the metabolic responses for the maltose condition can be observed compared to all other conditions (see also appendix for further metabolites). Additionally, a much higher peak was observed for trehalose-6-phosphate (T6P) (Figure 4.5), indicating a possible difference in the activity in the trehalose cycle under maltose conditions compared to glucose. An increase in trehalose cycle activity could partly explain the decrease in biomass yield and increase in respiratory activity compared to glucose. Nevertheless, an increase in activity alone would not be sufficient to explain the observed yield drop of 8%. Possible other mechanisms responsible for this decrease in yield could be cycling of maltose within the cell, such as between the cytosol and vacuole or extracellular space.

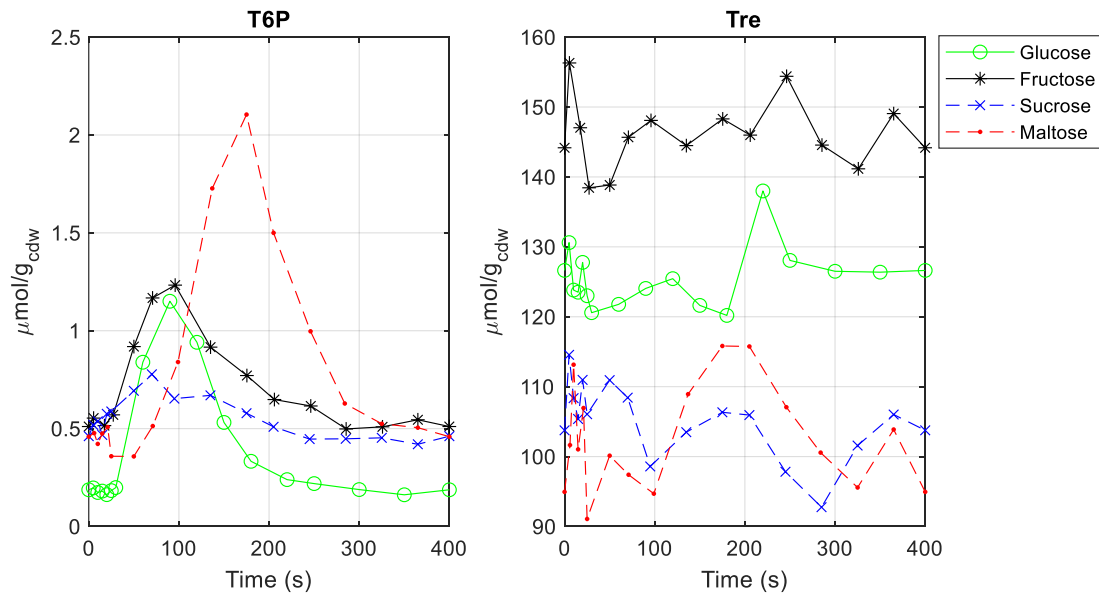


Figure 4.5. Concentration measurements of intracellular metabolites of the trehalose cycle during a 400s feast/famine cycle for glucose (green), fructose (black), sucrose (blue) and maltose (red). Dashed lines indicate disaccharide sugars, full lines indicate monosaccharide sugars.

Energy homeostasis - Nucleotides

An important finding for the glucose feast/famine regime was increased energy and AxP (sum of ATP+ADP+AMP) homeostasis compared to cells grown under continuous sugar-limited conditions, *i.e.* the so-called “ATP paradox” was not observed [32] (Figure 4.6). This phenomenon describes the observation that upon a glucose pulse the sum of adenylate nucleotides in the cell decreases although more substrate becomes available [34,35]. Here, cells adapted to feast/famine have stable AxP levels (Appendix, Figure A4.2), for all sugars used. Furthermore, from the adenylate energy charge [36], it can be observed that energy homeostasis was maintained throughout the feast/famine cycle. Interestingly, again a significant delay was observed for maltose conditions, with the energy charge lagging ~30 s behind compared to the other sugars.

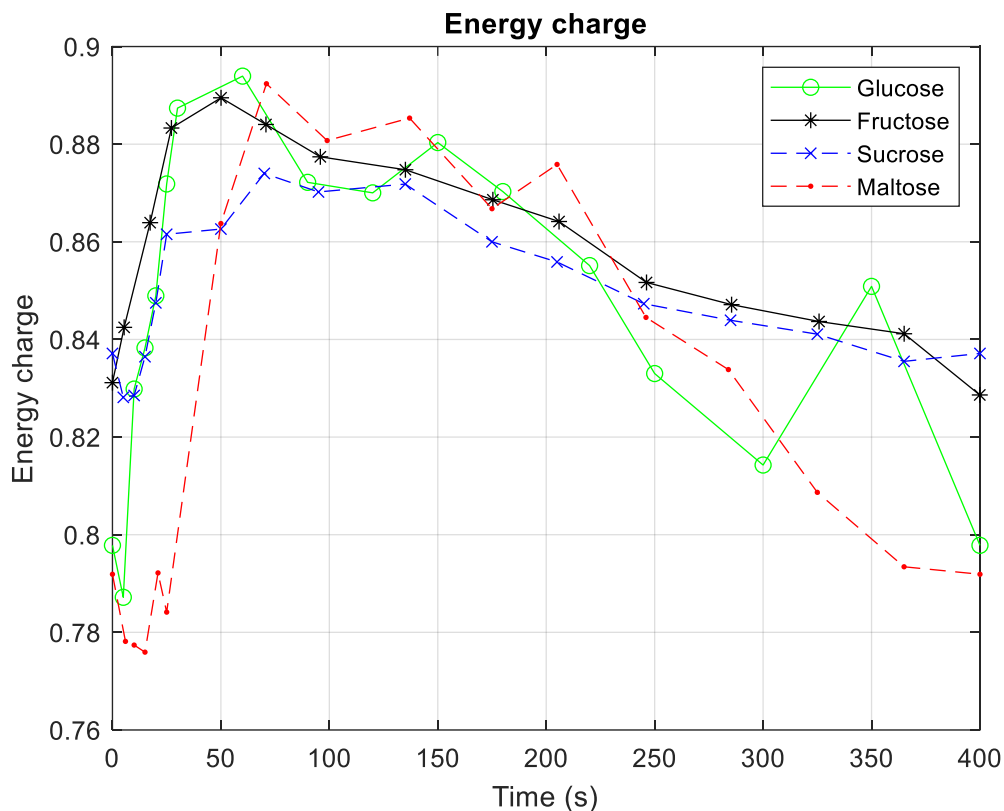


Figure 4.6. Energy charge (EC) during a 400s feast/famine cycle for glucose (green), fructose (black), sucrose (blue) and maltose (red) as substrate. Dashed lines indicate disaccharide sugars, full lines indicate monosaccharide sugars.

Proteome Adaptations

As was demonstrated in Chapter 2 for glucose as substrate, the change in metabolic response between steady-state and feast/famine conditions could not be explained by metabolite and enzyme kinetics alone. The model could only be fitted to the experimental data by additional adjustment of specific protein concentrations, especially the hexose transporter(s) and hexokinase/glucoquinase (see Chapter 2). Therefore, changes in the proteome composition between steady-state chemostat and dynamic feast/famine conditions for the different sugar substrates were expected and measured.

Non-targeted proteome comparison

The whole proteome was compared between conditions using label-free quantification. In total, 1126 proteins from 4748 peptides were identified in biological duplicates, covering 18% of metabolic proteins (345 out of 1928) reported in the KEGG database (https://www.kegg.jp/kegg-bin/download_htext?htext=sce00001).

Sucrose, fructose and glucose appeared to be the most differentiated conditions with 12 enzymes uniquely upregulated under glucose, 13 for sucrose and 15 for fructose (Figure 4.7). Proteins considered here have a fold change larger than 0.25, with an abundance of more than 0.02 % of the total proteome. Maltose in contrast only had 2 unique differentially regulated proteins. Only one protein was increased for all conditions, Ald6p. Ald6p, an aldehyde dehydrogenase, is responsible for the conversion of (accumulated) acetaldehyde into acetyl-CoA under stress conditions [37]. This could be linked to the increased acetate production under feast/famine conditions compared to steady state.

Under fructose and sucrose conditions, Ssa4p is upregulated (see Figure 4.7). Ssa4p is chaperone protein which is part of the *S. cerevisiae* SSA subfamily of cytosolic Hsp70 proteins. Hsp70 proteins are molecular chaperones, binding newly-translated proteins to assist in proper folding and prevent aggregation/misfolding [38]. Knockout of Ssa4p was found to result in a phenotype which is non-distinguishable from the wildtype, however, its expression has been found to be linked to heat shock, cold and ethanol stress, diauxic shift [39–42]. The observation here, a consistent increase for all substrates during dynamic substrate conditions, is a new condition of upregulation.

Common between glucose, fructose and sucrose are Tef1p and Glk1p, an elongation factor and a paralogue to hexokinase with different kinetic properties, especially with regards to allosteric regulation by T6P [43], which was also shown to be an essential enzyme to fit the kinetic model, described in Chapter 2.

Comparing the protein levels with the decrease from steady-state to feast/famine, condition specific changes were observed. As before, a change is identified when a fold change larger than 0.25, with an abundance of more than 0.02 % of the total proteome is observed. There was no protein commonly decreased for all substrates (Figure 4.8). Under sucrose feast/famine there were 31 proteins decreased, while for maltose only 9 proteins were lower concentrated. Downregulated for glucose, maltose and sucrose conditions, was Hsp26p, a molecular chaperone (see Figure 4.8). Hsp26p is barely expressed in unstressed cells, however strongly induced by among other conditions, carbon starvation [44,45]. This indicates that under feast/famine conditions, on average, cells appear to experience less stress from carbon starvation compared to steady-state conditions.

There was a common decrease for maltose and glucose for hexokinase I (Hxk1p), but this was not observed for sucrose and fructose. Furthermore, the abundance of glutamate dehydrogenase I (Gdh1p) was reduced in both conditions, which was earlier described to be regulated by carbon sources [46], but not yet by carbon source dynamics.

In earlier work, upregulation of the transcription factors Cyc8p, Wtm1p and Rap1p, with downregulation of Hog1p was found during batch cultivations comparing sucrose and glucose [47]. However, under chemostat conditions in this work no significant changes were observed for these specific proteins. Many other transcription factors and signaling proteins were below detection limit and, as such, could not be evaluated.

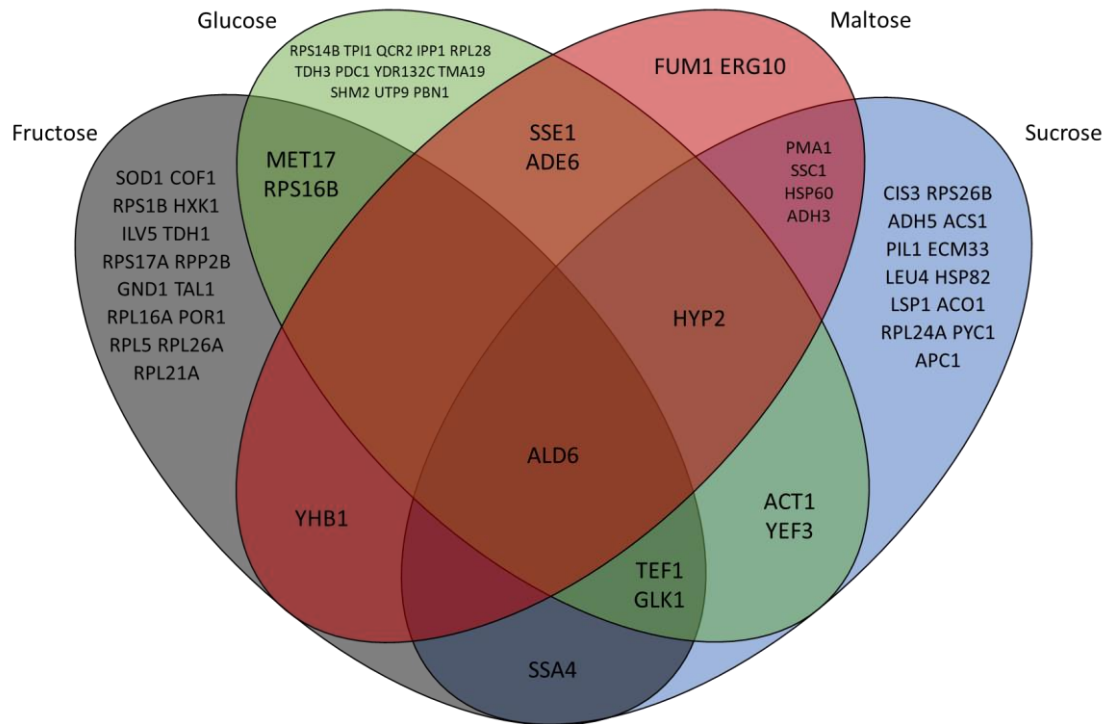


Figure 4.7. A Venn diagram of upregulated proteins (> 0.25 fold change, > 0.02% of proteome) from steady state to feast famine for all four substrates.

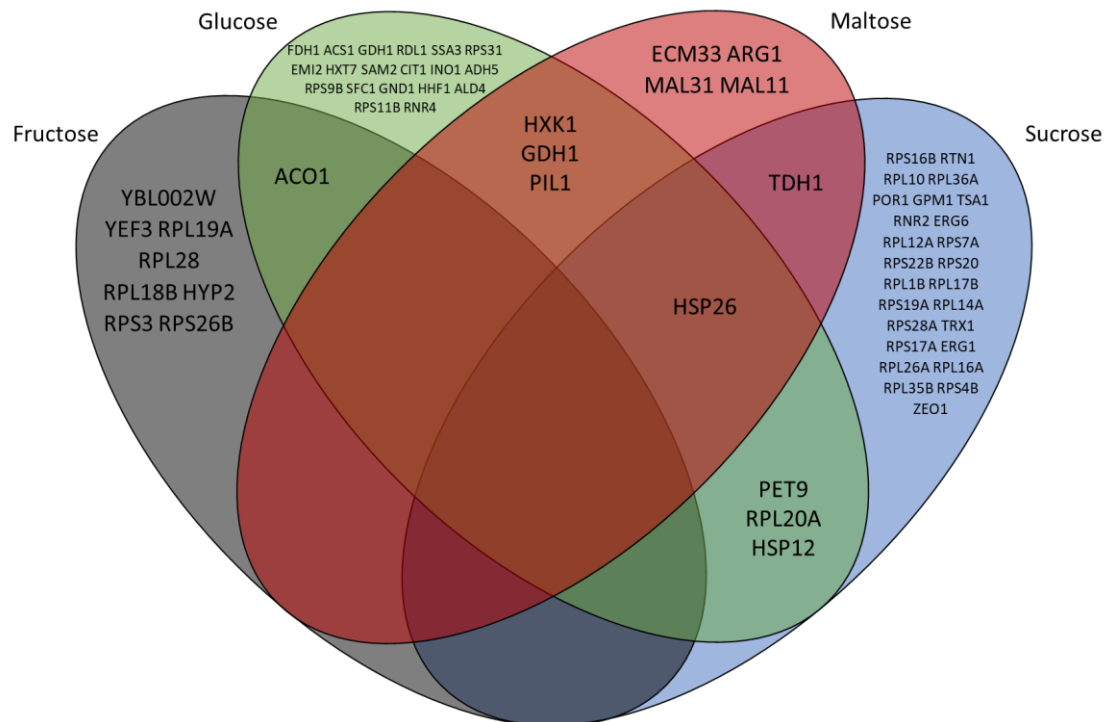


Figure 4.8. A Venn diagram of downregulated proteins (> 0.25 fold change, > 0.02% of proteome) from steady state to feast famine for all four substrates.

Pathway enrichment

A pathway enrichment analysis was performed based on the gene ontology biological process terms (GO terms) [48]. This allows for the identification of global changes in protein groups related to specific biological functions. The analysis was performed using a Fisher's exact test, selecting for proteins groups of more than 10 proteins of which at least 2/3 of proteins were significantly differentially expressed [49].

Considering the changes from steady-state to feast/famine conditions, for each of the different substrates, no significant changes were observed in specific biological functions. Thus, while these conditions exhibit different metabolic responses, these changes seem mostly based on post-translational modifications and kinetics, rather than changes on the proteomic level.

Next to analyzing the changes between steady-state and feast/famine conditions, this GO analysis was also performed on the feast/famine proteome measurements between the different substrates (see Figure 4.9). Significant changes were observed related to cytoplasmic translation and translational termination for all other sugar conditions compared to glucose, which was earlier observed for CEN.PK113-7D comparing sucrose to glucose growth conditions [47]. Additionally, proteins related to the cellular response to oxidative stress were found to be significantly enriched for all sugar conditions compared to glucose, which could be related to the increased respiration observed for sucrose and especially maltose conditions. A higher expression of proteins related to glycolytic processes was found for glucose conditions compared to the other sugars, which can be related to the higher glucose uptake flux, which potentially required a larger glycolytic capacity.

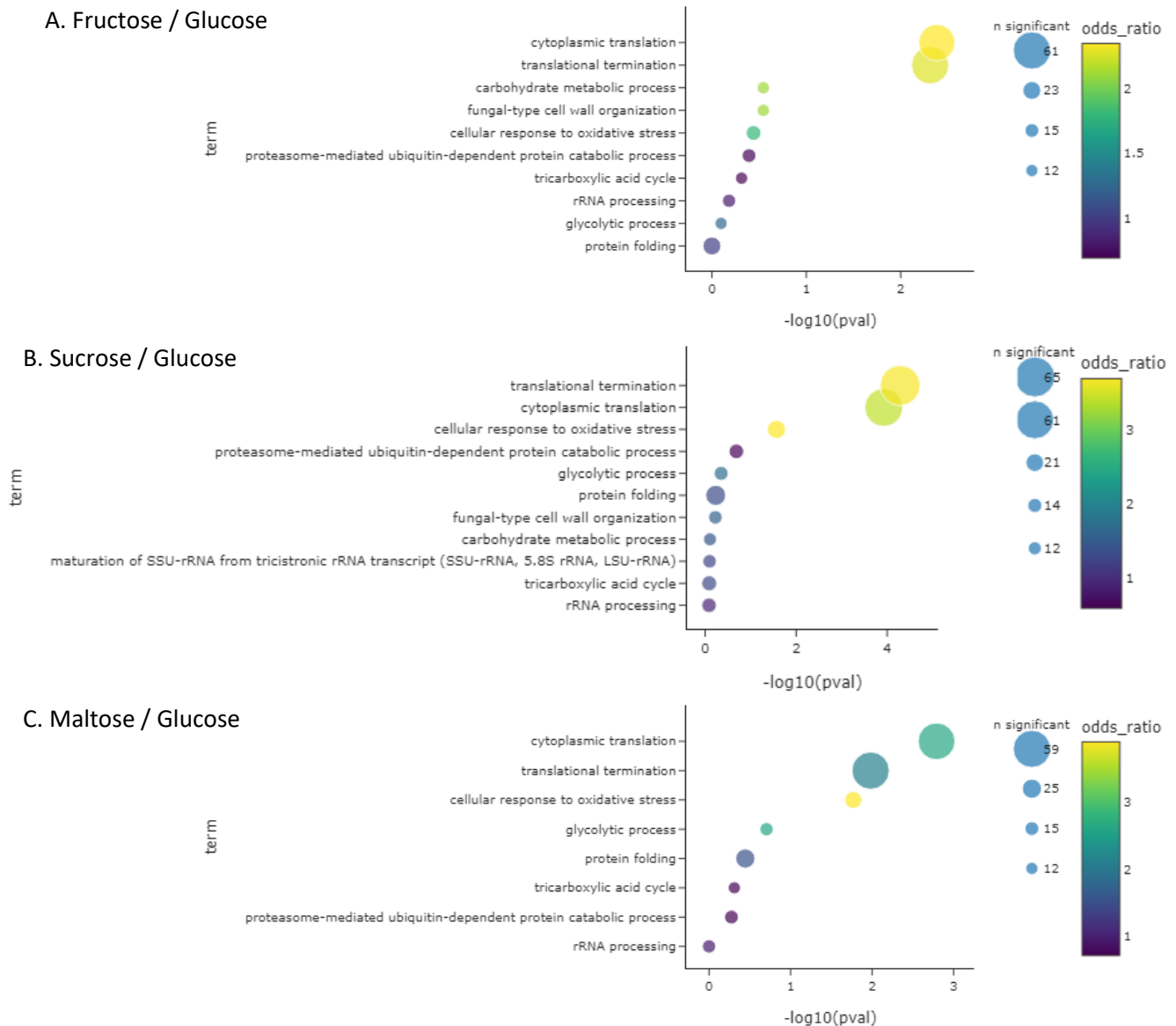


Figure 4.9. Enrichment analysis by Fisher's exact test for significant proteins between glucose and the three other substrates under feast/famine conditions. For all significant terms the p-value, group size and the enrichment (odds) factor are displayed. Plots were generated in Python, using a visualization toolbox developed by Schessner et al. [49].

Proteome adaptation within the glycolysis pathway

As the entry point of central carbon metabolism, a special focus was given to the proteome changes in hexose transporters and glycolysis. As discussed in Chapters 2 and 3 (glucose conditions), the upregulation of proteins of the lower glycolysis (especially TDH) from steady-state to feast/famine in combination with the downregulation of hexose transporters and proteins in the upper glycolysis was assumed to provide robustness to cope with extracellular perturbations. These changes should also prevent a putative phosphate 'deadlock' [50]. Especially, HXT and HXK decreased by more than 30%, lower glycolytic enzymes like TPI and TDH which are known to be abundant still increased by nearly 30%. Downstream of TDH changes in protein concentrations were less pronounced.

While the changes with maltose as substrate partially followed the ones with glucose, this was not the case for fructose and sucrose as substrates (Figure 4.10). Instead, for these two substrates, an

upregulation of transporters and upper glycolytic proteins was observed, without significant upregulation of lower glycolysis. The largest observed increase of glycolytic enzymes was actually observed for sucrose, with an increase of 41% for GLK (upper glycolysis). The inverse trends compared to glucose and maltose might be strongly linked to the lower affinity of the fructose transporter and reduced dynamics from its higher K_M value. The upregulation of transporters was highest with sucrose as substrate, where glucose and fructose are transported over the membrane.

This distinct difference between the protein adaptation observed for glucose & maltose and fructose & sucrose, in combination with the observed differences in uptake rates and especially metabolic response, highlights a yet unknown difference in regulation of central carbon metabolism under dynamic substrate conditions for these different sugars.

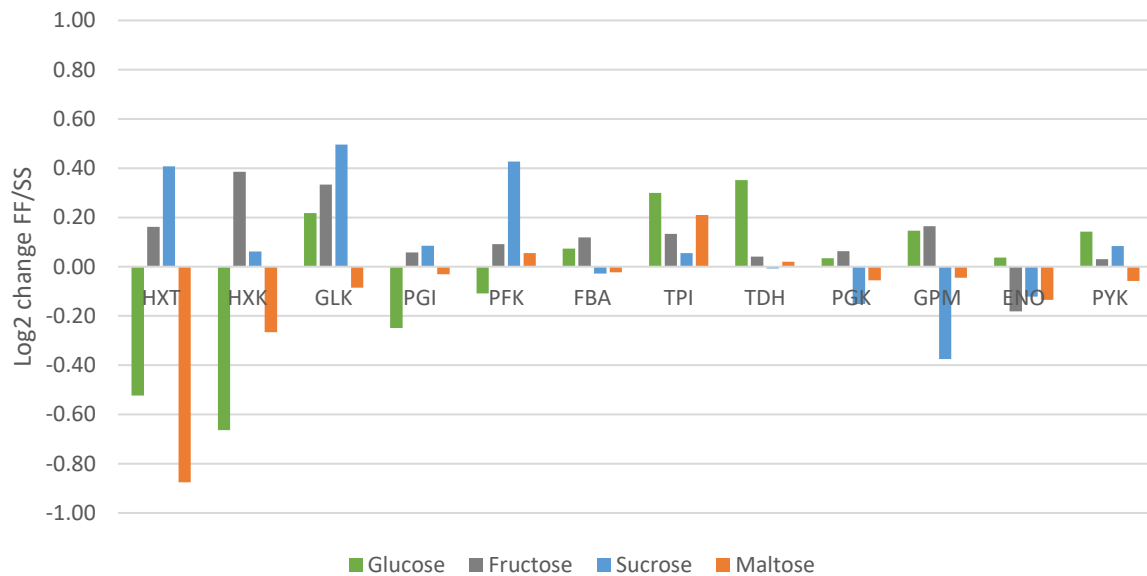


Figure 4.10. The log₂ changes observed in protein concentrations between steady-state chemostat and feast/famine conditions for hexose and maltose transporters as well as glycolytic enzymes.

Conclusions

The differential metabolic response of *S. cerevisiae* to different substrates under dynamic conditions highlights the importance to consider the intricacies of metabolic regulation when designing any bioprocess. While the sugar substrates are chemically very similar, they surprisingly elicited a specific different metabolic response under dynamic substrate conditions.

Substrate gradients of maltose lead to a decrease in biomass yield, while this same effect was not observed for glucose, fructose and sucrose. Striking is also the difference observed in uptake rate, with a very high initial uptake rate being observed with glucose, a similar uptake rate between maltose and fructose and a significantly lower uptake rate with sucrose. This indicates clearly that the kinetic properties of transporters influence metabolism, however, the significant differences in proteome adaptation between especially glucose & maltose vs fructose & sucrose substrate conditions suggests that beyond the effect of substrate transport, the substrate signaling of these different sugars also plays an important role in the metabolic response. The energy charge, which can be used as a proxy for the energetic stability of the cell, was observed to be stable for all substrates under dynamic feast/famine conditions, contrary to what was expected based on results from single-pulse experiments or limitation to excess shifts where for example maltose-accelerated death was observed. Keeping the diverse industrial feedstocks, such as molasses, in mind, this highlights the importance to look beyond glucose as model sugar substrate in exploring the regulation of metabolism under dynamic conditions and consider further evaluation of these other sugar substrates.

However, the interpretation of data itself is currently still challenging, showing gaps in the current understanding of regulation under dynamic conditions. While for glucose conditions, especially with respect to metabolomics, proteomics and fluxomics, several datasets are available, datasets for other carbon sources are sparse. Of special interest is the generation of comprehensive datasets that will include flux distributions. This should include flux data from ¹³C labelling experiments, in combination with kinetic modelling, which may assist with the evaluation of different hypotheses on the regulation of the metabolic response to feast/famine conditions. In this way, the effect of the different glycolytic proteome adaptation can be evaluated, and its effect on the metabolic response can be quantified and compared to the obtained metabolomics dataset.

An additional challenge is the existence of physiological differences between strains. As was concluded from earlier work, significant differences with respect to the consumption of different sugars can be observed between different strains of *S. cerevisiae* [51]. Botman et al. [28] observed large differences in cAMP response between different sugar substrates, however, certain *S. cerevisiae* strains, such as the strain used in this work, CEN.PK113-7D, are deficient in cAMP [29]. To what extent such differences in the substrate signaling pathways affected the observed metabolic response remains to be elucidated.

Materials & Methods

Strain and Culture Conditions

The haploid yeast *Saccharomyces cerevisiae* CEN.PK113-7D, obtained from the *Centraalbureau van Schimmelcultures* (Fungal Biodiversity Center, Utrecht, The Netherlands), was used in this study. The cultivations were performed using a low-salt Verduyn minimal medium [52] with a fructose/glucose concentration of 7.5 g/L or a maltose/sucrose concentration of 7.12 g/L, with a feed of the same composition. 1L-Erlenmeyer flasks containing 100 mL medium were inoculated with cells from a cryovial (glycerol, -80°C) and the inoculation cultures were subsequently grown for 10 h at 200 rpm and 30 °C. The inoculation culture was used to inoculate a 7 L bioreactor (Applikon Biotechnology B.V., Delft, The Netherlands) containing a working volume of 4 L, controlled by a Biostat B Plus controller (Sartorius AG, Göttingen, Germany). The reactor was aerated with pressurized air at 1 L/min (0.25 vvm) using a Smart series mass flow controller 5850S (Brooks Instrument, Hatfield, PA, USA). The reactor was operated at 0.3 bar overpressure, at 30 °C, with a stirrer speed of 600 rpm. The pH of the broth was maintained at 5.0 by automated addition of either 4M KOH or 2M H₂SO₄. Once the batch phase was completed (indicated by a fast decrease in CO₂ signal and a sharp increase in dissolved oxygen (DO)), the chemostat phase (steady-state) was started at a dilution rate of 0.1 h⁻¹ for 50 h. DO was not controlled but was well above > 60% during the whole chemostat phase. After about 5 residence times, sampling for proteomics was performed.

Dynamic Feast Famine Setup

After five residence times (50 h) of continuous feeding, the feeding was changed to a block-wise feeding regime, leading to a feast/famine regime [32]. Cycles of 400 s were applied by a feeding medium for 20 s, followed by a period of 380 s of no feeding. The medium pump was controlled using an automatic timer (PTC-1A, Programmable timing controller, Omega Engineering Inc., Stamford, CT, USA). During the 20-second feeding period, 43 ± 1 mL of fresh medium were added. The same volume was subsequently withdrawn for 260s at a flow rate of 0.166 ± 0.001 mL s⁻¹ maintaining the broth volume nearly constant at 4 L. After about 5 residence times (450 cycles), sampling for proteomics was performed.

Sample acquisition and analysis

Extracellular metabolites

For the analysis of extracellular metabolites, 1.5 ml broth was taken using a syringe containing ~26 g pre-cooled (-20 °C) stainless steel beads, which was subsequently filtered as described by Mashego et al. [53]. Extracellular acetate, ethanol, glucose and glycerol concentration were measured using HPLC or enzymatic assay, as described by Canelas et al. [54]. Biomass concentrations (cell dry weight) were determined using a gravimetric method described by Suarez-Mendez et al. [32]. The CO₂ and O₂ fractions in the off-gas were determined using a combined infrared/paramagnetic NGA2000 analyzer (Rosemount Analytics, St. Louis, MO, USA).

Intracellular metabolites

Samples for the measurement of intracellular metabolites were taken by rapidly withdrawing 1 ml of broth and quenching it in 5 ml cold (-40 °C) methanol, as described by Lange et al. and Canelas et al. [52,55]. Taken samples were weighted, and subsequently poured into a filtration setup (using a Supor-200 cellulose membrane, 0.2 µm, 47 mm, Pall Corporation), which already contained 15 ml pre-cooled (-40 °C) methanol. After this, vacuum was applied, followed by the addition of 15 ml cold (-40 °C) methanol to wash the biomass [56]. The filter with the washed biomass was subsequently transferred to a 50 ml falcon tube containing 30 ml of a 75% (v/v) ethanol solution, preheated to 75 °C. To this, 100 µl ¹³C yeast cell extract was added as internal standard [57]. The tube was then shaken and put

into a water bath at 95 °C for 3 minutes to extract the intracellular metabolites. After extraction, the tubes were immediately cooled in an ice bath, and the filter was removed. The cell extract was subsequently stored at -80 °C and later concentrated through complete evaporation of the aqueous ethanol solution and resuspended into 500 µl milliQ water, as described by Mashego et al. [58]. The resuspended samples were centrifuged at 15000 g for 5 minutes at 1 °C, and the supernatant was transferred to a new tube, which was subsequently centrifuged again to remove all solid components in the sample. The obtained supernatant was then transferred into a screw-capped vial and stored at -80 °C. Samples were analysed by GC-MS [57–59] and LC-MS [60].

Proteomics analysis

For each proteome sampling timepoint, a sample normalized to 10 OD units was withdrawn into an eppendorf tube and immediately centrifuged at 8000 g for 5 min at 4 °C. Supernatant was discarded, the pellet was resuspended in 2 mL saline solution (0.9% NaCl) (cooled beforehand at 4°C) and centrifuged again (8000 g, 5 min, 4 °C). The supernatant was discarded once more, again resuspended in 2 mL saline solution and centrifuged (8000 g, 5 min, 4 °C). Then, the supernatant was discarded and the sample was snap-frozen using liquid nitrogen and stored at -80 °C until further analysis. For each timepoint, duplicate samples were taken. To process the samples for proteomics analysis, the cell mass was normalized to a dry weight of 1.6 mg and then mechanically lysed using 0.5-mm zirconium beads and a PreCellys homogenizer. Proteins were isolated using Bligh and Dyer extraction [61], followed by reduction, alkylation, and digestion using trypsin. The samples were analysed in technical triplicates by liquid chromatography tandem mass spectrometry (LC-MS/MS) using a Vanquish UHPLC coupled to a Q Exactive Plus Orbitrap MS (Thermo Fisher Scientific, Waltham, MA, USA). Peptides were separated using reverse-phase chromatography using a gradient of water with 0.1% formic acid (solvent A) and acetonitrile with 0.1% formic acid (solvent B) from 2% B to 45% B in 50 min. Data-dependent acquisition (DDA) was performed with a resolution setting at 70,000 within the 400- to 1,600-m/z range and a maximum injection time of 75 ms, followed by high-energy collision-induced dissociation activated (HCD) MS/MS on the top 15 most abundant precursors using a resolution setting of 17,500 and a 200- to 2,000-m/z range with a maximum injection time of 50 ms. The minimum intensity threshold for MS/MS was 1,000 counts, and peptide species with 1 and >8 charges were excluded. MS/MS spectra were analysed with the SEQUEST HT search engine and Proteome Discoverer, version 2.3, against the proteins of *Saccharomyces cerevisiae* (Uniprot, *S. cerevisiae* CEN.PK113-7D, ID:UP000013192) [29]. Label-free quantification was performed using the top three unique peptides measured for each protein. Retention time alignment was performed on the most abundant signals obtained from nonmodified peptides measured in all samples, and results were corrected for the total ion intensities measured for each sample. The data was analysed for statistical differences using Perseus 1.6.10.45 [62]. A two sample test was used to determine the significance of the fold change, with a significance level threshold of $p < 0.01$, and at least 2 unique peptides per protein.

Data availability

The dataset on proteome fold changes between chemostat and feast/famine conditions, analyzed in this study, can be found in the 4TU.ResearchData repository at <https://doi.org/10.4121/19008833> and <https://doi.org/10.4121/21541416>. The analyzed metabolomics dataset for chemostat and feast/famine conditions can be found in the same repository at <https://doi.org/10.4121/21692057>.

References

1. Guillaume C, Delobel P, Sablayrolles J-M, Blondin B: **Molecular Basis of Fructose Utilization by the Wine Yeast *Saccharomyces cerevisiae* : a Mutated HXT3 Allele Enhances Fructose Fermentation.** *Appl Environ Microbiol* 2007, **73**:2432–2439.
2. Özcan S, Johnston M: **Function and Regulation of Yeast Hexose Transporters.** *Microbiol Mol Biol Rev* 1999, **63**:554–569.
3. Berthels N, Cordero R, Bauer F, Thevelein J, Pretorius I: **Discrepancy in glucose and fructose utilisation during fermentation by wine yeast strains.** *FEMS Yeast Res* 2004, **4**:683–689.
4. Bisson LF, Fraenkel DG: **Involvement of kinases in glucose and fructose uptake by *Saccharomyces cerevisiae*.** *Proc Natl Acad Sci* 1983, **80**:1730–1734.
5. Diderich JA, Schepper M, van Hoek P, Luttik MAH, van Dijken JP, Pronk JT, Klaassen P, Boelens HFM, de Mattos MJT, van Dam K, et al.: **Glucose Uptake Kinetics and Transcription of HXT Genes in Chemostat Cultures of *Saccharomyces cerevisiae*.** *J Biol Chem* 1999, **274**:15350–15359.
6. Bowski L, Saini R, Ryu DY, Vieth WR: **Kinetic modeling of the hydrolysis of sucrose by invertase.** *Biotechnol Bioeng* 1971, **13**:641–656.
7. Badotti F, Dário MG, Alves SL, Cordioli MLA, Miletti LC, de Araujo PS, Stambuk BU: **Switching the mode of sucrose utilization by *Saccharomyces cerevisiae*.** *Microb Cell Factories* 2008, **7**:4.
8. Marques WL, Raghavendran V, Stambuk BU, Gombert AK: **Sucrose and *Saccharomyces cerevisiae* : a relationship most sweet.** *FEMS Yeast Res* 2016, **16**:fov107.
9. Verstrepen KJ, Iserentant D, Malcorps P, Derdelinckx G, Van Dijck P, Winderickx J, Pretorius IS, Thevelein JM, Delvaux FR: **Glucose and sucrose: hazardous fast-food for industrial yeast?** *Trends Biotechnol* 2004, **22**:531–537.
10. Barnett JA: **The Utilization of Disaccharides and Some Other Sugars RY Yeasts.** In *Advances in Carbohydrate Chemistry and Biochemistry*. Elsevier; 1981:347–404.
11. Serrano R: **Energy Requirements for Maltose Transport in Yeast.** *Eur J Biochem* 1977, **80**:97–102.
12. Han E-K, Cotty F, Sottas C, Jiang H, Michels CA: **Characterization of AGT1 encoding a general alpha-glucoside transporter from *Saccharomyces*.** *Mol Microbiol* 1995, **17**:1093–1107.
13. Weusthuis RA, Adams H, Scheffers WA, van Dijken JP: **Energetics and kinetics of maltose transport in *Saccharomyces cerevisiae*: a continuous culture study.** *Appl Environ Microbiol* 1993, **59**:3102–3109.
14. Rich PR: **The molecular machinery of Keilin's respiratory chain.** *Biochem Soc Trans* 2003, **31**:1095–1105.
15. Postma E, Verduyn C, Kuiper A, Scheffers WA, Van Dijken JP: **Substrate-accelerated death of *Saccharomyces cerevisiae* CBS 8066 under maltose stress.** *Yeast* 1990, **6**:149–158.

16. Van Urk H, Mark PR, Scheffers WA, Van Dijken JP: **Metabolic responses of *Saccharomyces cerevisiae* CBS 8066 and *Candida utilis* CBS 621 upon transition from glucose limitation to glucose excess.** *Yeast* 1988, **4**:283–291.
17. Rolland F, Winderickx J, Thevelein J: **Glucose-sensing and -signalling mechanisms in yeast.** *FEMS Yeast Res* 2002, **2**:183–201.
18. Broach JR: **Nutritional Control of Growth and Development in Yeast.** *Genetics* 2012, **192**:73–105.
19. Conrad M, Schothorst J, Kankipati HN, Van Zeebroeck G, Rubio-Teixeira M, Thevelein JM: **Nutrient sensing and signaling in the yeast *Saccharomyces cerevisiae*.** *FEMS Microbiol Rev* 2014, **38**:254–299.
20. Peeters K, Thevelein JM: **Glucose Sensing and Signal Transduction in *Saccharomyces cerevisiae*.** In *Molecular Mechanisms in Yeast Carbon Metabolism*. Edited by Piškur J, Compagno C. Springer Berlin Heidelberg; 2014:21–56.
21. Belinchón MM, Gancedo JM: **Glucose controls multiple processes in *Saccharomyces cerevisiae* through diverse combinations of signaling pathways.** *FEMS Yeast Res* 2007, **7**:808–818.
22. Santangelo GM: **Glucose Signaling in *Saccharomyces cerevisiae*.** *Microbiol Mol Biol Rev* 2006, **70**:253–282.
23. Belinchón MM, Gancedo JM: **Different signalling pathways mediate glucose induction of SUC2, HXT1 and pyruvate decarboxylase in yeast: Glucose induction of SUC2, HXT1 and Pdc in yeast.** *FEMS Yeast Res* 2007, **7**:40–47.
24. Gancedo JM: **Yeast Carbon Catabolite Repression.** *Microbiol Mol Biol Rev* 1998, **62**:334–361.
25. Peeters K, Van Leemputte F, Fischer B, Bonini BM, Quezada H, Tsytlonok M, Haesen D, Vanthienen W, Bernardes N, Gonzalez-Blas CB, et al.: **Fructose-1,6-bisphosphate couples glycolytic flux to activation of Ras.** *Nat Commun* 2017, **8**:922.
26. Cullen PJ, Sprague GF: **The Regulation of Filamentous Growth in Yeast.** *Genetics* 2012, **190**:23–49.
27. Lemaire K, Van de Velde S, Van Dijck P, Thevelein JM: **Glucose and Sucrose Act as Agonist and Mannose as Antagonist Ligands of the G Protein-Coupled Receptor Gpr1 in the Yeast *Saccharomyces cerevisiae*.** *Mol Cell* 2004, **16**:293–299.
28. Botman D, O'Toole TG, Goedhart J, Bruggeman FJ, van Heerden JH, Teusink B: **A yeast FRET biosensor enlightens cAMP signaling.** *Mol Biol Cell* 2021, **32**:1229–1240.
29. Nijkamp JF, van den Broek M, Datema E, de Kok S, Bosman L, Luttik MA, Daran-Lapujade P, Vongsangnak W, Nielsen J, Heijne WH, et al.: **De novo sequencing, assembly and analysis of the genome of the laboratory strain *Saccharomyces cerevisiae* CEN.PK113-7D, a model for modern industrial biotechnology.** *Microb Cell Factories* 2012, **11**:36.
30. Vieth E: **Fitting piecewise linear regression functions to biological responses.** *J Appl Physiol* 1989, **67**:390–396.

31. Schumacher R, Wahl S: **Effective Estimation of Dynamic Metabolic Fluxes Using ¹³C Labeling and Piecewise Affine Approximation: From Theory to Practical Applicability.** *Metabolites* 2015, **5**:697–719.
32. Suarez-Mendez C, Sousa A, Heijnen J, Wahl A: **Fast “Feast/Famine” Cycles for Studying Microbial Physiology Under Dynamic Conditions: A Case Study with *Saccharomyces cerevisiae*.** *Metabolites* 2014, **4**:347–372.
33. Jurica MS, Mesecar A, Heath PJ, Shi W, Nowak T, Stoddard BL: **The allosteric regulation of pyruvate kinase by fructose-1,6-bisphosphate.** *Structure* 1998, **6**:195–210.
34. Somsen OJG, Hoeben MA, Esgalhado E, Snoep JL, Visser D, Heijden RTJM, Heijnen JJ, Westerhoff HV: **Glucose and the ATP paradox in yeast.** *Biochem J* 2000, **352**:593–599.
35. Walther T, Novo M, Rössger K, Létisse F, Loret M-O, Portais J-C, François J-M: **Control of ATP homeostasis during the respiro-fermentative transition in yeast.** *Mol Syst Biol* 2010, **6**.
36. Ball WJ, Atkinson DE: **Adenylate energy charge in *Saccharomyces cerevisiae* during starvation.** *J Bacteriol* 1975, **121**:975–982.
37. Aranda A, del Olmo MI M lí: **Response to acetaldehyde stress in the yeast *Saccharomyces cerevisiae* involves a strain-dependent regulation of several ALD genes and is mediated by the general stress response pathway.** *Yeast Chichester Engl* 2003, **20**:747–759.
38. Mayer MP, Bukau B: **Hsp70 chaperones: Cellular functions and molecular mechanism.** *Cell Mol Life Sci* 2005, **62**:670–684.
39. Werner-Washburne M, Becker J, Kusic-Smithers J, Craig EA: **Yeast Hsp70 RNA levels vary in response to the physiological status of the cell.** *J Bacteriol* 1989, **171**:2680–2688.
40. Quan X, Rassadi R, Rabie B, Matusiewicz N, Stochaj U: **Regulated nuclear accumulation of the yeast hsp70 Ssa4p in ethanol-stressed cells is mediated by the N-terminal domain, requires the nuclear carrier Nmd5p and protein kinase C.** *FASEB J* 2004, **18**:899–901.
41. Kandror O, Bretschneider N, Kreydin E, Cavalieri D, Goldberg AL: **Yeast adapt to near-freezing temperatures by *STRE/Msn2,4*-dependent induction of trehalose synthesis and certain molecular chaperones.** *Mol Cell* 2004, **13**:771–781.
42. Boorstein WR, Craig EA: **Structure and regulation of the SSA4 HSP70 gene of *Saccharomyces cerevisiae*.** *J Biol Chem* 1990, **265**:18912–18921.
43. Blázquez MA, Lagunas R, Gancedo C, Gancedo JM: **Trehalose-6-phosphate, a new regulator of yeast glycolysis that inhibits hexokinases.** *FEBS Lett* 1993, **329**:51–54.
44. Ferreira RM, de Andrade LR, Dutra MB, de Souza MF, Flosi Paschoalin VM, Silva JT: **Purification and characterization of the chaperone-like Hsp26 from *Saccharomyces cerevisiae*.** *Protein Expr Purif* 2006, **47**:384–392.
45. Lien PTK, Viet NTM, Mizuno T, Suda Y, Irie K: **Pop2 phosphorylation at S39 contributes to the glucose repression of stress response genes, HSP12 and HSP26.** *PLOS ONE* 2019, **14**:e0215064.

46. DeLuna A, Avendano A, Riego L, Gonzalez A: **NADP-glutamate dehydrogenase isoenzymes of *Saccharomyces cerevisiae*. Purification, kinetic properties, and physiological roles.** *J Biol Chem* 2001, **276**:43775–43783.
47. Soares Rodrigues CI: **Quantitative analysis of *Saccharomyces cerevisiae*'s growth and metabolism on sucrose.** 2021, doi:10.4233/UUID:83069B1B-4680-443D-AEA7-9FAE746514DB.
48. Ashburner M, Ball CA, Blake JA, Botstein D, Butler H, Cherry JM, Davis AP, Dolinski K, Dwight SS, Eppig JT, et al.: **Gene ontology: tool for the unification of biology. The Gene Ontology Consortium.** *Nat Genet* 2000, **25**:25–29.
49. Schessner JP, Voytik E, Bludau I: **A practical guide to interpreting and generating bottom-up proteomics data visualizations.** *Proteomics* 2022, **22**:2100103.
50. van Heerden JH, Wortel MT, Bruggeman FJ, Heijnen JJ, Bollen YJM, Planque R, Hulshof J, O'Toole TG, Wahl SA, Teusink B: **Lost in Transition: Start-Up of Glycolysis Yields Subpopulations of Nongrowing Cells.** *Science* 2014, **343**:1245114–1245114.
51. Rodrigues CIS, Wahl A, Gombert AK: **Aerobic growth physiology of *Saccharomyces cerevisiae* on sucrose is strain-dependent.** *FEMS Yeast Res* 2021, **21**:foab021.
52. Canelas AB, ten Pierick A, Ras C, Seifar RM, van Dam JC, van Gulik WM, Heijnen JJ: **Quantitative Evaluation of Intracellular Metabolite Extraction Techniques for Yeast Metabolomics.** *Anal Chem* 2009, **81**:7379–7389.
53. Mashego MR, van Gulik WM, Vinke JL, Visser D, Heijnen JJ: ***In vivo* kinetics with rapid perturbation experiments in *Saccharomyces cerevisiae* using a second-generation BioScope.** *Metab Eng* 2006, **8**:370–383.
54. Canelas AB, Ras C, ten Pierick A, van Gulik WM, Heijnen JJ: **An *in vivo* data-driven framework for classification and quantification of enzyme kinetics and determination of apparent thermodynamic data.** *Metab Eng* 2011, **13**:294–306.
55. Lange HC, Eman M, van Zuijlen G, Visser D, van Dam JC, Frank J, de Mattos MJT, Heijnen JJ: **Improved rapid sampling for *in vivo* kinetics of intracellular metabolites in *Saccharomyces cerevisiae*.** *Biotechnol Bioeng* 2001, **75**:406–415.
56. Douma RD, de Jonge LP, Jonker CTH, Seifar RM, Heijnen JJ, van Gulik WM: **Intracellular metabolite determination in the presence of extracellular abundance: Application to the penicillin biosynthesis pathway in *Penicillium chrysogenum*.** *Biotechnol Bioeng* 2010, **107**:105–115.
57. Wu L, Mashego MR, van Dam JC, Proell AM, Vinke JL, Ras C, van Winden WA, van Gulik WM, Heijnen JJ: **Quantitative analysis of the microbial metabolome by isotope dilution mass spectrometry using uniformly ¹³C-labeled cell extracts as internal standards.** *Anal Biochem* 2005, **336**:164–171.
58. Mashego MR, Wu L, Van Dam JC, Ras C, Vinke JL, Van Winden WA, Van Gulik WM, Heijnen JJ: **MIRACLE: mass isotopomer ratio analysis of U-¹³C-labeled extracts. A new method for accurate quantification of changes in concentrations of intracellular metabolites.** *Biotechnol Bioeng* 2004, **85**:620–628.

59. Cipollina C, ten Pierick A, Canelas AB, Seifar RM, van Maris AJA, van Dam JC, Heijnen JJ: **A comprehensive method for the quantification of the non-oxidative pentose phosphate pathway intermediates in *Saccharomyces cerevisiae* by GC-IDMS.** *J Chromatogr B* 2009, **877**:3231–3236.
60. Seifar RM, Ras C, van Dam JC, van Gulik WM, Heijnen JJ, van Winden WA: **Simultaneous quantification of free nucleotides in complex biological samples using ion pair reversed phase liquid chromatography isotope dilution tandem mass spectrometry.** *Anal Biochem* 2009, **388**:213–219.
61. Sapcariu SC, Kanashova T, Weindl D, Ghelfi J, Dittmar G, Hiller K: **Simultaneous extraction of proteins and metabolites from cells in culture.** *MethodsX* 2014, **1**:74–80.
62. Tyanova S, Temu T, Sinitcyn P, Carlson A, Hein MY, Geiger T, Mann M, Cox J: **The Perseus computational platform for comprehensive analysis of (prote)omics data.** *Nat Methods* 2016, **13**:731–740.

Appendix

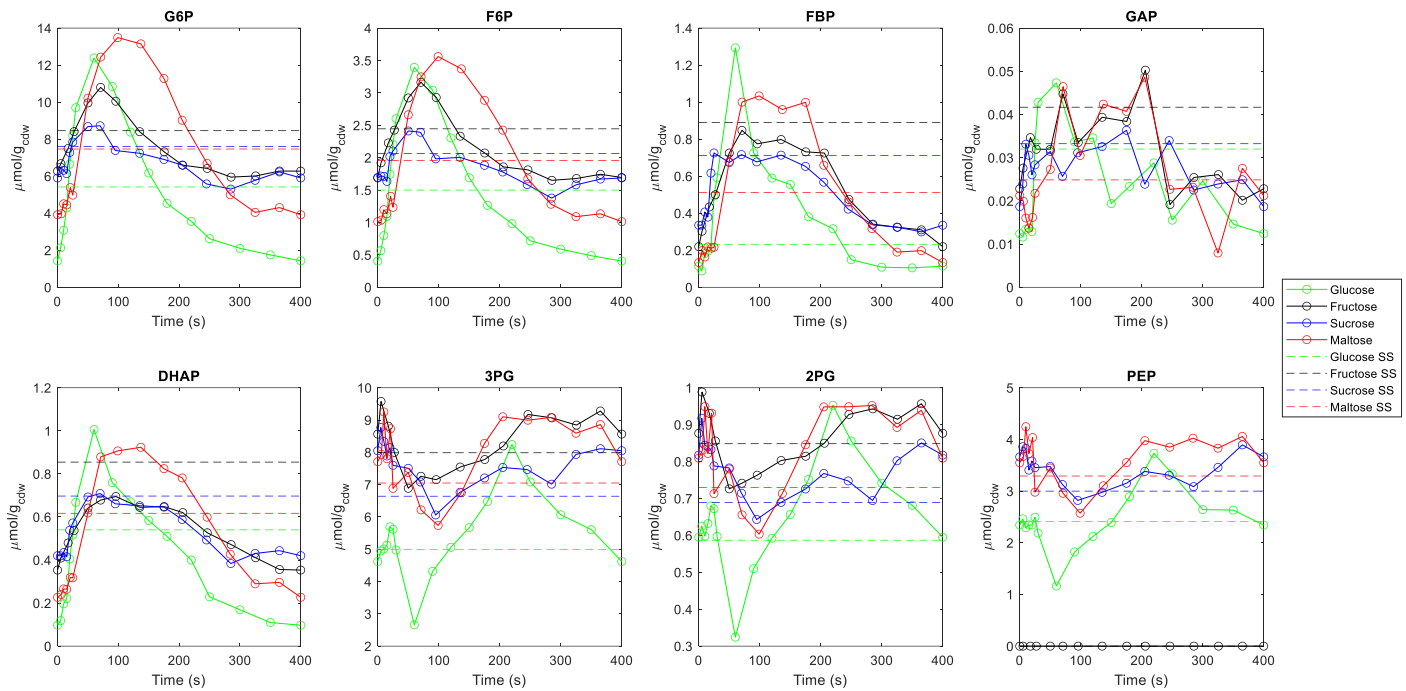


Figure A4.1. Concentration measurement of intracellular glycolytic metabolites during a 400s feast/famine cycle for glucose (green), fructose (black), sucrose (blue) and maltose (red). Dashed lines indicate the steady state level for each metabolite for the different sugars respectively.

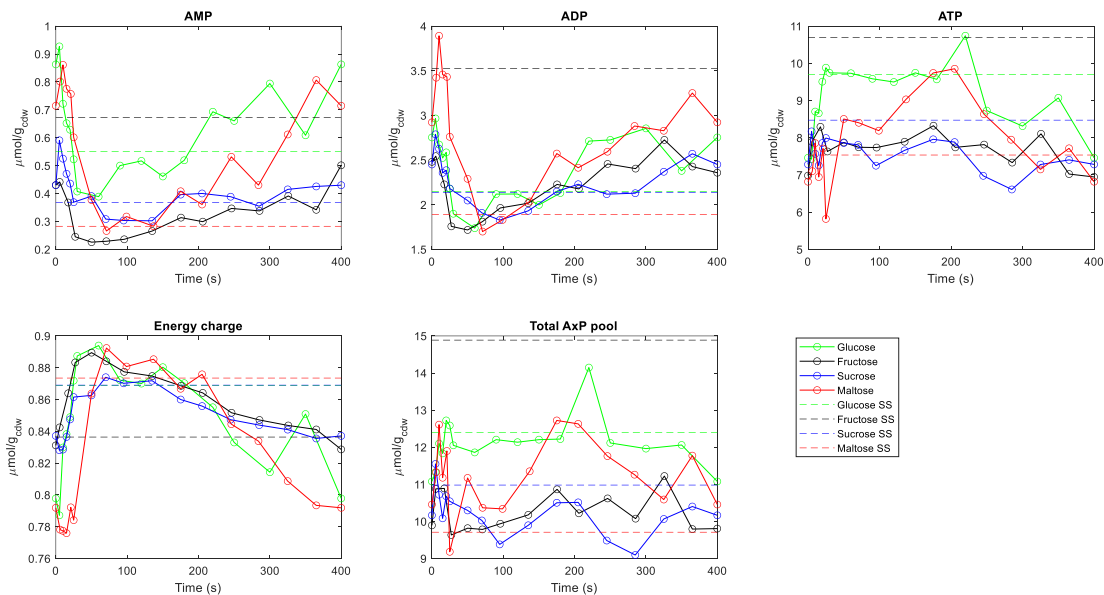


Figure A4.2. Concentration measurement of intracellular nucleotides during a 400s feast/famine cycle for glucose (green), fructose (black), sucrose (blue) and maltose (red). Dashed lines indicate the steady state level for each metabolite for the different sugars respectively.

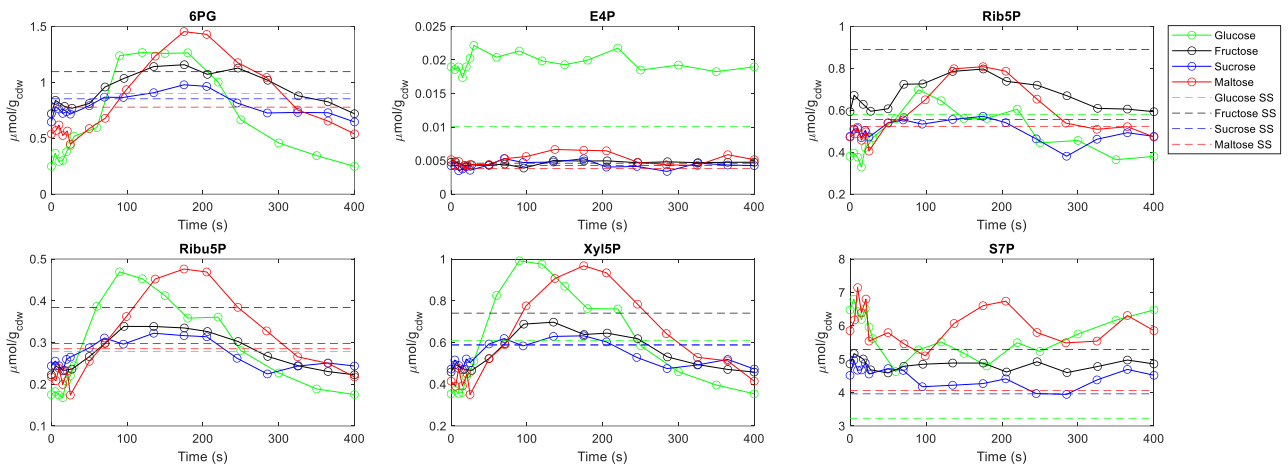


Figure A4.3. Concentration measurement of intracellular metabolites of the pentose phosphate pathway during a 400s feast/famine cycle for glucose (green), fructose (black), sucrose (blue) and maltose (red). Dashed lines indicate the steady state level for each metabolite for the different sugars respectively

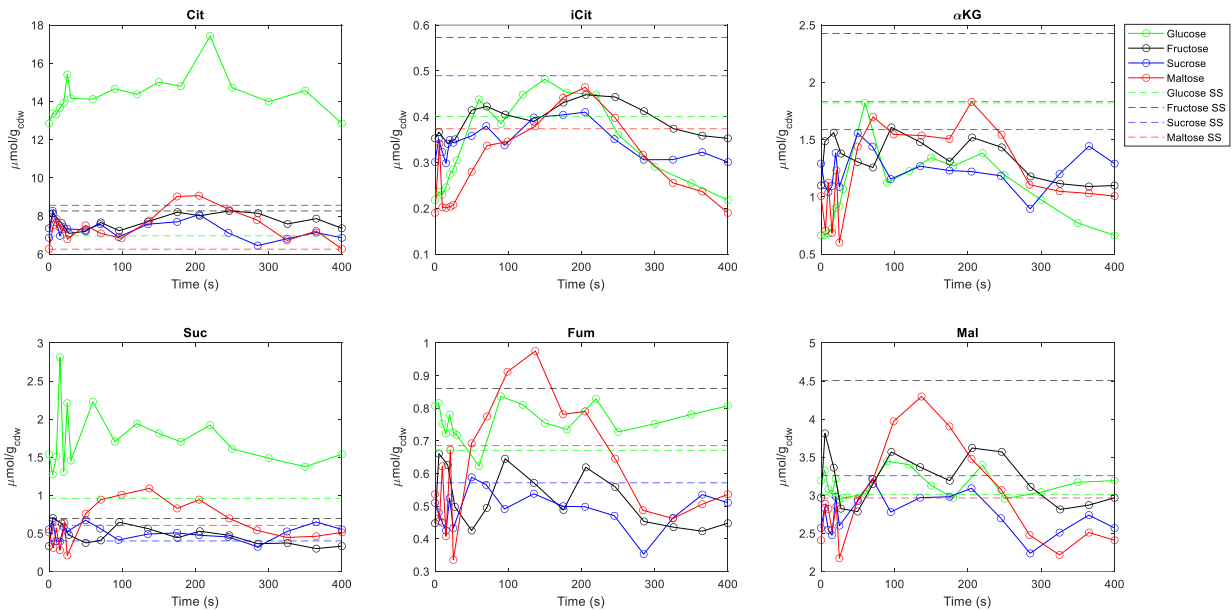


Figure A4.4. Concentration measurement of intracellular metabolites of the TCA cycle during a 400s feast/famine cycle for glucose (green), fructose (black), sucrose (blue) and maltose (red). Dashed lines indicate the steady state level for each metabolite for the different sugars respectively.

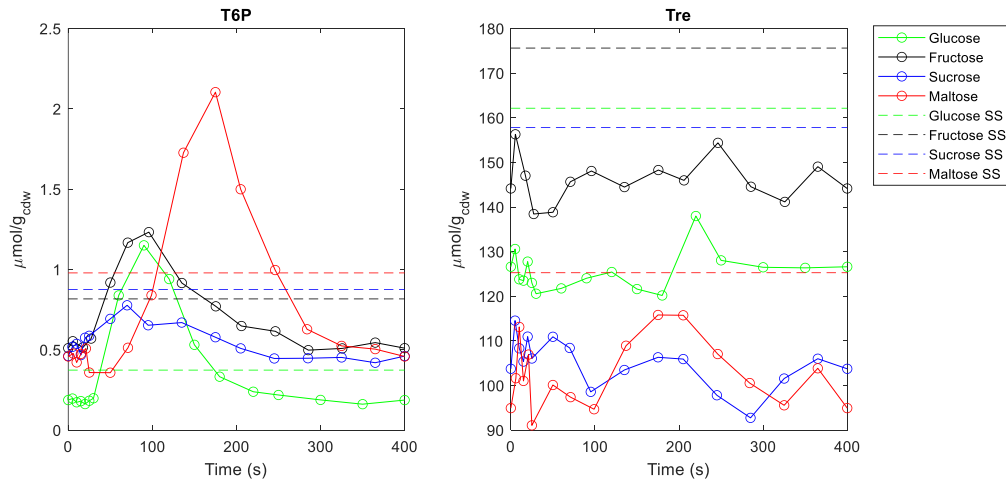


Figure A4.5. Concentration measurement of intracellular metabolites of the trehalose cycle during a 400s feast/famine cycle for glucose (green), fructose (black), sucrose (blue) and maltose (red). Dashed lines indicate the steady state level for each metabolite for the different sugars respectively.

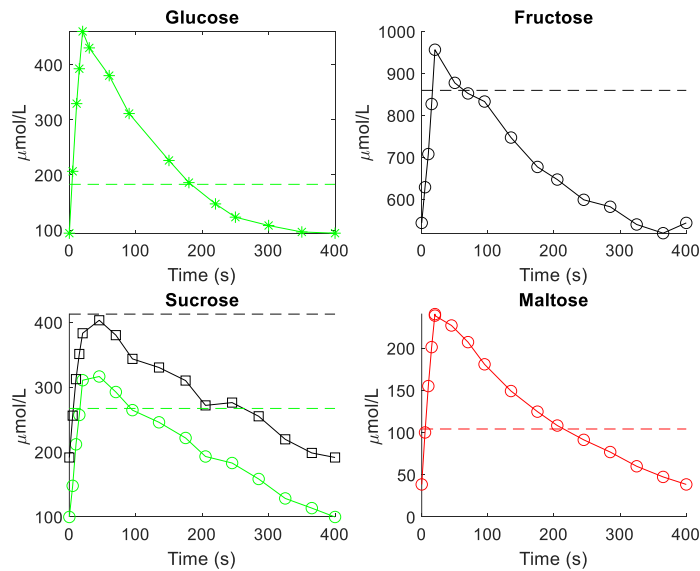


Figure A4.6. The measured extracellular sugar concentrations during four different cultivation conditions: Glucose, fructose, sucrose and maltose as substrates. Glucose concentrations are shown in green, fructose concentrations in black and maltose concentrations in red. Dashed lines indicate steady-state concentrations, and dots indicate feast/famine concentrations over the 400s cycle.

5

Outlook

Outlook

The presented research generated a better understanding of the metabolism of *Saccharomyces cerevisiae* through the integration of multi-omics datasets to produce a validated model. This model can now be applied for the prediction and design of novel *S. cerevisiae* processes. There are many experimental and modelling challenges beyond the focus of the thesis which are outlined below:

1. Accounting for differences in enzyme kinetics due to isoenzyme expression, intracellular pH and post-translational modifications

In Chapter 2, experimental data from fluxomics, metabolomics and proteomics was integrated into a large dynamic kinetic model, to identify the key mechanisms in the adaptation of *S. cerevisiae* to repetitive dynamic substrate conditions. In this model, multiple novel approaches were used. Next to fitting the model to the estimated flux distribution, model predictions of ^{13}C labelling enrichment were compared to the experimentally measured enrichment. This allowed for identification of missing kinetic regulatory mechanisms, which were mainly observed within the trehalose cycle.

Within the trehalose cycle, the trehalase reaction is carried out by an acid and a neutral enzyme (Ath1 and Nth1, respectively) [1], of which *in vivo* fluxes were quantified under feast/famine conditions. Within the model, we were able to reproduce the cytosolic Nth1 trehalase activity, but only if the cytosolic trehalose was artificially kept low by allocating the bulk of the trehalose to the vacuolar compartment. Other experimental work however shows that trehalose is expected to be mostly allocated to the cytosol [2]. Additionally, the predicted K_M for trehalose (0.13 mM) in the NTH1 reaction is significantly lower compared to the experimentally quantified value of 3-8 mM [3]. These discrepancies point towards an appreciable knowledge gap with respect to the regulation of the trehalose cycle.

Likely candidates for this missing regulation are post-translational modifications (PTMs). PTMs regulate the activity of individual enzymes through covalent binding of specific molecular attachments, such as through phosphorylation, acetylation or ubiquitination [4]. Within glycolysis and the trehalose cycle, many enzymes, such as Nth1, are regulated through phosphorylation [5]. While qualitative data on PTMs of enzymes in the central carbon metabolism of *S. cerevisiae*, including in the trehalose cycle, is available (den Ridder et al., 2022), a quantitative kinetic understanding of their impact on the activity of enzymes is as of yet still lacking. Future work ought to be focused on combining metabolic flux measurements with accurate quantitative measurements of PTMs [6] to elucidate this relationship.

In this work, we also touched upon the importance of the presence of different isoenzymes. While often simplified in kinetic models, the expression of different isoforms of the same enzyme differs between growth conditions, such as glyceraldehyde 3-phosphate dehydrogenase (GAPDH) genes [7]. We could show that especially the expression of glucokinase vs. hexokinase was relevant to explain the adaptation in metabolic response under dynamic feast/famine conditions. These isoenzymes are differently inhibited by trehalose-6-P. The effect of isoenzymes on the metabolic response under dynamic substrate conditions ought to be further investigated, for example by investigating the metabolic response of a *S. cerevisiae* strain containing only a minimal set of glycolytic genes, as was developed by Solis-Escalante et al. [8]. Additionally, the effect of individual enzymes may be evaluated using knock-outs. Next to the effect of differences in kinetics due to enzyme isoforms, the effect of intracellular pH on enzyme kinetics should also be considered in future modelling efforts, as

glucose pulses are known to significantly affect the intracellular pH of the cell [9,10]. While the enzymatic activity of glycolytic enzymes, especially GAPDH, has been shown to be very sensitive to pH [11], thus far, no dynamic kinetic models of yeast investigating the metabolic response to glucose pulses have included dependency on pH. Including the pH-dependency of enzymes has in fact been shown essential in reproducing metabolic responses in models of skeletal muscle cell glycogenolysis [12].

2. Spatial and temporal dimension of metabolism: Experimental challenges to determining intracellular transport & compartmentation

The holy grail of eukaryotic systems biology is to be able to measure the complete spatial and temporal state of the entire metabolism. As was highlighted in chapter 2 of this work, the temporal state of metabolism was provided as an input to the model, however, data on the spatial state of metabolism, regarding compartmentation of cofactors and metabolites involved in the trehalose cycle and glucose transport, was severely lacking. Canelas et al. [13] performed a thermodynamic analysis of the glycolytic reactions using whole cell as well as compartment specific NAD/NADH ratio measurements. With whole cell measurements, glycolysis appeared thermodynamically not feasible, which clearly showed the impact of redox factor compartmentation generating different potentials. To assess the kinetics driving the various intracellular redox reactions, the compartment-specific metabolite concentrations have to be determined. This presents an additional challenge for measuring the actual *in vivo* concentrations in eukaryotic cells.

Compartment-specific concentrations can be measured using fluorescent biosensors. These biosensors, composed of fluorescent proteins and an allosteric binding domain, change the fluorescent signal based on the analyte concentration (Figure 5.1). For example, the fluorescence intensity is changed by conformational changes in the sensor complex upon binding of the analyte [14,15]. These biosensors were applied for high-throughput screening of large mutant libraries using FACS. For example, mutants with NADPH-dependent systems were identified and isolated [16]. Next to FRET sensors for NADH, NADPH biosensors have been employed to study the influence of cellular processes on NADPH availability [17] and dynamic changes in NADPH concentrations [18].

Advantage of these biosensors is that they allow for single cell measurements, revealing the metabolic heterogeneity within a population [19]. However, a disadvantage is that a fluorescence microscope is required to provide a live readout of the single cell biosensor fluorescence, and thus these biosensors cannot be used to monitor the compartment-specific metabolite concentrations in cells in larger cultivations, such as reactors (although these conditions may be mimicked with microfluidics). Additionally, no absolute quantitative values can be obtained, and measurements are further complicated by interactions such as pH and ionic strength [20].

Another option is to utilize so-called equilibrium-based sensor reactions [13] (Figure 5.1). By overexpressing an enzyme catalysing an equilibrium-based reaction, a near equilibrium can be established between different metabolite pools involved in the reaction. From the equilibrium constant and involved measured metabolite concentrations, an undetermined metabolite concentration can be determined. To be sure that such a reaction operates close to equilibrium it should have a high capacity compared to the *in vivo* reaction rate. Sometimes native reactions can be used for this purpose [21]. If not, a heterologous enzyme can be expressed to act as sensor reaction, however, it should be verified that this does significantly not interfere with the host metabolism. An example is the expression of mannitol-1-phosphate dehydrogenase from *E.coli* in *S. cerevisiae*,

converting fructose-6-phosphate and NADH into mannitol-1-phosphate and NAD⁺ and vice versa, which appeared to be essentially a dead-end reaction in *S. cerevisiae* [13]. If this reaction is expressed exclusively in a specific compartment, and the measured metabolites are exclusively present in this specific compartment, then the compartment-specific concentration of the undetermined metabolite be determined. Several of these sensor reactions have been developed, such as for measuring the cytosolic NADH/NAD⁺ and NADPH/NADP⁺ ratios, or cytosolic Pi [13,21–23]. Using mannitol-1-phosphate dehydrogenase expressed in the cytosol as sensor reaction highly dynamic changes in the cytosolic NADH/NAD⁺ ratio, as result of glucose and combined glucose/acetaldehyde pulses to a steady state glucose limited chemostat, could be measured [13].

These sensors may additionally be employed to provide information on the compartment-specific labelling of metabolites, allowing not only for compartment-specific metabolomics, but also fluxomics.

Disadvantage of this sensor reaction-based technique is that only population average signals can be obtained as larger samples are required for quantification. Any single cell variation in redox ratios cannot be observed.

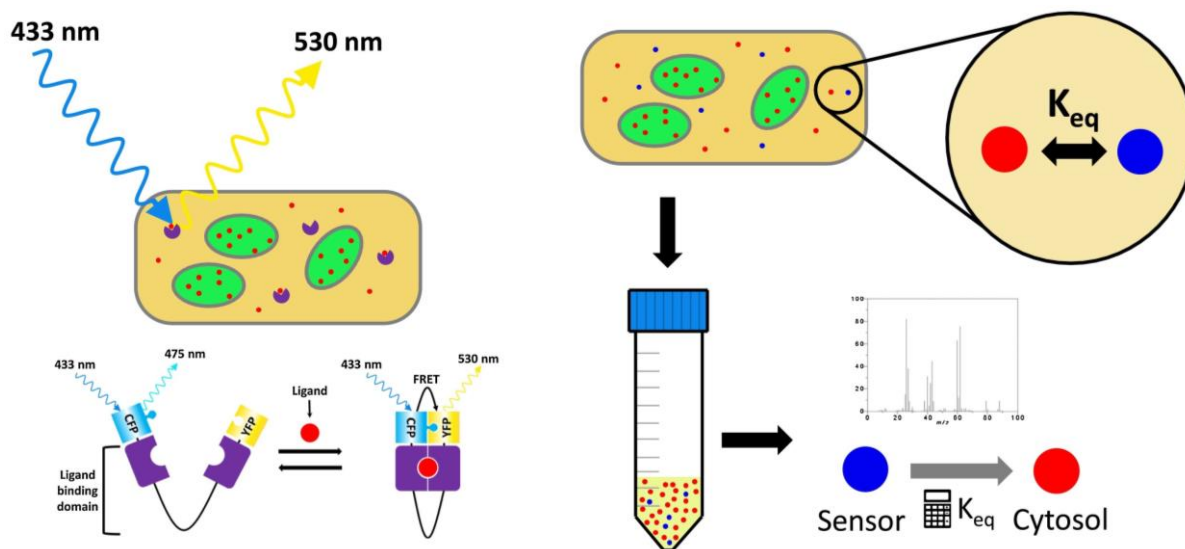


Figure 5.1. Left: Cytosolic fluorescence-based sensor (adapted from Komatsu et al. [24]): This sensor works based on the principle of Förster resonance energy transfer (FRET), i.e., energy is transferred from a donor to an acceptor fluorophore. The energy transfer only occurs when both fluorophores are in proximity of each other, and the distance is influenced by binding of the ligand. The fluorescence signals of YFP versus CFP are subsequently used to evaluate the ligand concentration [24]. Right: Cytosolic equilibrium-based sensor: By overexpressing an enzyme catalysing a close to equilibrium reaction, equilibrium between metabolites of interest and measurable pools can be established. From the equilibrium constant (K_{eq}) and involved measured metabolite concentrations, the metabolite of interest can be determined. With the equilibrium reaction expressed only in the cytosol, and the measured metabolites (blue) exclusively present in the cytosol, the compartment specific concentration of the metabolite of interest (red) can be determined [13].

The described sensors, both equilibrium- and fluorescence-based, are able to provide these single cell measurements, but are limited to only a subset of metabolites. The current GC- and LC-MS techniques are able to measure the full scope of the metabolism within a discrete temporal space, but are unable to provide the spatial property of metabolites of the cell, especially important within eukaryotic cells. However, even with future improvements in resolution and accuracy of MS

technology, the spatial property of the metabolism will not be resolved using regular extraction techniques. Promising developments to resolve this issue are made in the field of single-cell metabolomics [25]. MALDI-MSI (matrix assisted laser desorption/ionization mass spectrometry imaging) is utilized to sample the spatial distribution of metabolites within samples. With a lateral resolution down to 1.4 μm [26], this technique was utilized to analyse single-cell organisms with subcellular resolution. Due to the need of sample preparation, this technique, as of yet, cannot be utilized to measure single-cell and subcellular metabolome changes under dynamic conditions. However, with future developments in metabolome quenching techniques and organelle purification, MS imaging may well help provide full inside into the actual metabolic spatial and temporal state of single cells.

3. Population dynamics

A topic that has remained relatively underexplored in this work is cell population dynamics. Effects such as cell synchronization allow for major changes in intracellular flux distribution, even under stable extracellular conditions [27]. Zhang et al. [27] observed significant changes in the flux distribution of storage metabolism and the oxidative PPP/glycolysis split ratio after pulsing G0 cells with glucose, as cells simultaneously transition to the G1 phase. As cell synchronization is also likely to occur under the repeated feast/famine conditions utilized in this work, future research ought to also consider to what extent this effect influences the observed metabolic responses.

Additionally, during this research, we have studied the metabolic response of an entire population of cells in a reactor, assuming a homogeneous culture. However, this is only the average metabolic response, as from cell to cell, these responses are known to differ drastically [28]. This heterogeneity, caused by differences in, for example, expression of proteins, is also described in the form of bet-hedging. Cultures will contain a mixture of more robust fast-growing cells and more stress-resistant slow-growing cells. The advantage of this is that the population as a whole can grow both fast and be resistant to unexpected stresses in the environment [29]. This however also means that our models only describe the average kinetics of the whole population and not the kinetics of its subpopulations. To truly understand the impact of these subpopulations on the metabolic response of the population as a whole, and on the prediction ability of kinetic metabolic models, further research must be performed.

4. Model limitations and data quality

In this research, we have investigated the regulation of yeast central carbon metabolism under dynamic conditions using kinetic modelling. Nevertheless, this approach also has several limitations. Firstly, every model is, by definition, false. In order to completely capture the entire metabolism of a cell, one would need a model at least as complex as the cell itself. As we cannot currently create nor simulate such a model, several assumptions and shortcuts must be taken to create a representative model of yeast central carbon metabolism. In the presented model, several parts of the central carbon metabolism, such as the pentose phosphate pathway and TCA cycle were lumped into simplified sink reactions, as no or limited data was available on the concentrations and compartmentation of the metabolites in these pathways. A consequence of this choice is that the activity and regulation of these pathways cannot be accurately represented. Secondly, the model quality and reliability are limited by the quality of the used experimental data. This includes noise in the experimental dataset itself, but also variation between different datasets. Especially when fitting

a model to a dataset, this noise must be considered, as without proper normalization and regularization, this noise may lead to incorrect and misleading conclusions [30]. For example, within the dataset used in our work, we observed a relative error of ~50% in measurements of GAP, whereas the relative error in G6P was only ~5%. By applying weights to the different metabolite model errors, this was considered in this work (See Chapter 2). Still however, for the simulation of the dynamic feast/famine regime only dataset was used to fit the model. Future work should aim to include multiple and larger datasets, in which the variation due to the metabolic response is significantly larger compared to the data noise, to produce more reliable conclusions on the regulation of central carbon metabolism under dynamic substrate conditions.

References

1. Garre E, Matallana E: **The three trehalases Nth1p, Nth2p and Ath1p participate in the mobilization of intracellular trehalose required for recovery from saline stress in *Saccharomyces cerevisiae*.** *Microbiol Read Engl* 2009, **155**:3092–3099.
2. Keller F, Schellenberg M, Wiemken A: **Localization of trehalase in vacuoles and of trehalose in the cytosol of yeast (*Saccharomyces cerevisiae*).** *Arch Microbiol* 1982, **131**:298–301.
3. Veisova D, Macakova E, Rezaczkova L, Sulc M, Vacha P, Sychrova H, Obsil T, Obsilova V: **Role of individual phosphorylation sites for the 14-3-3-protein-dependent activation of yeast neutral trehalase Nth1.** *Biochem J* 2012, **443**:663–670.
4. Müller MM: **Post-Translational Modifications of Protein Backbones: Unique Functions, Mechanisms, and Challenges.** *Biochemistry* 2018, **57**:177–185.
5. Tripodi F, Nicastro R, Reghellin V, Coccetti P: **Post-translational modifications on yeast carbon metabolism: Regulatory mechanisms beyond transcriptional control.** *Biochim Biophys Acta BBA - Gen Subj* 2015, **1850**:620–627.
6. den Ridder M, Knibbe E, van den Brandeler W, Daran-Lapujade P, Pabst M: **A systematic evaluation of yeast sample preparation protocols for spectral identifications, proteome coverage and post-isolation modifications.** *J Proteomics* 2022, **261**:104576.
7. Linck A, Vu X-K, Essl C, Hiesl C, Boles E, Oreb M: **On the role of GAPDH isoenzymes during pentose fermentation in engineered *Saccharomyces cerevisiae*.** *FEMS Yeast Res* 2014, **14**:389–398.
8. Solis-Escalante D, Kuijpers NGA, Barrajon-Simancas N, van den Broek M, Pronk JT, Daran J-M, Daran-Lapujade P: **A Minimal Set of Glycolytic Genes Reveals Strong Redundancies in *Saccharomyces cerevisiae* Central Metabolism.** *Eukaryot Cell* 2015, **14**:804–816.
9. Orij R, Brul S, Smits GJ: **Intracellular pH is a tightly controlled signal in yeast.** *Biochim Biophys Acta BBA - Gen Subj* 2011, **1810**:933–944.
10. Ramos S, Balbin M, Raposo M, Valle E, Pardo LA: **The Mechanism of Intracellular Acidification Induced by Glucose in *Saccharomyces cerevisiae*.** *Microbiology* 1989, **135**:2413–2422.
11. Luzia L, Lao-Martil D, Savakis P, van Heerden J, van Riel N, Teusink B: **pH dependencies of glycolytic enzymes of yeast under *in vivo* -like assay conditions.** *FEBS J* 2022, **289**:6021–6037.
12. Vinnakota K, Kemp ML, Kushmerick MJ: **Dynamics of Muscle Glycogenolysis Modeled with pH Time Course Computation and pH-Dependent Reaction Equilibria and Enzyme Kinetics.** *Biophys J* 2006, **91**:1264–1287.
13. Canelas AB, van Gulik WM, Heijnen JJ: **Determination of the cytosolic free NAD/NADH ratio in *Saccharomyces cerevisiae* under steady-state and highly dynamic conditions.** *Biotechnol Bioeng* 2008, **100**:734–743.
14. Hung YP, Yellen G: **Live-Cell Imaging of Cytosolic NADH–NAD⁺ Redox State Using a Genetically Encoded Fluorescent Biosensor.** In *Fluorescent Protein-Based Biosensors*. Edited by Zhang J, Ni Q, Newman RH. Humana Press; 2014:83–95.

15. Liu Y, Landick R, Raman S: **A Regulatory NADH/NAD⁺ Redox Biosensor for Bacteria.** *ACS Synth Biol* 2019, **8**:264–273.
16. Siedler S, Schendzielorz G, Binder S, Eggeling L, Bringer S, Bott M: **SoxR as a Single-Cell Biosensor for NADPH-Consuming Enzymes in *Escherichia coli*.** *ACS Synth Biol* 2014, **3**:41–47.
17. Spielmann A, Baumgart M, Bott M: **NADPH-related processes studied with a SoxR-based biosensor in *Escherichia coli*.** *MicrobiologyOpen* 2019, **8**:e00785.
18. Goldbeck O, Eck AW, Seibold GM: **Real Time Monitoring of NADPH Concentrations in *Corynebacterium glutamicum* and *Escherichia coli* via the Genetically Encoded Sensor mBFP.** *Front Microbiol* 2018, **9**:2564.
19. Botman D, van Heerden JH, Teusink B: **An Improved ATP FRET Sensor For Yeast Shows Heterogeneity During Nutrient Transitions.** *ACS Sens* 2020, **5**:814–822.
20. Okumoto S, Jones A, Frommer WB: **Quantitative Imaging with Fluorescent Biosensors.** *Annu Rev Plant Biol* 2012, **63**:663–706.
21. Bekers KM, Heijnen JJ, van Gulik WM: **Determination of the *in vivo* NAD:NADH ratio in *Saccharomyces cerevisiae* under anaerobic conditions, using alcohol dehydrogenase as sensor reaction: Determination of *in vivo* NAD:NADH ratio in *S. cerevisiae*.** *Yeast* 2015, **32**:541–557.
22. Zhang J, Sassen T, ten Pierick A, Ras C, Heijnen JJ, Wahl SA: **A fast sensor for *in vivo* quantification of cytosolic phosphate in *Saccharomyces cerevisiae*: In Vivo Cytosolic Phosphate in *S. cerevisiae*.** *Biotechnol Bioeng* 2015, **112**:1033–1046.
23. Zhang J, Pierick A ten, van Rossum HM, Maleki Seifar R, Ras C, Daran J-M, Heijnen JJ, Aljoscha Wahl S: **Determination of the Cytosolic NADPH/NADP Ratio in *Saccharomyces cerevisiae* using Shikimate Dehydrogenase as Sensor Reaction.** *Sci Rep* 2015, **5**.
24. Komatsu N, Aoki K, Yamada M, Yukinaga H, Fujita Y, Kamioka Y, Matsuda M: **Development of an optimized backbone of FRET biosensors for kinases and GTPases.** *Mol Biol Cell* 2011, **22**:4647–4656.
25. Duncan KD, Fyrestam J, Lanekoff I: **Advances in mass spectrometry based single-cell metabolomics.** *The Analyst* 2019, **144**:782–793.
26. Kompauer M, Heiles S, Spengler B: **Atmospheric pressure MALDI mass spectrometry imaging of tissues and cells at 1.4- μ m lateral resolution.** *Nat Methods* 2017, **14**:90–96.
27. Zhang Z, Miliadis-Argeitis A, Heinemann M: **Dynamic single-cell NAD(P)H measurement reveals oscillatory metabolism throughout the *E. coli* cell division cycle.** *Sci Rep* 2018, **8**.
28. Lidstrom ME, Konopka MC: **The role of physiological heterogeneity in microbial population behavior.** *Nat Chem Biol* 2010, **6**:705–712.
29. Levy SF, Ziv N, Siegal ML: **Bet Hedging in Yeast by Heterogeneous, Age-Related Expression of a Stress Protectant.** *PLoS Biol* 2012, **10**:e1001325.
30. Misra BB: **Data normalization strategies in metabolomics: Current challenges, approaches, and tools.** *Eur J Mass Spectrom* 2020, **26**:165–174.

Acknowledgements

Although my name is the only one on the front page of this thesis, without the help and contributions of the many people around me over the years, this thesis would not exist.

First of all, I would like to thank Aljoscha, for offering me the opportunity to work on this project, and for your invaluable advice throughout the years! I have learned a lot from you, from experimental design, analysis of metabolomics data to metabolic modelling. You were always there to help me along in my project, often with many, many useful comments on my drafts and I really appreciate that. It was also very fun to teach AMN together with you these last years! Thank you very for being my mentor and supervisor during this PhD!

Pascale, I would like to thank you very much for your help and advice during my project! I really appreciate that you stepped in as my new promotor after the first year of my PhD, into a (for you) completely new project! Even though a lot of the modelling work was very much outside of your expertise, you were always able to offer me a new and valuable perspective on my data and analysis I had not considered yet. Thank you very much for all your support, I am very glad to have you as my promotor!

This work was performed as part of the Yeast3M project, in collaboration with colleagues DSM, TU Eindhoven and the Vrije Universiteit Amsterdam. David, my modelling partner in crime, I would like to thank you a lot for the intensive collaboration we had, developing the feast/famine kinetic model while corona was raging outside! I really enjoyed our regular modelling meetings with Ana, Ilse, and Hugo, and definitely learned a lot from you! Laura, thank you for introducing me to the world of single-cell metabolomics! It was really great working with you in the lab in Delft, sampling our reactors to produce the most wonderful fluorescent pictures! Bas and Natal, thank you for your invaluable advice during our Yeast3M progress meetings and for your fruitful collaboration on the papers we wrote together! I am very glad we had to opportunity to work together! Joep, I also want to thank you for your advice and essential industrial input during our meeting, and for offering me an opportunity at DSM as the next step in my career! Evelina and Johan, thank you for the useful discussions we had during our meetings!

Perhaps the most important contributors to this thesis are my students! Siem, thank you very much for designing the proteome allocation model that forms the backbone of chapter 3 of this thesis! I really enjoyed our many discussions and wish you all the best for your new PhD position at EBT! Caspar, thank you for all your hard work in the lab, constructing and testing our metabolite sensor strains! Unfortunately, that work did not make it in the final cut of this thesis, however we learned a lot, and it was a pleasure working with you! Ilse, you were presented with David's large kinetic model and managed to incorporate the feast/famine cycles into it, laying the basis for chapter 2 of this thesis! I really enjoying working together! Marije, even though we only met each other once in real life, at the very beginning of your project, due to the lockdown during your project, you were able to produce a great black-box model, helping us to understand sucrose uptake dynamics much better. Thank you for all your hard work! Ana, thank you for all your enthusiasm during the project, and of course for refining the feast/famine kinetic model Ilse had built before you! I really enjoyed working with you! Thijs, you helped me along greatly in expanding our knowledge of the feast/famine regime on different substrates, as is outlined in chapter 4 of this thesis. Thank for the great atmosphere in the lab and the fun discussions during our many meetings! Baukje, you were able to expand upon the proteome model Siem had constructed, improving it so we could publish it. It was great to work together with you, thank you for that! Hugo, towards the end of my project, you were able to shed light upon the various sugar substrate dynamics described in chapter 4 with your kinetic modelling. Thank you for your work and the great discussions during our meetings!

I also would like to thank to members of my defence committee! Thank you for agreeing to be part of my defence, for reviewing my work and for providing me with useful comments on how to further improve this thesis!

The next people I would like to thank are my many colleagues in BT. Leonor, thank you for being a great supervisor during my master thesis and for being a great friend and colleague during my PhD! I enjoyed our many discussions about PAOs, metabolomics and other very random things! Also, thank you for being my paranymph during these final days of my PhD! Florence, thank you for always offering a helpful hand whenever needed, for being a great friend and for our great discussions on yeast and trehalose! We had a lot of fun during our many drinks at the botanical garden and elsewhere in Delft! Thank you helping me wrap up this last chapter of my PhD by being my paranymph!

And of course, to my other colleagues in CSE: Eleni, I had a great time with you in our office, discussing substrate dynamics over our favourite coffee, and enjoying Greek lunches at the Fellowship! Jinrui, thank you for your help and useful advice on yeast metabolism, whenever I needed it! Karel, thank you for your great mentorship in the lab on molecular biology, I have learned many things from you, lots of which I still use every day! Also thank you for the fun we had during our botanical garden drinks! Mariana, I really appreciated your kindness and help in the lab during my PhD! Yaya, thank you for the great time and your help in setting up the big fermenters in our lab! Walter, thank you for your invaluable advice and help during our group meetings, and for your help in writing our paper together! Carla, thank you for always bringing a great atmosphere to the lab, and always being ready to help! Agi, I enjoyed our drinks bar shifts together and thank you for our useful modelling discussions! Maxime, thank you for your help with my proteomics questions and for the fun times during our lunches, drinks and bar shifts at the botanical! Hugo, I enjoyed our drinks in the botanical a lot, thanks for the great atmosphere! Joan, thank you for our great discussions and your help in the lab! Timmy, thanks for our fun discussions on resource allocation, and of course thank you very much for inviting me along to the many EBT lunches, drinks, and dinners! We had a great time together!

To the members of the analytical team: Patricia, thank you for your hard work in providing me with the GC-MS measurements of my many metabolomics samples! Cor, thank you for your expertise and help in getting the LC-MS measurements of my samples and for helping me to setup the HPLC systems! Martin, thank you very much for your advice on my proteomics experiments and for your help in getting metabolomics measurements! Johan, thank you for measuring my many TOC samples and for the great conversations during lunch! Carol, thank you for the great time during our many lunches, drinks, and dinners!

I also want to thank the three heroes at MSD, Apilena, Astrid and Jannie. Thank you for always taking great care in preparing my media and reactors for my experiments! Without you, this thesis would not have been possible! I also really enjoyed the great conversations during our many lunches, thank you for all your kindness!

Next to MSD, I also want to express my thanks to the technicians in CSE, EBT and IMB. Dirk & Rob, thank you for always being ready to help with anything in the lab. Your help was indispensable to performing my experiments, and I am very grateful for all your assistance and all you have taught me over the years! Song, also many thanks to you for helping me in the lab whenever an issue popped up! Thank you also for the fun times during our drinks after work! Erik, thank you for your help during my experiments with Sophie, the fun times during drinks and dinners and especially for welcoming me into IMB! Ben, thank you for the fun discussions and for your help in the Molbio lab!

To my colleagues in my second home, IMB: Sophie, thank you for the fun times and discussions during our ^{13}C experiments! While it was a fairly stressful experiment to performed, we were definitely able to gather some nice data! Looking forward to working together for many coming years at DSM! Ewout, thank you for useful discussions we had on proteomics! Aafke, Anna, Celiné, Charlotte, Christiaan, Clara, Denzel, Eline, Flip, Jasmijn, Jean-Marc, Jonna, Jordi, Marcel, Maria, Marieke, Marijke, Nicole, Nicolò, Raul, Rinke, Robert, Sagarika, Sanne, Wijn and all others, thank you for the welcoming atmosphere in IMB, for the many useful discussions and for the fun times during drinks and conferences!

To my other colleagues and friends in BOC, BPE and EBT: Alexandra, Ali, Ana Maria, Angelos, Chris, Danny, David, Francesc, Gerben, Ingrid, Jan, Jules, Lemin, Luuk, Mariana, Marina, Marta, Maxim, Nina, Rodoula, Sam, Samarpita, Sergio, Simon, Stefan, Stefan, Timmy, Vanda and all the others, thank you for all our fun adventures in Delft, in the botanical garden and during lunches and barbecues! You all ensured that I had an absolutely great time during my PhD! Especially, I really appreciated the fun drinks and events after the lockdowns, when I really needed it again. Thank you all very much for all your kindness!

Finally, I would like to thank my family. Mama, Papa, Wouter & Marieke thank you for your love and kindness, for providing me a place to come home to and for all your support, even though what exactly I was working on may not have always been completely clear to you!

To conclude, thank you all very much, I could not have done it without you all!

- Koen

About the Author

Curriculum Vitae

Koen Verhagen was born on the 26th of September 1994 in Delft, the Netherlands. In 2012, he started his Bachelor's degree in Life Science & Technology at the Technische Universiteit Delft and the Universiteit Leiden in the Netherlands. He performed his Bachelor thesis, titled 'Obtaining and studying a N₂O-reducing enrichment from activated sludge', at the Environmental Biotechnology group in Delft, under the supervision of Dr. M. Conthe Calvo, Prof. M.C.M. van Loosdrecht and Dr. R. Kleerebezem. After receiving this degree in 2015, he went on to pursue a Master's degree in Life Science & Technology (Biochemical engineering specialization), also at the Technische Universiteit Delft, the Netherlands. As part of this degree, he joined the Cell Systems Engineering group, and wrote a thesis with the title 'Metabolic Analysis of Storage Accumulating Organisms' under the supervision of Dr. L. Guedes da Silva, Prof. S.A. Wahl and Prof. M.C.M. van Loosdrecht. Additionally, Koen performed a six months research internship at BASF in Ludwigshafen, Germany, supervised by Dr. A. Golabgir. After obtaining his Master's degree in 2017, he started a PhD project at the Technische Universiteit Delft, supervised by Prof. S.A. Wahl and Prof. P.A.S. Daran-Lapujade, the results of which are described in this thesis.

Since March 2022, he is working as an Associate Fermentation Scientist in DSM in Delft, the Netherlands.

List of Publications

Verhagen, K. J. A., van Gulik, W. M., & Wahl, S. A. (2020). **Dynamics in redox metabolism, from stoichiometry towards kinetics**. *Current opinion in biotechnology*, 64, 116-123., <https://doi.org/10.1016/j.copbio.2020.01.002>

Lao-Martil, D., Verhagen, K. J. A., Schmitz, J. P., Teusink, B., Wahl, S. A., & van Riel, N. A. (2022). **Kinetic Modeling of *Saccharomyces cerevisiae* Central Carbon Metabolism: Achievements, Limitations, and Opportunities**. *Metabolites*, 12(1), 74., <https://doi.org/10.3390/metabo12010074>

Verhagen, K. J. A., Eerden, S. A., Sikkema, B. J., & Wahl, S. A. (2022). **Predicting Metabolic Adaptation Under Dynamic Substrate Conditions Using a Resource-Dependent Kinetic Model: A Case Study Using *Saccharomyces cerevisiae***. *Frontiers in molecular biosciences*, 9., <https://doi.org/10.3389/fmolb.2022.863470>

Lao-Martil, D., Verhagen, K. J. A., Valdeira Caetano, A. H., Pardijs, I. H., van Riel, N. A. W. & Wahl, S. A. (2023). **Using Kinetic Modelling to Infer Adaptations in *Saccharomyces cerevisiae* Carbohydrate Storage Metabolism to Dynamic Substrate Conditions**. *Metabolites*, 13, 88. <https://doi.org/10.3390/metabo13010088>